

Site U1410¹

R.D. Norris, P.A. Wilson, P. Blum, A. Fehr, C. Agnini, A. Bornemann, S. Boulila, P.R. Bown, C. Cournede, O. Friedrich, A.K. Ghosh, C.J. Hollis, P.M. Hull, K. Jo, C.K. Junium, M. Kaneko, D. Liebrand, P.C. Lippert, Z. Liu, H. Matsui, K. Moriya, H. Nishi, B.N. Opdyke, D. Penman, B. Romans, H.D. Scher, P. Sexton, H. Takagi, S.K. Turner, J.H. Whiteside, T. Yamaguchi, and Y. Yamamoto²

Chapter contents

Background and objectives	1
Operations	2
Lithostratigraphy	4
Biostratigraphy	7
Paleomagnetism	10
Age-depth model and mass accumulation rates	12
Geochemistry	13
Physical properties	15
Stratigraphic correlation	17
References	18
Figures	19
Tables	56

Background and objectives

Integrated Ocean Drilling Program (IODP) Site U1410 (proposed Site SENR-23A; 41°19.6993'N, 49°10.1847'W; ~3400 m water depth) is a mid-depth site (~2950 meters below sea level [mbsl] paleodepth at 50 Ma) (Tucholke and Vogt, 1979) in the upper mid-depth end of the Expedition 342 Paleogene Newfoundland sediment drifts depth transect (Fig. F1). The site was positioned to capture a record of sedimentation ~1.5 km shallower than the largely sub-carbonate compensation depth (CCD) record drilled at Site U1403 (Figs. F2, F3). The location, well above the average late Paleogene CCD, should be sensitive to both increases and decreases in carbonate burial, whether these reflect variations in dissolution related to changes in the CCD, changes in carbonate production, or variations in background noncarbonate sedimentation. Our primary scientific objectives for drilling Site U1410 were

- To obtain an expanded record of lower to middle Eocene drift sedimentation that can be compared directly to the relatively condensed record at Site U1409 drilled on the edge of the drift;
- To capture fine-scale variations in carbonate preservation and lysocline shifts in carbonate-rich sediment that is ~400 m deeper than at Site U1408; and
- To evaluate the history of deep water and the CCD on sediment chemistry, grain size, and provenance.

Secondary objectives included the possible recovery of specific Paleogene hyperthermals such as the Middle Eocene Climatic Optimum (MECO) for comparison with the record of these events elsewhere, particularly Sites U1404, U1406, and U1408 along the Expedition 342 depth transect.

Site U1410 is a companion site to Site U1409, where we employed an offset drilling strategy to obtain advanced piston corer (APC) records through a thicker section of the same sediment drift. Drilling a similar pair of sites (U1407 and U1408) showed that the more expanded Site U1408 record is essentially a record similar to that at Site U1407 but with much more clay and a somewhat younger uppermost sediment record. We found largely the same geometry in the J-Anomaly Ridge sites, where the center of the drift has a massively expanded record of the same geological intervals that is present in relatively condensed sections at the ends of the drift. Hence, we expected that coring at Site U1410 would

¹Norris, R.D., Wilson, P.A., Blum, P., Fehr, A., Agnini, C., Bornemann, A., Boulila, S., Bown, P.R., Cournede, C., Friedrich, O., Ghosh, A.K., Hollis, C.J., Hull, P.M., Jo, K., Junium, C.K., Kaneko, M., Liebrand, D., Lippert, P.C., Liu, Z., Matsui, H., Moriya, K., Nishi, H., Opdyke, B.N., Penman, D., Romans, B., Scher, H.D., Sexton, P., Takagi, H., Turner, S.K., Whiteside, J.H., Yamaguchi, T., and Yamamoto, Y., 2014. Site U1410. In Norris, R.D., Wilson, P.A., Blum, P., and the Expedition 342 Scientists, *Proc. IODP*, 342: College Station, TX (Integrated Ocean Drilling Program). doi:10.2204/iodp.proc.342.111.2014

²Expedition 342 Scientists' addresses.



recover a sequence with more clay but otherwise similar gross stratigraphy to the more condensed companion Site U1409.

The primarily calcareous sequence expected at Site U1410 should record changes in ocean alkalinity and carbonate production. Sites U1403 and U1404 were mainly positioned to capture large-amplitude CCD deepening events such as the carbonate budget “overshoots” that are thought to be associated with the most extreme climate perturbations of the Cenozoic, such as those involved with the Paleocene/Eocene Thermal Maximum (PETM), the late middle Eocene, and the Eocene–Oligocene transition (EOT) (see the “[Site U1403](#)” and “[Site U1404](#)” chapters [Norris et al., 2014b, 2014c]). Transient shoaling of the CCD in generally carbonate rich sequences should be recorded at Site U1410 by decreases in carbonate preservation and decreasing carbonate content relative to clay or biosiliceous sediment, as we have already observed at Sites U1404–U1408. As an upper mid-depth site on the Newfoundland depth transect at ~3400 mbsl, Site U1410 was positioned to allow us to reconstruct small changes in carbonate content between the records of Sites U1406 (3850 mbsl) and U1408 (3022 mbsl) and should have a few intervals in which the sediment is 80%–90% carbonate but also intervals in which carbonate abundance falls in the record. Carbonate content was expected to be generally higher at sites in shallower water depth, such as the majority of the sites located on Southeast Newfoundland Ridge, but less than our shallowest depth Sites U1407 and U1408.

The relatively high carbonate contents anticipated in sediment at Site U1410 should permit the construction of detailed stable isotope records and calcareous microfossil biostratigraphy that can be tied by physical property records and magnetostratigraphy to Sites U1403–U1406 further downslope and Sites U1407 and U1408 upslope. Ties between sites on Southeast Newfoundland Ridge and those on J-Anomaly Ridge will allow the isotope stratigraphy and biochronology developed for Sites U1406–U1408 to be exported to the lower ends of the depth transect.

Ultimately, the goal is to use the combination of the lower and middle Eocene record at Sites U1407–U1410 and the younger Paleogene record at Site U1406 to produce composite stable isotope and carbonate content records that can be tied to the more intermittent geochemical records at Sites U1403–U1405. Our aim is to match carbonate-rich intervals across all of the J-Anomaly sites with the sites on Southeast Newfoundland Ridge to create an orbital-resolution record of fluctuations in ocean chemistry and deep water origins.

Site U1410 was proposed during Expedition 342 to test the hypothesis that there are several acoustically transparent drift packages on the Southeast Newfoundland Ridge that correlate to similar but more persistently developed reflector units on the toe of J-Anomaly Ridge (cored at Site U1403). Drilling on J-Anomaly Ridge showed that the uppermost acoustically transparent unit is of middle Eocene to early Miocene age and is separated from a thin, lower, acoustically transparent interval by a set of very well developed reflectors of early Eocene to Cretaceous age. In turn, drilling at Sites U1407–U1409 showed that drift sedimentation begins in the middle early Eocene. We hope to use Site U1410 to determine the onset of drift sedimentation in a record that is likely to have a higher fidelity than the relatively condensed records on the fringes of the sediment drifts.

We hypothesized that Site U1410 would provide an expanded record of primarily calcareous ooze and chalk of rough age-equivalence to sites in deeper water on J-Anomaly Ridge. In particular, Site U1410 should provide a high-deposition rate record of the middle and early Eocene as a counterpart to the largely sub-CCD record at Site U1403 and the shallower records at Sites U1407 and U1408. The combination of these records will improve age and water depth control on the behavior of the CCD in the North Atlantic during this key interval.

Operations

All times are local ship time (UTC – 2.5 h). See Table [T1](#) for coring summary.

Hole U1410A summary

Latitude: 41°19.6987'N

Longitude: 49°10.1995'W

Water depth below sea level (m): 3387.5

Date started: 1845 h, 20 July 2012

Date finished: 0500 h, 22 July 2012

Time on hole (days): 1.4

Seafloor depth (m drilling depth below rig floor [DRF]): 3399.0

Seafloor depth estimation method: mudline core

Rig floor to sea level (m): 11.75

Penetration depth (m drilling depth below seafloor [DSF]): 259.8

Cored interval (m): 259.8

Recovered length (m): 256.88

Recovery (%): 99

Total cores (number): 28

APC cores (number): 16

XCB cores (number): 12



Drilling system: 11 $\frac{1}{16}$ inch advanced piston corer (APC)/extended core barrel (XCB) bit with 136.00 m bottom-hole assembly (BHA)
 Objective: core from seafloor to ~250 m DSF or until science objectives are met
 Result: target reached; objectives achieved

Hole U1410B summary

Latitude: 41°19.6993'N
 Longitude: 49°10.1847'W
 Water depth below sea level (m): 3386.92
 Date started: 0500 h, 22 July 2012
 Date finished: 1620 h, 23 July 2012
 Time on hole (days): 1.5
 Seafloor depth (m DRF): 3398.7
 Seafloor depth estimation method: mudline core
 Rig floor to sea level (m): 11.78
 Penetration depth (m DSF): 245.2
 Cored interval (m): 245.2
 Recovered length (m): 244.84
 Recovery (%): 100
 Total cores (number): 28
 APC cores (number): 18
 XCB cores (number): 10
 Drilling system: 11 $\frac{1}{16}$ inch APC/XCB bit with 136.00 m BHA
 Objective: core from seafloor to ~250 m DSF
 Result: target reached; objectives achieved

Hole U1410C summary

Latitude: 41°19.6885'N
 Longitude: 49°10.1854'W
 Water depth below sea level (m): 3386.9
 Date started: 1620 h, 23 July 2012
 Date finished: 0915 h, 25 July 2012
 Time on hole (days): 1.7
 Seafloor depth (m DRF): 3398.7
 Seafloor depth estimation method: mudline core
 Rig floor to sea level (m): 11.78
 Penetration depth (m DSF): 243.8
 Cored interval (m): 243.8
 Recovered length (m): 238.81
 Recovery (%): 98
 Total cores (number): 27
 APC cores (number): 16
 XCB cores (number): 11
 Drilling system: 11 $\frac{1}{16}$ inch APC/XCB bit with 136.00 m BHA
 Objective: repeat cored sequence from Hole U1410B
 Result: target reached; objectives achieved

Description

The vessel arrived at Site U1410 at 1845 h on 20 July 2012 after a 3.46 nmi transit from Site U1409 in dynamic positioning mode that took 3.5 h at 1.0 kt. The plan for Site U1410 called for drilling three holes to ~250 m DSF. Holes U1410A, U1410B, and U1410C were successfully cored to 259.8, 245.2, and 243.8 m DSF, respectively. The total time spent at Site U1410 was 110.5 h (4.6 days).

Hole U1410A coring

A 8.53 m long mudline core established seafloor depth at 3399.0 m DRF (3387.3 mbsl). Hole U1410A was spudded at 2125 h on 20 July. Cores 342-U1410A-1H through 16H were recovered to 151.0 m DSF using nonmagnetic core barrels and the FlexIT core orientation tool. Core 16H experienced the first partial stroke. The XCB was deployed for Cores 17X through 28X to the final depth of 259.8 m DSF. The seafloor was cleared at 0500 h on 22 July, ending Hole U1410A. Overall core recovery for Hole U1410A was 256.88 m for the 259.8 m interval cored (98.9% recovery). The total time spent in Hole U1410A was 34.25 h.

Hole U1410B coring

The vessel was offset 20 m east. A 3.8 m long mudline core established the seafloor at 3398.7 m DRF (3386.9 mbsl). Hole U1410B was spudded at 0650 h on 22 July. Cores 342-U1410B-1H through 18H were recovered to 153.8 m DSF using nonmagnetic core barrels and the FlexIT core orientation tool. The XCB was deployed for Cores 19X through 28X to a final depth of 245.2 m DSF. The seafloor was cleared at 1620 h on 23 July, ending Hole U1410B. The overall recovery for Hole U1410B was 244.84 m over the 245.2 m cored (99.9% recovery). The total time spent in Hole U1410B was 35.25 h.

Hole U1410C coring

The vessel was offset 20 m south, and Hole U1410C was spudded at 1825 h on 23 July. A 6.82 m long mudline core established the water depth at 3398.7 m DRF (3386.9 mbsl). Cores 342-U1410C-1H through 16H were recovered to 146.8 m DSF using nonmagnetic core barrels. No core orientation was performed in Hole U1410C. The XCB was deployed for Cores 17X through 27X to a final depth of 243.8 m DSF. Overall recovery for Hole U1410C was 238.81 m out of 243.8 m cored (98.0% recovery). The seafloor was cleared, and the vessel was secured for transit at 0915 h on 25 July, ending Hole U1410C. The total time spent on Hole U1410C was 41.00 h.



Lithostratigraphy

At Site U1410, we recovered an ~260 m thick sedimentary succession of deep-sea sediment of Pleistocene to early Eocene age. The full sequence of lithostratigraphic units was only recovered in Hole U1410A. Holes U1410B and U1410C were terminated at 244.25 and 243.27 meters below seafloor (mbsf), respectively.

The sedimentary sequence at Site U1410 comprises four lithostratigraphic units (Figs. F4, F5, F6, F7, F8, F9; Table T2). Unit I is an ~34 m thick succession of Pleistocene sediment with alternating reddish brown clay, gray to dark brown muddy/clayey foraminiferal ooze with nannofossils, grayish brown foraminiferal sand, and occasional sand- to pebble-sized lithics (Fig. F5A, F5B). Unit II is an ~30 m thick succession of clay, clay with nannofossils, and nannofossil clay of early Miocene to Oligocene age (Figs. F5C, F5D, F6B). Manganese, present as discrete nodules or disseminated silt- to sand-sized flecks, and disseminated sulfides are common. Sedimentological and biostratigraphic information indicates that Unit II contains multiple hiatal surfaces in addition to the unconformities that define its upper and lower boundaries. Middle to upper Eocene Unit III is the thickest of the four units (63–68 m thick) and contains greenish gray to greenish nannofossil clay to greenish clayey nannofossil ooze with distinctive 10–25 cm thick bands of light gray to white nannofossil ooze (Figs. F5E, F6C). Lithostratigraphic Unit IV is a 48 m thick sequence of white to pinkish white nannofossil chalk with foraminifers and/or radiolarians of early Eocene age (Figs. F5F, F5G, F6D). This unit is divided into two subunits, with the lower subunit containing several chert beds. Hole U1410A is the deepest hole and thus contains the thickest record of Unit IV. Coring in Hole U1410C recovered only 47 cm of the upper part of Subunit IVb. No part of Subunit IVb was recovered from Hole U1410B (Table T2).

Lithostratigraphic units and boundaries are defined by changes in lithology (as identified by visual core description and smear slide observations), physical properties, color reflectance (L^* , a^* , and b^*), and biogenic content (calcium carbonate and silica) (Fig. F4). The lithologic differences observed between units are primarily attributable to varying abundances of nannofossils, diatoms, radiolarians, and foraminifers (Figs. F7, F8, F9). Lithologic descriptions are based on sediment recovered from Hole U1410A and refined with observations from Holes U1410B and U1410C. The Unit I/II boundary is a sharp contact between banded brown to gray Pleisto-

cene sediment and underlying greenish gray clay of late Miocene age. The basal boundary of Unit II is also sharp and corresponds to a temporal hiatus between overlying lower Oligocene clay and nannofossil clay and underlying middle Eocene sediment that alternates between white nannofossil ooze and dark green nannofossil clay. The Unit III/IV boundary is defined by the transition from alternating green nannofossil clay and white nannofossil ooze to pinkish white, carbonate-rich nannofossil ooze with foraminifers and radiolarians.

Unit I

Intervals: 342-U1410A-1H-1, 0 cm, to 4H-5, 85 cm; 342-U1410B-1H-1, 0 cm, to 5H-2, 135 cm; 342-U1410C-1H-1, 0 cm, to 4H-5, 87 cm

Depths: Hole U1410A = 0–34.35 mbsf; Hole U1410B = 0–34.15 mbsf; Hole U1410C = 0–32.67 mbsf

Age: Pleistocene

Lithology: nannofossil ooze to nannofossil foraminiferal ooze, silty clay with nannofossils or foraminifers, clay, and muddy foraminiferal sand

Unit I is an ~34 m thick succession of Pleistocene sediment with reddish brown (5YR 5/3) to dark greenish gray (10Y 4/1) clay, gray (N6 and 10YR 5/1) and dark brown (5Y 4/2) to dark greenish gray (10Y 4/1) muddy/clayey foraminiferal ooze with nannofossils, and grayish brown (2.5Y 5/2) foraminiferal sand (Fig. F5A, F5B). Sediment in the uppermost interval of Unit I (0 to ~12 mbsf) contains radiolarians and diatoms of varying abundances (Figs. F6, F7, F8, F9). These siliceous components are found only in Units I and IV and further distinguish Unit I sediment from that of underlying Unit II. The upper half of Unit I (0 to ~15 mbsf) contains discrete layers and patches of coarse sand- to small pebble-sized lithics, which are clearly ice rafted debris. The sediment of Unit I is heavily to completely bioturbated throughout, with the exception of some sandy layers that are only slightly bioturbated. The Unit I/II boundary is defined by a sharp contact between brown and gray Pleistocene sediment and underlying greenish gray clay and dark greenish gray nannofossil clay of late Miocene age in the upper part of Unit II. This contact, which occurs in Cores 342-U1410A-4H, 342-U1410B-5H, and 342-U1410C-4H (~34 mbsf), is expressed as a decrease in magnetic susceptibility from ~150 instrument units (IU) in Unit I to <20–50 IU in Unit II (Fig. F4) and a decrease in bulk density (see “Physical properties”). Core 342-U1410C-4H contains a thin (<5 cm) interval of lithogenic sand that directly overlies a sharp contact. This is likely a winnowed deposit that formed during the >5 m.y.



duration of the unconformity that separates Units I and II.

Unit II

Intervals: 342-U1410A-4H-5, 85 cm, to 7H-7, 62 cm; 342-U1410B-5H-2, 135 cm, to 8H-4, 7 cm; 342-U1410C-4H-5, 87 cm, to 7H-7, 24 cm

Depths: Hole U1410A = 34.35–64.17 mbsf; Hole U1410B = 34.15–63.27 mbsf; Hole U1410C = 32.67–63.54 mbsf

Age: late Miocene to Oligocene

Lithology: clay, clay with nannofossils, and nannofossil clay

Unit II is an ~30 m thick succession of clay, clay with nannofossils, and nannofossil clay of late Miocene to Oligocene age (Fig. F4). Colors range from light olive-gray (5Y 6/2) to olive-gray (5Y 6/2), greenish gray (10GY 5/1 and 10Y 6/1), and dark greenish gray (5G 4/1) for the clay and greenish gray (5GY 5/1 and 10Y 5/1) to dark greenish gray (10GY 4/1) for the nannofossil clay (Fig. F5C, F5D). The abundance of foraminifers decreases substantially compared to overlying Unit I, and siliceous biogenic components are absent (Figs. F6, F7, F8, F9). Minor lithologies and accessories include centimeter-scale manganese nodules, disseminated manganese as small dark flecks, dark green glauconite-rich horizons, and dark gray to black concentrations of sulfides. Sulfide mineralization is typically associated with burrows, creating a mottled appearance. Small (1 mm to <1 cm) concentrations of angular, silt- to very fine sand-sized quartz (confirmed by shipboard X-ray diffraction [XRD] analysis) are present throughout Unit II as discrete patches/blebs or, more rarely, as discontinuous lenses within the nannofossil clay (Figs. F5D, F10). We hypothesize that this angular quartz is ice-raftered debris that was subsequently reworked and concentrated by bioturbation.

Sharp contacts define the upper and lower stratigraphic boundaries of Unit II in all holes and coincide with abrupt changes in color and lithology (Fig. F4). Additionally, prominent surfaces within Unit II typically associated with sediment containing abundant glauconite and/or manganese directly below are observed separating distinct intervals. For example, a sharp surface at Section 342-U1410A-5H-4, 43 cm, separates overlying upper Miocene nannofossil clay from underlying lower Miocene nannofossil clay with silt. Although the lithologies across this surface are generally similar, there is a temporal gap of as much as 7 m.y. (see “**Biostratigraphy**”). Additional surfaces within Unit II likely represent other hiatuses that further biostratigraphic investigation could potentially resolve.

Unit III

Intervals: 342-U1410A-7H-7, 62 cm, to 23X-1, 150 cm; 342-U1410B-8H-4, 7 cm, to 25X-CC, 35 cm; 342-U1410C-7H-7, 24 cm, to 23X-CC, 37 cm

Depths: Hole U1410A = 64.17–211.50 mbsf; Hole U1410B = 63.27–216.27 mbsf; Hole U1410C = 63.54–214.22 mbsf

Age: middle Eocene

Lithology: nannofossil clay, clayey nannofossil ooze, and nannofossil ooze

Unit III is a 63–68 m thick succession of predominantly dark greenish gray (5GY 5/1) to greenish gray (10Y 5/1 and 10Y 6/1) nannofossil clay to greenish gray clayey nannofossil ooze (Figs. F4, F5E, F6B, F6C, F7, F8, F9). Distinctive 10–25 cm thick bands of light gray (10Y 7/1 and 10Y 8/1) to white (N 8) nannofossil ooze occur as a secondary, interbedded lithology (Figs. F5E, F6B, F6C). The white nannofossil ooze and greenish gray clay are differentiated by physical properties including color reflectance (L^*), magnetic susceptibility, natural gamma radiation (NGR) (Fig. F11), and carbonate content, which varies from ~30 wt% in the dark layers to ~80 wt% in the light layers (Fig. F4). The frequency of the lighter colored, more nannofossil rich bands is variable throughout Unit III, with some cores containing no light-colored bands and other cores displaying a strikingly rhythmic banded appearance (e.g., Core 342-U1410A-12H; Fig. F11). Intervals of alternating greenish gray nannofossil clay and white nannofossil ooze of middle Eocene age were also recovered at Southeast Newfoundland Ridge Sites U1407 and U1408, all in Unit III. A similar succession, although diminished in its visual appearance, was also recovered in Oligocene–Miocene age sediment at J-Anomaly Ridge (e.g., Site U1405).

Bioturbation is moderate to heavy throughout Unit III, with *Zoophycos*, *Planolites*, and *Chondrites* burrows mottling both the greenish gray and white sediment. Green horizons with elevated concentrations of glauconite and chlorite occur throughout the light greenish gray beds of Unit III, but these are conspicuously absent from the white nannofossil oozes. The concentration of green horizons is higher in the uppermost portion of the light greenish gray nannofossil clay intervals immediately underlying the white/green contacts.

Section 342-U1410A-17X-2 contains a 14 cm thick (153.13–153.27 mbsf) conglomerate with foraminiferal sand matrix (Fig. F12). The clasts are 0.5 to >5 cm in size and composed of the dominant nannofossil clay and clayey nannofossil ooze lithology that is observed throughout Unit III. Examination of calcareous nannofossils sampled from a clast and from the



foraminiferal sand matrix indicates an age of nannofossil Subzone NP15b (middle Eocene) for both (see “**Biostratigraphy**”), which is consistent with the age of the sediment directly under and overlying the conglomerate bed (Fig. F12). We interpret the conglomerate to record erosion, reworking, and winnowing during a period of intensified bottom-current energy. The conglomerate bed in Section 342-U1410A-17X-2 is overlain by an ~11 m thick, internally chaotic interval containing several sharp surfaces, commonly at high angles, that juxtapose lighter clayey nannofossil ooze against darker nannofossil clay. This interval is similar in sedimentary characteristics and age (calcareous nannofossil Subzone NP15b) to an interpreted slump deposit in nearby Site U1409 (see Fig. F16 in the “Site U1409” chapter [Norris et al., 2014d]). Erosion and reworking during the phase that created the conglomerate lag deposit could have produced a relatively rough seafloor topography, which subsequently promoted mass wasting and other soft-sediment deformation in the overlying deposits.

The Unit III/IV boundary is defined by the transition from interbedded gray and white nannofossil clay and ooze to pinkish white, carbonate-rich nannofossil chalk with foraminifers and white nannofossil chalk with radiolarians. The carbonate content of sediments decreases at the Unit III/IV boundary from an average of ~90 wt% in Unit IV to an average of ~50 wt% in Unit III.

Unit IV

Intervals: 342-U1410A-23X-2, 0 cm, through 28X-CC, 58 cm; 342-U1410B-26X-1, 0 cm, through 28X-CC, 32 cm; 342-U1410C-24X-1, 0 cm, through 27X-1, 47 cm

Depths: Hole U1410A = 211.50–258.91 mbsf; Hole U1410B = 225.49–244.25 mbsf; Hole U1410C = 214.00–243.27 mbsf

Age: early Eocene

Lithology: nannofossil chalk with foraminifers and/or radiolarians

Unit IV is a 48 m thick sequence of dominantly nannofossil chalk with foraminifers and/or radiolarians of early Eocene age. Unit IV is divided into two lithologically similar subunits on the basis of the occurrence of interbedded chert at 245.07 mbsf in Hole U1410A (Fig. F4). The chert-rich Subunit IVb was recovered only in Hole U1410A. Unit IV is distinguished from overlying Unit III primarily by the abrupt change in lithology from greenish gray nannofossil clay to white nannofossil chalk, a change that is apparent in most physical property measurements (see “**Physical properties**”). A significant increase in siliceous biogenic components, especially

radiolarians, further distinguishes Unit IV from overlying Unit III, which is essentially barren of siliceous microfossils (Figs. F6, F7, F8, F9).

Subunit IVa

Intervals: 342-U1410A-23X-2, 0 cm, through 26X-6, 47 cm; 342-U1410B-26X-1, 0 cm, through 28X-CC, 32 cm; 342-U1410C-24X-1, 0 cm, through 26X-CC, 39 cm

Depths: Hole U1410A = 211.50–245.07 mbsf; Hole U1410B = 225.49–244.25 mbsf; Hole U1410C = 214.22–239.83 mbsf

Age: early Eocene

Lithology: nannofossil chalk with foraminifers and/or radiolarians

Subunit IVa is a 20–34 m thick succession of white (N8) to pinkish white (7.5YR 8/2 and 7.5YR 8/3) nannofossil chalk with foraminifers and radiolarians (Fig. F5F). Subtle changes in color, from pinkish white to reddish brown (5YR 4/3), occur at the centimeter to decimeter scale in some parts of the succession. Intervals of slightly brighter pink nannofossil chalk are more abundant in radiolarians. Heavy bioturbation, evidenced by faint mottling, occurs throughout Subunit IVa. Underlying Subunit IVb is distinguished by the first occurrence of chert.

Subunit IVb

Intervals: 342-U1410A-26X-6, 47 cm, through 28X-CC, 58 cm; 342-U1410C-27X-1, 0 cm; through 27X-1, 47 cm

Depths: Hole U1410A = 245.07–258.91 mbsf; Hole U1410C = 242.80–243.27 mbsf

Age: early Eocene

Lithology: nannofossil chalk with foraminifers and/or radiolarians and chert

Subunit IVb is a 14 m thick nannofossil chalk with foraminifers and/or radiolarians distinguished from Subunit IVa by several thin (<5 cm) brown (7.5YR 6/4) chert layers. Coring of Subunit IVb in Holes U1410B and U1410C was not attempted because of the significantly slower drilling encountered in Hole U1410A as a result of the chert layers. The brief recovery of this subunit in Hole U1410C is incidental.

Summary

The sedimentary sequence at Site U1410 comprises four lithostratigraphic units. Unit I is an ~34 m thick succession of Pleistocene sediment with alternating reddish brown clay, gray to dark brown muddy/clayey foraminiferal ooze with nannofossils, grayish brown foraminiferal sand, and occasional sand- to pebble-sized lithics (Fig. F5A, F5B). Unit II is an ~30 m thick succession of clay, clay with nannofossils, and nan-



nofossil clay of late Miocene to Oligocene age (Fig. F5C, F5D). Manganese, present as discrete nodules or disseminated silt- to sand-sized flecks, and disseminated sulfides are common. Sedimentological and biostratigraphic information indicates that Unit II contains multiple hiatus surfaces in addition to the unconformities that define its upper and lower boundaries. Middle to lower Eocene Unit III is the thickest of the four units (63–68 m) and contains greenish gray to greenish nannofossil clay and greenish clayey nannofossil ooze with distinctive 10–25 cm thick bands of light gray to white nannofossil ooze (Fig. F5E). Unit IV is a 48 m thick sequence of white to pinkish white nannofossil chalk with foraminifers and/or radiolarians of middle Eocene to early Eocene age. This unit is divided into two generally similar subunits, with the lower subunit containing several chert beds.

The lithostratigraphy of Site U1410 strongly resembles that of Sites U1408 and U1409 in terms of the appearance, lithology, degree of bioturbation, and sedimentary succession of units for Units I–III and, to a lesser degree, Unit IV. We observed three lithostratigraphic commonalities among all sites drilled to date on the Southeast Newfoundland Ridge (Sites U1407–U1410). They include

1. Cyclic banding between light greenish gray nannofossil clay and white (or lighter greenish gray) nannofossils ooze of middle Eocene age,
2. Cherts and other silicified sediments in the lower Eocene, and
3. A step change in calcium carbonate content in sediment during nannofossil Zone NP14 (around the lower to middle Eocene boundary).

Biostratigraphy

Coring at Site U1410 recovered a 260 m thick sequence of Pleistocene to lower Eocene nannofossil ooze and nannofossil clay, with foraminifers and radiolarians. Nannofossils, planktonic foraminifers, and benthic foraminifers are present through most of the succession. Short barren intervals occur between thin Pleistocene, upper Miocene, and lower Miocene–Oligocene sequences. Radiolarians are only present in the uppermost Pleistocene and lower Eocene. Thin Pleistocene, upper Miocene, and lower Miocene–Oligocene sequences overlie a middle Eocene through lower Eocene succession. Hiatuses or highly condensed intervals occur between the lower Pleistocene and upper Miocene (7.1 m.y. duration), upper and lower Miocene (7.4 m.y. duration), lower Miocene and upper Oligocene (5.4 m.y. duration), and lower Oligocene and middle Eocene (7.4 m.y. duration). The Oligocene is highly condensed and

may also contain significant hiatuses. Sedimentation rates are 0.2 cm/k.y. through the Oligocene, 1.3–2.6 cm/k.y. through the middle Eocene, and 0.6 cm/k.y. through the lower Eocene.

Benthic foraminifers are generally rare (the “present” category) throughout the recovered succession with the exception of the Miocene to Oligocene, in which they are abundant to dominant. Benthic foraminifer preservation is good to very good through most of the recovered Eocene sequence. Moderate to poor preservation occurs in the Miocene to Oligocene and the early Eocene.

An integrated calcareous and siliceous microfossil biozonation is shown in Figure F13. An age-depth plot including biostratigraphic and paleomagnetic datums is shown in Figure F22. Datum and zonal determinations from nannofossils, planktonic foraminifers, and radiolarians are in close agreement. Microfossil and paleomagnetic datums are given in Table T3. A summary of calcareous and siliceous microfossil abundances and preservation is given in Figure F14.

Calcareous nannofossils

Calcareous nannofossil biostratigraphy is based on analysis of core catcher and additional working section-half samples in Hole U1410A. Depth positions and age estimates of biostratigraphic marker events are shown in Table T4. Calcareous nannofossil occurrence data are shown in Table T5. Note that the distribution charts are based on shipboard study only and are therefore biased toward age-diagnostic species.

At Site U1410, the preservation of calcareous nannofossils is generally good and moderate to good in the middle Eocene and moderate in the upper Miocene, lower Miocene–Oligocene, and lower Eocene. The uppermost sediment in Hole U1410A contains abundant nannofossils indicative of Pleistocene Zones NN20/NN21–NN17 indicated by the top of *Pseudemiliania lacunosa* in Sample 342-U1410A-1H-CC (8.48 mbsf) and the top of *Discoaster pentaradiatus* in Sample 4H-3, 100 cm (31.51 mbsf). Samples 4H-3, 100 cm (31.51 mbsf), through 4H-CC (37.52 mbsf) are noncalcareous and do not contain nannofossils. The short interval from Sample 4H-CC to 5H-3, 100 cm (31.51–41.00 mbsf), is assigned to upper Miocene Zone NN9 based on the presence of *Discoaster hamatus*. The underlying sediment, from Sample 5H-3, 100 cm, to 5H-CC (41.00–46.45 mbsf), is noncalcareous and barren of nannofossils.

The interval from Sample 342-U1410A-5H-CC through 6H-5, 50 cm (46.45–53.00 mbsf), is assigned to lower Miocene–upper Oligocene Zones NN3–NN1



based on the top of *Sphenolithus belemnos* in Sample 5H-CC (46.45 mbsf), the base of *Discoaster druggii* in Sample 6H-3, 50 cm (50.00 mbsf), and the top of *Sphenolithus ciperoensis* in Sample 6H-5, 50 cm (50.00 mbsf). A short, poorly preserved interval, from Sample 6H-5, 50 cm, through 7H-3, 50 cm (50.00–59.55 mbsf), is late Oligocene in age (Zones NP24–NP25) based on the presence of *Dictyococcites bisectus* and *S. ciperoensis*.

The identification of Zone NP23 in Sample 342-U1410A-7H-7, 62 cm (64.17 mbsf), and Zone NP17 in Sample 342-U1410B-4H-CC, 6.5 cm (64.25 mbsf), indicates the presence of a hiatus of ~8 m.y., representing the upper Eocene to lower Oligocene.

Samples 342-U1410A-7H-7, 70 cm, through 28X-CC (64.25–258.69 mbsf) are assigned to middle to upper Eocene nannofossil Zones NP17–NP12 based on the top of *Chiasmolithus grandis* in Sample 7H-7, 70 cm (64.25 mbsf), the top and base of *Chiasmolithus gigas* in Samples 17X-2, 87 cm (153.37 mbsf), and 21X-2, 70 cm (190.74 mbsf), the base of *Blackites inflatus* in Sample 23X-6, 108 cm (216.28 mbsf), the base of *Discoaster sublodoensis* in Sample 24X-CC (227.06 mbsf), the top of *Tribrachiatus orthostylus* in Sample 26X-5, 90 cm (244.00 mbsf), and the presence of *Discoaster lodoensis* at the base of the section in Sample 28X-CC (258.69 mbsf).

Radiolarians

Radiolarian biostratigraphy is based on analysis of all core catcher samples from Hole U1410A. No samples from Hole U1410B or U1410C were examined. Radiolarians are present in the uppermost part of Hole U1410A (Cores 342-U1410A-1H and 2H) but are absent from the underlying Pleistocene–middle Eocene interval, from Core 3H to 22X (27.88–208.03 mbsf). Radiolarians are very abundant and well preserved in the upper part of the lower Eocene (Cores 23X through 25X; 218.4–233.2 mbsf) and common but poorly preserved in the lowermost Cores 26X through 28X (246.1–258.7 mbsf). Depth positions and age estimates of biostratigraphic marker events are shown in Table T6, and the radiolarian distribution is shown in Table T7. Note that the distribution charts are based on shipboard study only and are therefore biased toward age-diagnostic species.

Sample 342-U1410A-1H-CC (8.48 mbsf) contains a well-preserved Pleistocene–Holocene radiolarian assemblage assigned to Zone RN17 based on the absence of *Stylatractus universus*. Sample 2H-CC (18.4 mbsf) contains rare radiolarians of no biostratigraphic utility. Samples 3H-CC through 22X-CC (20.6–208.03 mbsf) are barren of radiolarians.

Below 208.03 mbsf, Hole U1410A contains a continuous radiolarian succession from Zone RP11 to RP8. Sample 342-U1410A-23X-CC (218.4 mbsf) is assigned to Zone RP11 based on the presence of the primary index species *Dictyomitra mongolfieri* and the absence of *Eusyringium lagena*, the primary index species for Zone RP12. The scarcity of *D. mongolfieri* suggests that this sample lies in lowermost Zone RP11. Sample 24X-CC (227.1 mbsf) is assigned to Zone RP10 based on the presence of *Lithochytris vespertilio* and the absence of *D. mongolfieri*. The event that defines the base of Zone RP10, the faunal crossover from *Theocotyle nigriniae* to *Theocotyle cryptocephala*, is poorly expressed in Hole U1410A. *T. cryptocephala* is much less common than *T. nigriniae* in both samples that span the Zone RP10–RP11 interval. Sample 25X-CC (233.2 mbsf) is assigned to Zone RP9 based on the presence of *Lamptonium fabaeforme constrictum* and the absence of *Lamptonium vespertilio* and *T. cryptocephala*. Samples 26X-CC through 28X-CC (246.1–258.7 mbsf) contain common radiolarians of poor to moderate preservation and are assigned to Zone RP8 based on the presence of the primary index, *Buryella clinata*. The top of *Buryella tetradiaca* is recorded at the top of the zone (Sample 26X-CC; 246.1 mbsf).

Planktonic foraminifers

Core catchers and additional samples from Hole U1410A working section halves were examined. Samples contain planktonic foraminifers from the Pleistocene through lower Eocene. Depth positions and age estimates of identified biostratigraphic marker events are shown in Table T8. The stratigraphic distribution of planktonic foraminifers is shown in Table T9.

The uppermost interval from Sample 342-U1410A-1H-CC to 2H-CC (8.48–18.36 mbsf) contains *Globorotalia truncatulinoides* and *Globorotalia inflata*, indicative of Pleistocene age. Sections 342-U1410A-3H-CC through 4H-5 (27.88–34.51 mbsf) contain a poorly preserved low-diversity assemblage dominated by *G. inflata*, *Neogloboquadrina dutertrei*, and *Neogloboquadrina pachyderma*, suggesting an age of late Pliocene–Pleistocene. An upper Miocene assemblage was recovered from Samples 4H-6, 100–102 cm, through 5H-3, 100–102 cm (36.01–41.01 mbsf), with the co-occurrence of *Globoturborotalita nepenthes*, *Globorotalia plesiotumida*, and *Sphaeroidinellopsis seminulina* and the absence of *Globorotalia tumida* and *Sphaeroidinella dehiscens*, suggesting Subzone M13b to Zone M14.

Three barren intervals occur from Sample 342-U1410A-5H-4, 100–102 cm, to 5H-5, 100–102 cm

(42.51–44.01 mbsf); from Sample 6H-6, 100–102 cm, to 6H-CC (55.01–56.20 mbsf); and in Sample 7H-7, 28–30 cm (63.84 mbsf). Samples 5H-6, 90–92 cm, to 6H-4, 100–102 cm (45.41–52.01 mbsf), contain no planktonic foraminifers or poorly preserved and impoverished assemblages of early Miocene age (Zone M3 or older) consisting of *Catapsydrax dissimilis*, *Globorotalia praescitula*, and *Globigerinoides immaturus*. A poorly preserved and impoverished assemblage of Oligocene age (unzoned) exists from Sample 7H-2, 100–102 cm, to 7H-5, 100–102 cm (58.53–61.9 mbsf).

Sample 342-U1410A-7H-7, 100–102 cm, contains diverse globigerinathekids, *Subbotina senni*, *Turborotalita carcoselleensis*, and *Turborotalita cerroazulensis*, suggesting middle Eocene Zone E13. Well-preserved and diverse planktonic foraminifers of early to middle Eocene age are found in Samples 7H-CC through 23X-5, 102–104 cm (65.66–215.53 mbsf). The top and base of *Orbulinoides beckmanni* demarcates the top and base of Zone E12 in Samples 8H-4, 110–112 cm, and 9H-CC (71.11–84.56 mbsf). The top of *Guembelitrioides nuttalli* marks the base of Zone E11 in Sample 10H-6, 90–92 cm (90.56 mbsf). Although the top of *Morozovella aragonensis* marks the base of Zone E10, this species occurs only sporadically through the middle Eocene of Hole U1410A. Therefore, we have used the base of *Morozovella lehneri* in Sample 17X-4, 120–122 cm (156.71 mbsf), to approximate this zonal boundary. The base of *Globigerinatheka kugleri* occurs in Sample 17X-CC (160.82 mbsf) and marks the base of Zone E9. The base of *G. nuttalli* in Sample 22X-2, 100–102 cm (201.51 mbsf) indicates the base of Zone E8, and the base of *Turborotalita frontosa* in Sample 23X-5, 102–104 cm (215.53 mbsf), marks the base of Subzone E7b.

The early Eocene interval from Sample 342-U1410A-23X-CC to 27X-CC (218.43–255.14 mbsf) contains poorly preserved planktonic foraminifers ranging from Subzone E7a through Zone E5. The base of *Acarinina cuneicamerata* in Sample 26X-2, 114–115 cm (239.75 mbsf), indicates the base of Subzone E7a, whereas the top of *Morozovella subbotinae* in Sample 27X-CC (252.83 mbsf) marks the top of Zone E5.

Benthic foraminifers

Benthic foraminifers were examined semiquantitatively in core catcher samples from Hole U1410A. Additional working section half samples taken from Cores 342-U1410A-4H through 27X were examined for preservation and relative abundance of benthic foraminifers. Benthic foraminifers at this site are predominantly rare (the “present” category) relative to total sediment particles >150 µm in the Pleistocene

and Eocene, and more abundant in the Miocene and Oligocene (Fig. F14; Tables T10, T11).

Preservation of benthic foraminifer tests is generally good to very good in the middle Eocene, the Miocene, and Oligocene, but the lower Eocene successions contain poorly to moderately preserved benthic foraminifers (Fig. F14).

With the exception of well-preserved Sample 342-U1410A-1H-CC (8.48 mbsf), the Pleistocene faunas of Samples 1H-CC through 3H-CC (8.48–27.88 mbsf) are moderately preserved and dominated by *Cibicidoides* sp., *Cibicidoides kullenbergi*, *Cibicidoides wuellerstorfi*, *Pullenia bulloides*, *Turrilina* sp., and *Uvigerina peregrina* (Table T10).

The moderately preserved Miocene benthic foraminifer assemblage (Samples 342-U1410A-4H-CC and 5H-CC; 37.52–46.45 mbsf) is characterized by high-productivity fauna with abundant *Cassidulina subglobosa*, *Dentalina* sp., *Gyroidinoides* sp., *Plectofrondicularia* sp., *Pleurostomella tenius*, *Stilostomella subspinosa*, and *Turrilina* sp.

Poorly preserved Oligocene benthic foraminifers are found in Sample 342-U1410A-6H-CC (56.20 mbsf). This sample contains abundant glauconite grains and fish teeth, indicative of a condensed sequence with low sedimentation rate. Because of this condensed nature, benthic foraminifers, potentially exposed on the seafloor for a long interval of time, are severely fragmented and dissolved.

Samples 342-U1410A-7H-CC through 28X-CC (65.66–258.69 mbsf) show typical early to middle Eocene fauna dominated by calcareous taxa. Abundant calcareous taxa in the middle Eocene are *Anomalinoides* sp., *Bulimina* sp., *Cassidulina subglobosa*, *Cibicidoides praemundulus*, *Dentalina* sp., *Nuttallides truempyi*, *Oridorsalis umbonatus*, *Pullenia bulloides*, and stilostomellids (including *Stilostomella gracillima*, *Stilostomella lepidula*, and *Stilostomella subspinosa*) (Table T10). In addition to the taxa described above, the lower Eocene and lowermost middle Eocene (Samples 342-U1410A-21X-CC through 28X-CC; 199.13–258.69 mbsf) are characterized by the occurrence of *Alabamina dissonata*, *Aragonina aragonensis*, and *Cibicidoides eocaenus*.

The lower to middle Eocene assemblages described above suggest a normal deepwater environment, but Sample 342-U1410A-11H-CC (103.18 mbsf) is exceptional in that it contains a benthic foraminifer assemblage dominated by the infaunal taxa *Bigenerina* sp. and *Stilostomella* spp. together with abundant *N. truempyi* and lacks other epifaunal species. A short-term increase in infaunal taxa can be also found within the MECO-equivalent sequence (Section 342-

U1410A-8H-CC; 75.39 mbsf), comparable to observations from the same level at Site U1408.

Paleomagnetism

We completed a paleomagnetism study of APC and XCB cores from Holes U1410A–U1410C with the primary objective of establishing a magnetostratigraphic age model for the site. The natural remanent magnetization (NRM) of each archive section half was measured at 2.5 cm intervals before and after demagnetization treatment in a peak alternating field (AF) of 20 mT for all cores from Hole U1410A. For all other cores, we only measured NRM after 20 mT demagnetization. Archive-half measurement data were processed by removing measurements made within 7.5 cm of section ends and from disturbed intervals described in the Laboratory Information Management System database. Cores 342-U1410A-1H through 16H and 342-U1410B-1H through 18H were azimuthally oriented using the FlexIT orientation tool (Table T12). All other cores were not oriented.

We also collected 178 discrete samples from working section halves to verify the archive section half measurement data and to measure anisotropy of magnetic susceptibility (AMS) and bulk susceptibility of Site U1410 sediment. Discrete samples were collected and stored in 7 cm³ plastic cubes and typically taken from the least disturbed region closest to the center of each section from Hole U1410A. Selected samples were subjected to measurements of AMS, including bulk susceptibility, and NRM after 20 mT AF demagnetization. Twenty-two samples were selected for step-wise demagnetization at 0, 10, 20, 30, 40, and 60 mT. All discrete sample data are volume corrected to 7 cm³.

Results

Downhole paleomagnetism data after 20 mT demagnetization are presented for Holes U1410A, U1410B, and U1410C in Figures F15, F16, and F17, respectively. Similar to paleomagnetism results from previous Expedition 342 sites, section-half measurement data from cores recovered using the XCB are difficult to interpret because of biscuiting and substantial core disturbance. We chose to interpret only results obtained from APC cores except for a few cases in which discrete samples provide additional constraints on magnetozone identification in XCB-recovered intervals.

We report the following principal features in the paleomagnetism data at Site U1410. First, we observed several trends in downhole magnetization intensity.

Second, inclinations are biased toward positive values, whereas declinations alternate around 180° and cluster at ~0° and ~180°. Third, the geomagnetic field transitions correlated to Chrons C18n.1n–C18n.1r–C18n.2n are recorded in exceptional detail in Hole U1410B. The same reversal transitions were observed in similar detail at Site U1408; the two paleomagnetism records are remarkably coherent.

Downhole trends in magnetic intensity

Downhole magnetic intensity values show downhole trends that are consistent among all three holes and generally correspond to lithostratigraphic units. Magnetic intensity is invariant and high (~10⁻² A/m) in the uppermost ~35 m. This interval corresponds to the reddish brown to green Pleistocene nannofossil oozes, nannofossil and foraminifer oozes, and silty clay of lithostratigraphic Unit I (see “[Lithostratigraphy](#)”). From ~40 to ~100 mbsf, magnetic intensity generally remains high (~10⁻² A/m) but is distinguished from the interval above by frequent horizons of low magnetic intensity (as low as ~10⁻⁴ A/m). This interval corresponds to the upper Miocene to Oligocene greenish gray clay and nannofossil clay of Unit II and the uppermost part of the middle Eocene green and greenish gray nannofossil clay and nannofossil ooze of Unit III. Although the contact between Units II and III is clearly distinguished by magnetic susceptibility, it is not obvious in the magnetic intensity record. From ~100 to 150 mbsf, magnetic intensity gradually decreases from 10⁻² to 10⁻⁴ A/m. This interval is entirely within Unit III. Below ~150 mbsf, Holes U1410A and U1410B have two distinctive intervals that show gradual increases in intensity, from ~10⁻⁵ to ~10⁻⁴ A/m at ~150–220 mbsf and from ~10⁻⁵ to ~10⁻³ A/m below ~220 mbsf. In contrast, Hole U1410C shows almost constant intensity (~10⁻⁴ A/m) below ~150 mbsf. Downhole trends in magnetic susceptibility below ~150 mbsf are similar among all three holes. The difference in downhole magnetic intensity trends among the three holes in this lowest interval is unclear, but it may be attributable to different degrees of core disturbance in these XCB-recovered intervals.

Inclination bias and declination clustering

Inclination bias indicates that there is a substantial drilling overprint even after 20 mT AF demagnetization. Because of this strong inclination bias, we often cannot identify paleomagnetism polarity solely based on shipboard inclination data. However, azimuthally oriented APC cores show ~180° alternation of declination, and these values cluster at ~0° and ~180°. We interpret intervals with declination values of ~0° (~180°) to indicate normal



(reversed) magnetozones. A magnetozone with a primary normal polarity should not display inclinations less than ~40°, barring sedimentary inclination shallowing biases. Notably, intervals with ~180° declination almost always correspond to inclination values that are more shallow than those in the intervals with declination of ~0°. Thus, the drilling overprint mainly obscures remanent inclination but not declination, similar to the paleomagnetism results from Sites U1403 and U1404.

Comparison between pass-through and discrete sample data

AF demagnetization results for 109 discrete samples are summarized in Table T13. Of the 22 samples treated with a peak AF demagnetization field of 60 mT, 13 reveal reasonably stable components of magnetization (e.g., Fig. F18A, F18B). These samples have remanent magnetizations that are strong enough to be measured by the onboard JR-6A spinner magnetometer. The remaining samples typically display NRM intensities that decrease by an order of magnitude following AF demagnetization in a 20 mT field. This behavior indicates that a drilling overprint probably obscures the primary magnetic signal. An example of such a magnetic overprint can be seen in Figure F18C. Nevertheless, these results are useful for verifying the 20 mT pass-through paleomagnetism data from the archive section halves.

Magnetization intensity and declination are generally consistent between the discrete samples and the archive section half samples from APC-recovered intervals (Fig. F15). In contrast, inclinations measured in discrete samples from XCB-recovered intervals are often more shallow than their counterpart values in the archive section half samples from APC core intervals. These observations indicate that cores from XCB-recovered intervals have a relatively severe overprint.

Magnetostratigraphy

The shipboard downhole results reveal a series of normal and reversed magnetozones between Cores 342-U1410A-1H and 24X (~0–218 mbsf), between Cores 342-U1410B-1H and 15H (~0–121 mbsf), and between Cores 342-U1410C-2H and 13H (13–118 mbsf). These magnetostratigraphies can be easily correlated among all three holes.

By utilizing radiolarian, foraminifer, and nannofossil biostratigraphic datums from Hole U1410A (see “[Biostratigraphy](#)”), we can correlate magnetozones to the geomagnetic polarity timescale (GPTS). The shipboard magnetostratigraphic age model is based on Hole U1410A, for which we have the most bio-

stratigraphic datums. Extension of this age model to the magnetozonation observed in Holes U1410B and U1410C is contingent on the accuracy of the stratigraphic correlation between holes, which is corroborated by lithostratigraphic horizons, biostratigraphic datums, and physical property features (see “[Stratigraphic correlation](#)”). Our correlation is presented in Table T14 and Figures F15, F16, F17, and F19.

We correlate the polarity transitions from the top of Core 342-U1410A-1H to 4H at ~32.95 mbsf to Chron C1n (Brunhes) to upper Chron C2An.1n (~2.6 Ma). We do not observe Chrons C2r.1r and C2r.1n (Réunion) in any hole at Site U1410 in this interval. We do not interpret this as a hiatus, but rather the inability of the wide-bore pass-through magnetometer to resolve these extremely short and rarely observed chronos in this Pleistocene sediment. We correlate the well-resolved magnetozonation observed in Sections 342-U1410A-8H-3 (~68.68 mbsf) to 24X-1 (~218.06 mbsf) to lower Chron C18n.1n (~39.5 Ma) continuously downhole to upper Chron C21r (~47.4 Ma). Paleomagnetism data from archive section halves and discrete samples suggest a magnetostratigraphy can be developed in deeper intervals at Site U1410, but it cannot be resolved in sufficient detail with these shipboard data to correlate with confidence to the GPTS. Magnetozone correlations for Holes U1410B and U1410C are similar to Hole U1410A, with the exceptions that we did not interpret XCB-recovered intervals in the former holes and we did not observe the Chron 18n.1r/18n.2n boundary in Hole U1410C.

The correlations described above provide a shipboard chronostratigraphic framework for interpreting the Pleistocene and middle Eocene sediment record at Site U1410. The most salient implications of this age model are that

- Average linear sedimentation rates during the Pleistocene at Site U1410 range from 1.47 to 2.35 cm/k.y. (Fig. F22),
- The difficulty in correlating magnetozones between Cores 342-U1410A-5H and 7H to the GPTS can be attributed to the highly condensed nature of this interval and the likelihood of several significant hiatuses inferred from the nannofossil biostratigraphy, and
- Average linear sedimentation rates during the middle Eocene at Site U1410 are similar to those calculated for Sites U1407–U1409. Sedimentation rates are highest during Chron C20n (2.63 cm/k.y. from ~42.3 to 43.4 Ma) and are ~75% lower before and after this interval. Notably, the interval of highest average linear sedimentation rate (LSR) at Site U1410 is one chron



younger than at Site U1409, the downslope conjugate site to Site U1410.

Detailed record of a geomagnetic field transition

At Site U1408, we found that the geomagnetic field transitions from Chrons C18n.1n to C18n.1r to C18n.2n are recorded in exceptional detail in all three holes over ~7 m of stratigraphic section. A very similar record is observed between ~67 and 74 mbsf in Hole U1410B (Fig. F20). The remarkable coherence in the record between the two distant sites suggests that the paleomagnetism record faithfully reflects geomagnetic field behavior rather than diagenetic artifacts. A thorough, shore-based paleomagnetism and rock magnetic study is necessary, however, to fully characterize and understand the geomagnetic field transition behavior.

Magnetic susceptibility and anisotropy of magnetic susceptibility

Bulk magnetic susceptibility measured on 118 discrete samples is summarized in Table T15. Although discrete samples were collected from each core section from the entire depth of Hole U1410A, we chose to measure only odd-numbered samples, except in the interval between Cores 342-U1410A-8H and 16H, in which we measured every sample. Downhole variation in whole-round magnetic susceptibility (WRMS) and discrete sample magnetic susceptibility (DSMS) for Hole U1410A are shown in Figure F15. The WRMS data for Hole U1410A are shown in raw form; they have not been trimmed at section ends or filtered for obvious outliers, so noise in the data probably reflects edge effects or spurious measurements. We multiplied the WRMS data, which are in instrument units, by a factor of 0.577×10^{-5} to convert to approximate SI volume susceptibilities (see “Paleomagnetism” in the “Methods” chapter [Norris et al., 2014a]). WRMS and DSMS data agree very well after this conversion, and we attribute small absolute differences to the fact that the conversion factor applied to the WRMS data is not constant downhole because of changes in core diameter and density; only discrete samples provide calibrated susceptibility values in SI units. Both magnetic susceptibility data sets show the same first- and second-order cyclic trends, indicating that these trends are robust features of Site U1410 sediment.

AMS results for the discrete samples are also summarized in Table T15 and are shown in Figure F21. The eigenvalues associated with the maximum (τ_1), intermediate (τ_2), and minimum (τ_3) magnetic susceptibilities at Site U1410 show some downhole varia-

tions that correspond to changes in lithostratigraphy. We also observe a change in AMS values at the transition from APC to XCB coring technologies, with greater consistent divergence between principal eigenvalues indicative of more oblate fabrics in the XCB cores. In the clay-dominated lithostratigraphic Unit III, we observed consistently steeper inclinations of the minimum principal eigenvector (V_3) in the XCB-recovered interval, but we did not observe this trend in the nannofossil chalks of Unit IV. Thus, as expected, more lithified sediment is more resistant to coring-induced fabrics.

Triaxial fabrics are greatest and most variable in three discrete intervals: Cores 342-U1410A-1H, 17X, and 24X. These intervals are also characterized by high degrees of anisotropy (P) and stronger lineation fabrics. In Core 1H, we attribute this behavior to the high pore water content and lack of lithification in these young sediments. Core 17X is at the base of the interval of highest average LSR (Chron 20n; see “Magnetostratigraphy”) and in a highly disturbed interval described as a slump deposit (Fig. F12). Core 24X is characterized by a peak in bulk density values and a low in water content in the white nannofossil chalk of lithostratigraphic Subunit IVa (see “Physical properties”).

Age-depth model and mass accumulation rates

At Site U1410, we recovered a 260 m thick sequence of Pleistocene to lower Eocene nannofossil ooze and nannofossil clay with foraminifers and radiolarians. A relatively thick Pleistocene section overlies a condensed upper Miocene–upper middle Eocene section, which is followed by an expanded middle through lower Eocene succession. Hiatuses or highly condensed intervals occur between the lower Pleistocene and upper Miocene (7.1 m.y. duration), upper and lower Miocene (7.4 m.y. duration), lower Miocene and upper Oligocene (5.4 m.y. duration), and lower Oligocene and middle Eocene (7.4 m.y. duration). The Oligocene is highly condensed and may also contain substantial hiatuses. Sedimentation rates are 0.2 cm/k.y. through the Oligocene, 1.3–2.6 cm/k.y. through the middle Eocene, and 0.7 cm/k.y. through the lower Eocene.

Biostratigraphic and magnetostratigraphic datums from Hole U1410A (Table T3) were compiled to construct an age-depth model for this site (Fig. F22). A selected set of datums (Table T16) was used to create an age-depth correlation and calculate LSRs. Total mass accumulation rate (MAR), carbonate MAR (CAR), and noncarbonate MAR (nCAR) were calcu-

lated at 0.2 m.y. intervals using a preliminary ship-board splice rather than the sampling splice described in this volume (Table T17; Fig. F23).

Age-depth model

The age-depth model is tied to Pleistocene nannofossil and paleomagnetic datums in the upper 36 m of Hole U1410A. Nannofossil datums provide the sole tie points over a very condensed section that extends from the lower Pleistocene to the middle Eocene. This section includes two definite hiatuses and three very condensed intervals that probably also include hiatuses. Through the middle Eocene, nannofossil and paleomagnetic datums provide the primary tie points, with a single radiolarian datum serving as the final tie point in the core. Datums are in good agreement through the Eocene.

Linear sedimentation rates

This site is unique among sites drilled during this expedition in that it has a relatively expanded Pleistocene section with LSRs of 1.47–2.35 cm/k.y. This section is followed downhole by a condensed Pliocene–middle Eocene section with an average LSR of 0.19 cm/k.y. The middle to lower Eocene section has high LSRs in the upper part (1.98–2.63 cm/k.y.) that decrease progressively to a minimum of 0.66 cm/k.y. in the lower Eocene.

Mass accumulation rates

The Pleistocene sequence at Site U1410 has a MAR of 2.0 to 2.4 g/cm²/k.y., with a double peak largely driven by the LSR pattern. MAR is low in the Pliocene to middle Oligocene with a pattern of peak MAR values that correspond to changes in LSR. In the middle Eocene, MAR is 2.0–2.9 g/cm²/k.y., with roughly equal accumulation rates for carbonate and noncarbonate units. In the lower Eocene, carbonate contents increase to ~90 wt%, but overall MAR are significantly lower than the middle Eocene, with very low nCAR values.

Geochemistry

The geochemistry program during operations at Site U1410 included

- Analysis of interstitial gas compounds on headspace samples;
- Measurement of minor and trace element concentrations in interstitial water squeezed from whole-round samples from Hole U1410A;
- Inorganic carbon, total carbon, and total nitrogen determinations of solid sediment samples from multiple holes; and

- Characterization of organic matter by source rock pyrolysis.

Headspace gas samples

Headspace gas samples for routine safety monitoring were collected typically at a frequency of one sample per core in Hole U1410A (Table T18), generally in the bottom half of each core (i.e., Sections 4, 5, or 6). Methane increases very slightly downhole, with values between 2.11 and 6.72 ppmv. Higher molecular weight hydrocarbons were not detected in measurable amounts.

Interstitial water samples

Twenty-three interstitial water samples were squeezed from whole-round samples, which were typically taken at a frequency of one per core in Hole U1410A (Table T19). Whole-round samples were collected immediately after the cores were sectioned on the catwalk. In some cases, disturbed cores or low recovery precluded whole-round sampling, as in the case with Cores 342-U1410A-10H and 22X, which were too disturbed.

Results

Salinity, pH, alkalinity, ammonium, manganese, iron, and sulfate

The pH profile decreases uniformly throughout the hole from ~7.5 at the seafloor to 6.8 at 254 mbsf (Fig. F24). The salinity profile is near uniform at 36–38. In contrast, alkalinity shows low values of ~3.5 mM at the core top to 5.6 mM at the base of lithostratigraphic Subunit IVb (254 mbsf).

Manganese concentrations display a complex profile, with values of ~4–8 µM in lithostratigraphic Units I and II (0–130 mbsf), a maximum of ~15 µM near the base of Unit III (190 mbsf), and values varying between 11 and 4 µM in underlying Subunits IVa and IVb (220–254 mbsf).

Sulfate concentrations decrease downhole from a maximum of 30 mM at the top of the recovered sequence (lithostratigraphic Unit I) to <22 mM at the base. Ammonium concentrations are highly variable but are lowest at the core top (40 µM) and highest at the base (155 µM) in Subunit IVb (254 mbsf). An intermediate maximum of 105 µM occurs in Unit I (15 mbsf) and in the middle of Unit III (120 µM at 130 mbsf).

Calcium, magnesium, sodium, chloride, boron, and potassium

Calcium concentrations in Hole U1410A show an increasing downhole trend, from lithostratigraphic



Unit I through Subunit IVb (0–254 mbsf), in which a step increase from ~11 to ~24 mM occurs.

Magnesium concentrations mirror the calcium profile, which shows slightly decreasing values in Unit I through Subunit IVa where a step decrease from 54 to 39 mM occurs. Magnesium/calcium ratios show a smooth monotonic decline from ~4.9 at the core top to <2 at the base of the hole. Potassium concentrations show a decreasing downhole trend to a depth of 150 mbsf. Below this depth, the concentration profile is near uniform at ~11 mM.

Sodium concentrations range from 465 to 494 mM, with a weak overall increasing downhole trend. Chloride concentrations range from 535 to 580 mM, with no discernible downhole trend.

Interstitial water boron concentrations are low (~400 μM or less) at the core top and in lithostratigraphic Subunit VIa (220–240 mbsf) but rise to values between 450 and 580 μM in Unit II (30 mbsf) and Subunit IVa (210 mbsf). Otherwise, boron concentrations show a gentle decline downhole.

Discussion

The interstitial fluid profiles of sulfate, alkalinity, and ammonium in Hole U1410A reflect typical changes associated with organic carbon cycling. As with other sites drilled to date on Southeast Newfoundland Ridge (Sites U1407–U1409), interstitial water profiles display evidence of compartmentalization with pronounced abrupt downhole shifts in magnesium, manganese, and potassium at ~220–230 mbsf, suggesting that the unrecovered sequence of chert functions as an aquiclude. Overall, interstitial water profiles of potassium, calcium, and magnesium are consistent with those resulting from exchange with and alteration of basaltic basement at depth (Gieskes and Lawrence, 1981). Potassium and magnesium concentrations decrease and calcium concentrations increase with depth (Fig. F24). Inflections at ~240 mbsf correspond to an increase in alkalinity and indicate possible dissolution/reprecipitation of carbonate, which is high in the nannofossil chalk that comprises the basal lithostratigraphic Subunit IVb (see “[Lithostratigraphy](#)”).

Depth profiles of alkalinity and manganese concentrations are well correlated with each other. This covariation of alkalinity and manganese concentrations indicates modest organic matter degradation associated with manganese reduction. Alkalinity, manganese, and iron show multiple peaks through the recovered sequences, which implies the presence of complex diffusional processes and organic matter reservoirs and subsequent organic matter degradation in each peak. Peak concentrations of manganese

(16 μM) and iron (80 μM) are attained in lithostratigraphic Unit III. Disseminated pyrite formation in Unit II is reflected in the low iron content (0–4 μM), indicating syndepositional removal under highly reducing conditions. Both redox-sensitive metals not only reflect the generally reducing character of the sediment but also the difference between the clay contents of Unit III and the rest of the remaining units (see “[Lithostratigraphy](#)”). Sulfate concentrations steadily decrease with depth suggesting diffusion of seawater sulfate rather than solely microbial sulfate reduction.

The boron profile shows low values (380 μM) in the top of the sedimentary section (0–30 mbsf) and then increases sharply to high values (500–600 μM) at 30–40 mbsf, from where values decrease downhole back to low levels (400 μM) at 240 mbsf and then increase one more time toward the bottom of the hole. The sharp downhole increase near the top of the hole occurs near the boundary between lithostratigraphic Units I and II (35 mbsf; see “[Lithostratigraphy](#)”), where physical properties profiles also show step changes. Unit I is an ~34 m thick succession of Pleistocene sediment with alternating reddish brown clay, gray to dark brown foraminiferal ooze, grayish brown foraminiferal sand, and occasional sand- to pebble-sized lithics. Unit II is an ~30 m thick succession of clay-rich sediment of early Miocene to Oligocene age. The boron increase at the bottom of the hole corresponds to Subunit IVb, consisting of (pinkish) white nannofossil chalk of Eocene age containing several chert beds.

Boron has been demonstrated in laboratory experiments and from field studies to be leached from terrigenous sediments into fluids (e.g., James et al., 2003; Deyhle and Kopf, 2002). The boron profile at Site U1410 suggests that the boron supply varied significantly in the different lithostratigraphic units.

Sediment samples

Sediment plugs (5 cm^3) for downhole analysis of sediment elemental geochemistry were taken from Cores 342-U1410A-1H through 24X at an average resolution of one sample per section, adjacent to the moisture and density samples (Table T20).

Results

Concentrations of inorganic carbon vary from 0.04 to 12.4 wt% in Holes U1410A–U1410C (Table T20; Fig. F25). These concentrations are equivalent to 0.7–93 wt% CaCO_3 , assuming that all of the carbonate is calcite.

Carbonate concentrations are 5–50 wt% in Pleistocene nannofossil ooze of lithostratigraphic Unit I



and decrease to 0–20 wt% in upper Miocene to Oligocene clay of Unit II, which is consistent with low carbonate levels observed in other Oligocene-age sequences recovered during Expedition 342. In the expanded middle Eocene sequence represented by Unit III (see “[Lithostratigraphy](#)”), the alternating clay-rich bedding and white nannofossil ooze layers have fluctuating carbonate values of 30–85 wt%, with a few peaks of ~85 wt% carbonate. The clay and ooze layers are further differentiated by physical properties including color reflectance (L^*), magnetic susceptibility, and NGR. Carbonate content increases to 90 wt% in Unit IV, which corresponds to early Eocene–age sediment.

Total organic carbon (TOC) values are typically 0.1–0.3 wt% throughout the sediment column. TOC values, together with total nitrogen values, appear to decrease downhole from lithostratigraphic Unit III to IV. Organic matter is thermally immature and relatively well preserved with low T_{\max} values (380°–420°C). Organic matter is a mixture of Type II (algal and microbial) and Type III (land plant) kerogen.

Discussion

Based on shipboard age models, the low-carbonate interval (80–83 mbsf) immediately above Chron C19n corresponds to the MECO, which is widely regarded as the terminal Eocene hyperthermal event (e.g., Bohaty et al., 2009), marked by high temperatures and deep sea carbonate dissolution.

The striking intervals of rhythmic greenish gray nannofossil clay and white nannofossil ooze of middle Eocene age were also recovered at Southeast Newfoundland Ridge Sites U1407 (lithostratigraphic Unit III), U1408 (Unit III), and U1409 (Unit III). A similar succession, although diminished in its visual appearance, was also recovered in Oligocene–Miocene sediment at J-Anomaly Ridge sites (e.g., Site U1405).

As with other sites drilled to date on the Southeast Newfoundland Ridge (Sites U1407–U1410), the most prominent change in Hole U1410A is a step increase (from 50 to 90 wt% CaCO_3 ; ~100 mbsf) in sediment during nannofossil Zone NP14 (around the early/middle Eocene boundary). This step correlates with shifts in several proxies (e.g., color reflectance, magnetic susceptibility, NGR, TOC, and total nitrogen values) and marks a transition from pelagic chalk sedimentation to clay deposition in the initial stages of sediment drift development.

Physical properties

We made physical properties measurements on whole-round sections, section halves, and discrete

samples from section halves. Gamma ray attenuation (GRA) bulk density, magnetic susceptibility, P -wave velocity, and NGR measurements were made on whole-round sections using the Whole-Round Multisensor Logger (WRMSL) and Natural Gamma Radiation Logger. Compressional wave velocity on section halves was also measured at a frequency of two in each section (at ~50 and 100 cm) using a P -wave caliper (PWC). For moisture and density (MAD) analyses, one discrete sample was collected in each section (typically at ~35 cm from the top of a section) from Hole U1410A. The Section Half Multisensor Logger (SHMSL) was used to measure spectral reflectance and magnetic susceptibility on archive section halves.

Magnetic susceptibility

Overall, magnetic susceptibility ranges from -2 to 291 IU (Fig. [F26](#)). In lithostratigraphic Unit I (0 to ~35 mbsf), magnetic susceptibility is high and variable (8–291 IU) and increases (from ~30 to 120 IU) downhole. Magnetic susceptibility decreases sharply to 20 IU at the Unit I/II boundary. In Unit II, magnetic susceptibility averages 30 IU, but is also characterized by many superimposed peaks that correlate among all three holes. A sharp decrease to ~5 IU is observed at the contact with underlying Unit III. Magnetic susceptibility values remain much more uniform (0–20 IU) throughout Unit III, but high-frequency variations are observed between ~70 and 120 mbsf in all three holes. In Subunits IVa and IVb, magnetic susceptibility remains constant at ~4 and 13 IU, respectively.

Density and porosity

Two methods were used to measure bulk density at Site U1410. The GRA density method provides an estimate from whole-round sections, whereas the MAD method, applied to 183 discrete samples from Hole U1410A, provides a second, independent measure of bulk density, as well as dry bulk density, grain density, water content, and porosity.

At Site U1410, bulk density ranges from 1.5 to 2.4 g/cm³ and gradually increases downhole. The downhole profile of MAD bulk density is consistent with that of GRA bulk density; however, MAD bulk density is on average ~2% lower than GRA density in the APC-cored section (Fig. [F26](#)). In lithostratigraphic Unit I, density varies from 1.6 to 1.8 g/cm³ and decreases to 1.5 g/cm³ at the Unit I/II boundary (35 mbsf). Bulk density increases downhole from 1.5 to 1.9 g/cm³ in Units II and III. Two superimposed peaks that correlate among all three holes occur within this interval, at ~50 and 160 mbsf. Bulk density values fluctuate

between 1.8 and 2.1 g/cm³ in Unit IV, and increase to ~2.0 g/cm³ at the bottom of Subunit IVb.

Water content in sediment from Hole U1410A ranges from 21 to 53 wt%, and porosity varies from 43 to 76 vol%. Generally, water content and porosity decrease downhole; this trend is expected because of sediment compaction. In Unit I, both properties display high values (30–48 wt% for water content and 55–70 vol% for porosity). In Unit II, water content and porosity fluctuate from 41 to 53 wt% and from 65 to 76 vol%, respectively. These physical properties gradually decrease downhole in Unit III (from 37 to 26 wt% for water content and 61 to 50 vol% for porosity). In Subunits IVa and IVb, water content and porosity fluctuate from 23 to 35 wt% and from 44 to 59 vol%, respectively.

Grain density ranges from 2.6 to 3.3 g/cm³ in Hole U1410A. From the top of the hole to ~20 mbsf, grain density values are high (>2.8 g/cm³), whereas below this interval, grain density values remain uniform and average ~2.75 g/cm³. High values may be the result of high manganese oxide content in the sediment. Alternatively, the high values may be an artifact of measuring sandy (foraminiferal) and silty clay that may not be completely saturated.

P-wave velocity

P-wave velocity was measured using the PWL on all whole-round sections and using the PWC on undisturbed section halves from Holes U1410A–U1410C.

P-wave velocity ranges from 1500 to 1650 m/s in PWL data and from 1490 to 1960 m/s in PWC data in all three holes. PWC values are consistently lower than the PWL values by ~20 m/s in the APC-cored section (Fig. F27). P-wave velocity gradually increases downhole and maximum velocities are recorded at the bottom of the hole. PWL measurements were not performed in the lower part of lithostratigraphic Unit III and Subunits IVb and IVc in Holes U1410A and U1410C (from ~160 mbsf to the bottom of each hole). PWC measurements show higher variations within this interval; we attribute this variability to the change in coring methods from APC to XCB.

Natural gamma radiation

NGR was measured on whole-round sections from Holes U1410A–U1410C. Overall, values range from 2 to 47 cps. Through lithostratigraphic Unit I, NGR increases downhole from 13 to 42 cps (Fig. F27), a trend that is in step with a decrease in carbonate content (see “Geochemistry”). In Unit II, NGR decreases to a minimum of <20 cps at ~48 mbsf in Hole

U1410A, ~50 mbsf in Hole U1410B, and ~45 mbsf in Hole U1410C. NGR values increase to 40 cps down-hole through the rest of Unit II but abruptly decrease to 30 cps at the Unit II/III boundary. Carbonate content increases abruptly across the Unit II/III boundary. In Unit III, NGR values remain relatively constant and fluctuate between 13 and 30 cps. Three shifts at ~82, 110, and 160 mbsf can be correlated among all three holes. All of these peaks correspond to alternations between greenish clay and whitish carbonate-rich clay layers (see “Lithostratigraphy”). The shift observed at ~160 mbsf coincides with a slight increase in carbonate content. NGR values rapidly decrease from 27 to 10 cps at the Unit III/IV boundary at ~215 mbsf; this shift corresponds to the transition from gray-green carbonate-poor sediment of Unit III to carbonate-rich white chalk of Unit IV. In the carbonate-rich Subunits IVa and IVb, NGR remains uniformly low (~10 cps).

Color reflectance

Color reflectance was measured on archive section halves from all three holes. The standard operating resolution of data acquisition was decreased from 2.5 to 5 cm in all three holes because the rate of core recovery required faster processing. Changes in color reflectance parameters a^* and b^* are consistent among all three holes (Fig. F28). In lithostratigraphic Unit I, values average ~1 for a^* and ~0 for b^* . In Unit II, a^* and b^* values show more variations (a^* and b^* range from -4 to 8.5 and from -5.5 to 16, respectively); this variability is associated with the large changes in sediment color (from light olive-gray to dark greenish gray) of this unit (see “Lithostratigraphy”). Through Unit III, a^* and b^* remain relatively constant, and a^* averages 0 whereas b^* averages -1. From the Unit III/IV boundary (~210 mbsf) to the base of Subunit IVb, a^* and b^* increase from -2 to 12 and from -3 to 8, respectively. The increase in a^* and b^* corresponds to the change from greenish to pinkish white sediment. In Subunit IVb, a^* and b^* remain constant, with a^* ranging from 4 to 8 and b^* ranging from 5 to 10).

L^* exhibits the same downhole trend in all three holes. From the top of the hole to ~40 mbsf, L^* decreases downhole from ~55 to 40. A shift to higher values, with a peak of 60, occurs at ~42 mbsf. Below this level, L^* values continue to increase slightly (from 50 to 65) to the bottom of Unit III. Two broad peaks occur at ~115 and ~150 mbsf within this interval. At the contact with the underlying Subunit IVa (at ~215 mbsf), L^* values increase sharply from 65 to 90, a shift that correlates with the transition from gray-green nannofossil clay to white nannofossil chalk. L^* values remain high and constant, with an



average value of 85, throughout Subunits IVa and IVb. The major variations in L^* recorded at Site U1410 occur at the same levels as changes in the NGR data series (Fig. F28). This pattern correlates to changes in calcium carbonate content (see “[Geochemistry](#)”).

Thermal conductivity

Twenty-eight measurements were completed on whole-round sections from Hole U1410A (Table T21). Overall, thermal conductivity ranges from 0.9 to 1.5 W/(m·K) (Fig. F29). In lithostratigraphic Unit I, thermal conductivity ranges from 0.9 to 1.4 W/(m·K). From the top of Unit II to the bottom of the hole, thermal conductivity values increase gradually downhole from ~1.1 to 1.5 W/(m·K). Thermal conductivity measurements approximately correlate to GRA bulk density values ($R^2 = \sim 0.58$) (Fig. F30).

Stratigraphic correlation

Sampling splice

We constructed a sampling splice for Site U1410 that is continuous to ~226 m core composite depth below seafloor (CCSF) based on unambiguous signals in magnetic susceptibility. Physical property data at Site U1410 are very similar to those from Site U1408—orbital cyclicity superimposed on clear long-term trends provided useful patterns to correlate among the three holes. Clear trends and patterns in NGR also aided verification of the splice (Fig. F31). Hole U1410A is the deepest hole drilled at this site, with a maximum depth of ~260 mbsf (~280 m CCSF). Holes U1410B and U1410C extended to 245.2 m mbsf (265.37 m CCSF) and 243.8 m mbsf (258.51 m CCSF), respectively. We are most confident about the correlation among the three holes for the upper ~170 m CCSF. Below this depth, some tie points are more tentative because of ambiguous patterns in physical properties. Across the middle to early Eocene transition, a distinct lithostratigraphic change from green clay-rich sediments to white calcium carbonate-rich strata is accompanied by a sharp down-hole decrease in magnetic susceptibility values to almost zero. As a result, correlations are tentative in the carbonate-rich interval. These tentative tie points are denoted in the offset and tie point tables (Tables T22, T23). Additional shore-based data will be used to verify the accuracy of the splice in this interval. Our correlation results in a growth rate of 6% for Holes U1410A–U1410C (Fig. F32).

Correlation during drilling operations

Based on correlation between WRMSL magnetic susceptibility data generated on cores from Hole U1410A and STMSL magnetic susceptibility data generated on cores from Holes U1410B and U1410C, we were able to guide drilling operations. Good estimates of seafloor depth enabled drilling operations to achieve the targeted lengths of mudline cores in Holes U1410B and U1410C, which were 3.8 and 6.8 m, respectively. Below the relatively thick (~35 m) Pleistocene–Pliocene cover, magnetic susceptibility values dropped; however, the signal was sufficient to guide drilling. Orbital cycles in both the Pleistocene and Eocene intervals yielded good depth control. Offsets among cores from adjacent holes decreased incrementally with depth because of varying resistance of the lithology while drilling. However, we were able to secure a continuous splice downhole to ~226 m CCSF, with only a few depth adjustments made while drilling in Holes U1410B and U1410C.

Correlation and splice construction

Orbital cyclicity in the WRMSL magnetic susceptibility data, in combination with similar, but lower resolution patterns and trends in NGR (see “[Physical properties](#)”) (Fig. F31) formed the primary signal for constructing the composite depth scale and splice. Core 342-U1410A-1H is defined as the anchor in the splice because it is the longest of the three mudline cores recovered. The clear cyclicity present in the uppermost, relatively thick (compared to other sites at J-Anomaly Ridge and South East Newfoundland Ridge) Pleistocene–Pliocene cover disappears in the very condensed Pliocene to late Eocene interval between ~35 and ~65 m CCSF. Throughout the Eocene drift deposit, between ~65 and ~228 m CCSF and corresponding to lithostratigraphic Unit III (see “[Lithostratigraphy](#)”), persistent orbital cyclicity is again present. Cycle amplitude is largest in the upper part of the sequence and drops to lower amplitudes below ~145 m CCSF. Tie points in the lower portion of the record are therefore more tentative and require shore-based verification.

At ~228 m CCSF, the transition from the middle to early Eocene is marked by different lithologies recovered in Hole U1410A with respect to Holes U1410B and U1410C. In Hole U1410A, a gradual transition in magnetic susceptibility and NGR values correspond to clear cycles in the lithology from greenish clay to white carbonate, whereas in Holes U1410B and U1410C, these cycles are absent. We interpret a gap in Hole U1410A and append Core 342-U1410A-



23X to the bottom of Core 342-U1410C-23X. Below, we interpret gaps between Cores 342-U1410B-25X and 26X and between Cores 342-U1410C-23X and 24X. No operational explanation is apparent for such gaps; rather, we consider the gaps in the composite depth scale reflective of lateral variability within the formation at the middle to early Eocene transition. Relatively strong APC coring disturbance, with variable expansion-compression profiles along the lengths of the cores, is recognizable in cores across all three holes at Site U1410. Cores 342-U1410A-27X and 28X were appended because this interval was not recovered in Holes U1410B and U1410C.

References

- Bohaty, S.M., Zachos, J.C., Florindo, F., and Delaney, M.L., 2009. Coupled greenhouse warming and deep-sea acidification in the middle Eocene. *Paleoceanography*, 24(2):PA2207. [doi:10.1029/2008PA001676](https://doi.org/10.1029/2008PA001676)
- Deyhle, A., and Kopf, A., 2002. Strong B enrichment and anomalous $\delta^{11}\text{B}$ in pore fluids from the Japan Trench forearc. *Mar. Geol.*, 183(1-4):1–15. [doi:10.1016/S0025-3227\(02\)00186-X](https://doi.org/10.1016/S0025-3227(02)00186-X)
- Norris, R.D., Wilson, P.A., Blum, P., Fehr, A., Agnini, C., Bornemann, A., Boulila, S., Bown, P.R., Cournede, C., Friedrich, O., Ghosh, A.K., Hollis, C.J., Hull, P.M., Jo, K., Junium, C.K., Kaneko, M., Liebrand, D., Lippert, P.C., Liu, Z., Matsui, H., Moriya, K., Nishi, H., Opdyke, B.N., Penman, D., Romans, B., Scher, H.D., Sexton, P., Takagi, H., Turner, S.K., Whiteside, J.H., Yamaguchi, T., and Yamamoto, Y., 2014a. Methods. In Norris, R.D., Wilson, P.A., Blum, P., and the Expedition 342 Scientists, *Proc. IODP*, 342: College Station, TX (Integrated Ocean Drilling Program). [doi:10.2204/iodp.proc.342.102.2014](https://doi.org/10.2204/iodp.proc.342.102.2014)
- Norris, R.D., Wilson, P.A., Blum, P., Fehr, A., Agnini, C., Bornemann, A., Boulila, S., Bown, P.R., Cournede, C., Friedrich, O., Ghosh, A.K., Hollis, C.J., Hull, P.M., Jo, K., Junium, C.K., Kaneko, M., Liebrand, D., Lippert, P.C., Liu, Z., Matsui, H., Moriya, K., Nishi, H., Opdyke, B.N., Penman, D., Romans, B., Scher, H.D., Sexton, P., Takagi, H., Turner, S.K., Whiteside, J.H., Yamaguchi, T., and Yamamoto, Y., 2014b. Site U1403. In Norris, R.D., Wilson, P.A., Blum, P., and the Expedition 342 Scientists, *Proc. IODP*, 342: College Station, TX (Integrated Ocean Drilling Program). [doi:10.2204/iodp.proc.342.104.2014](https://doi.org/10.2204/iodp.proc.342.104.2014)
- Norris, R.D., Wilson, P.A., Blum, P., Fehr, A., Agnini, C., Bornemann, A., Boulila, S., Bown, P.R., Cournede, C., Friedrich, O., Ghosh, A.K., Hollis, C.J., Hull, P.M., Jo, K., Junium, C.K., Kaneko, M., Liebrand, D., Lippert, P.C., Liu, Z., Matsui, H., Moriya, K., Nishi, H., Opdyke, B.N., Penman, D., Romans, B., Scher, H.D., Sexton, P., Takagi, H., Turner, S.K., Whiteside, J.H., Yamaguchi, T., and Yamamoto, Y., 2014c. Site U1404. In Norris, R.D., Wilson, P.A., Blum, P., and the Expedition 342 Scientists, *Proc. IODP*, 342: College Station, TX (Integrated Ocean Drilling Program). [doi:10.2204/iodp.proc.342.105.2014](https://doi.org/10.2204/iodp.proc.342.105.2014)
- Norris, R.D., Wilson, P.A., Blum, P., Fehr, A., Agnini, C., Bornemann, A., Boulila, S., Bown, P.R., Cournede, C., Friedrich, O., Ghosh, A.K., Hollis, C.J., Hull, P.M., Jo, K., Junium, C.K., Kaneko, M., Liebrand, D., Lippert, P.C., Liu, Z., Matsui, H., Moriya, K., Nishi, H., Opdyke, B.N., Penman, D., Romans, B., Scher, H.D., Sexton, P., Takagi, H., Turner, S.K., Whiteside, J.H., Yamaguchi, T., and Yamamoto, Y., 2014d. Site U1409. In Norris, R.D., Wilson, P.A., Blum, P., and the Expedition 342 Scientists, *Proc. IODP*, 342: College Station, TX (Integrated Ocean Drilling Program). [doi:10.2204/iodp.proc.342.110.2014](https://doi.org/10.2204/iodp.proc.342.110.2014)
- Gieskes, J.M., and Lawrence, J.R., 1981. Alteration of volcanic matter in deep-sea sediments: evidence from the chemical composition of interstitial waters from deep sea drilling cores. *Geochim. Cosmochim. Acta*, 45(10):1687–1703. [doi:10.1016/0016-7037\(81\)90004-1](https://doi.org/10.1016/0016-7037(81)90004-1)
- Gradstein, F.M., Ogg, J.G., Schmitz, M.D., and Ogg, G.M. (Eds.), 2012. *The Geological Time Scale 2012*: Amsterdam (Elsevier).
- James, R.H., Allen, D.E., and Seyfried, W.E., Jr., 2003. An experimental study of alteration of oceanic crust and terrigenous sediments at moderate temperatures (51 to 350°C): insights as to chemical processes in near-shore ridge-flank hydrothermal systems. *Geochim. Cosmochim. Acta*, 67(4):681–691. [doi:10.1016/S0016-7037\(02\)01113-4](https://doi.org/10.1016/S0016-7037(02)01113-4)
- Kirschvink, J.L., 1980. The least-squares line and plane and the analysis of palaeomagnetic data. *Geophys. J. R. Astron. Soc.*, 62(3):699–718. [doi:10.1111/j.1365-246X.1980.tb02601.x](https://doi.org/10.1111/j.1365-246X.1980.tb02601.x)
- Tucholke, B.E., and Vogt, P.R., 1979. Western North Atlantic: sedimentary evolution and aspects of tectonic history. In Tucholke, B.E., Vogt, P.R., et al., *Init. Repts. DSDP*, 43: Washington, DC (U.S. Govt. Printing Office), 791–825. [doi:10.2973/dsdp.proc.43.140.1979](https://doi.org/10.2973/dsdp.proc.43.140.1979)

Publication: 3 March 2014
MS 342-111



Figure F1. Bathymetric map for northwestern Southeast Newfoundland Ridge, northeast of J-Anomaly Ridge. Data are based upon multibeam mapping by KNR179-1 site survey. Single-channel seismic reflection profiles are shown in Figures F2 and F3.

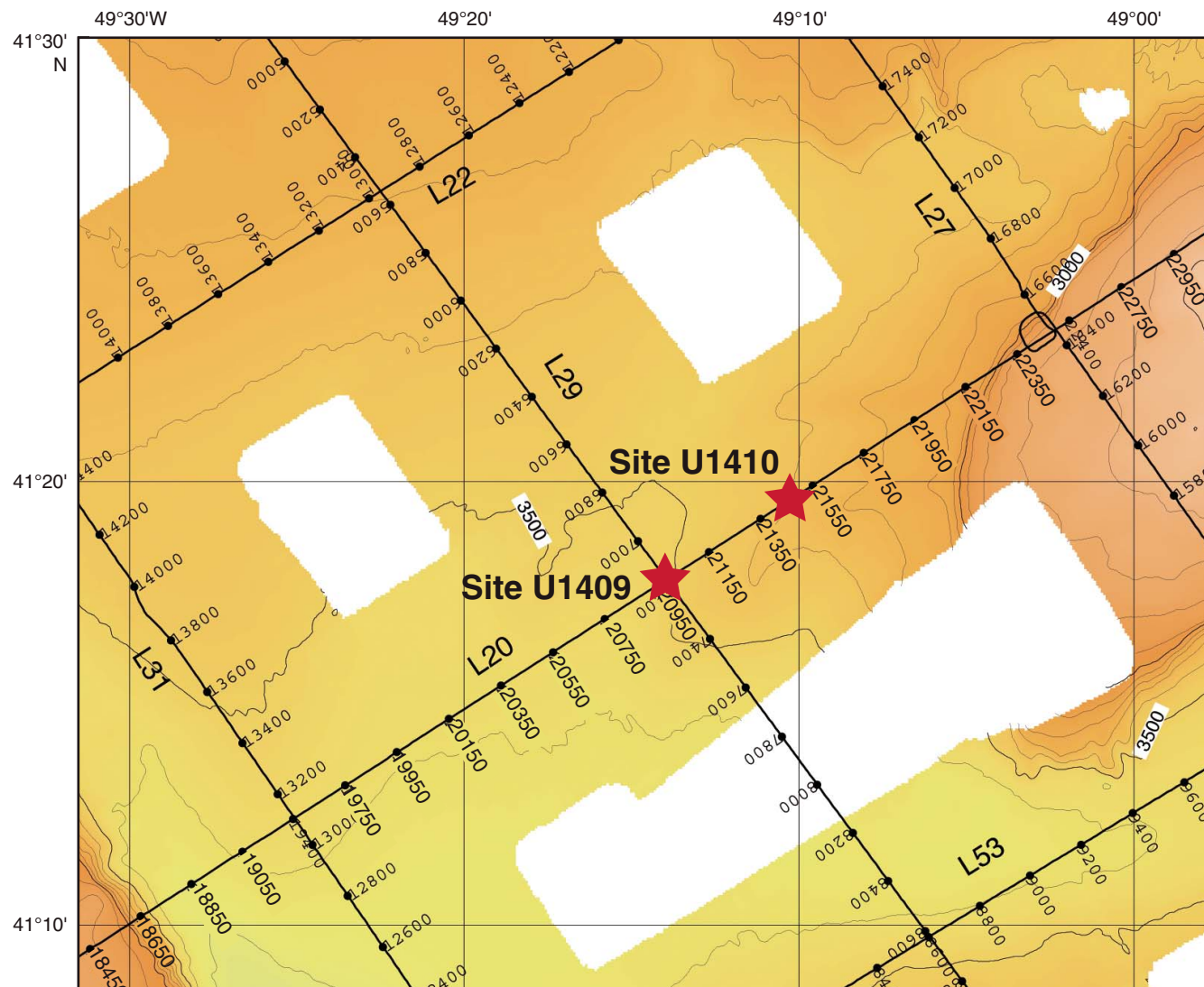


Figure F2. Single-channel seismic KNR179-1 Line 20. This is the southwest–northeast line crossing Site U1410 (at shotpoint [SP] 21480). White boxes represent approximate depth of penetration at Sites U1409 and U1410.

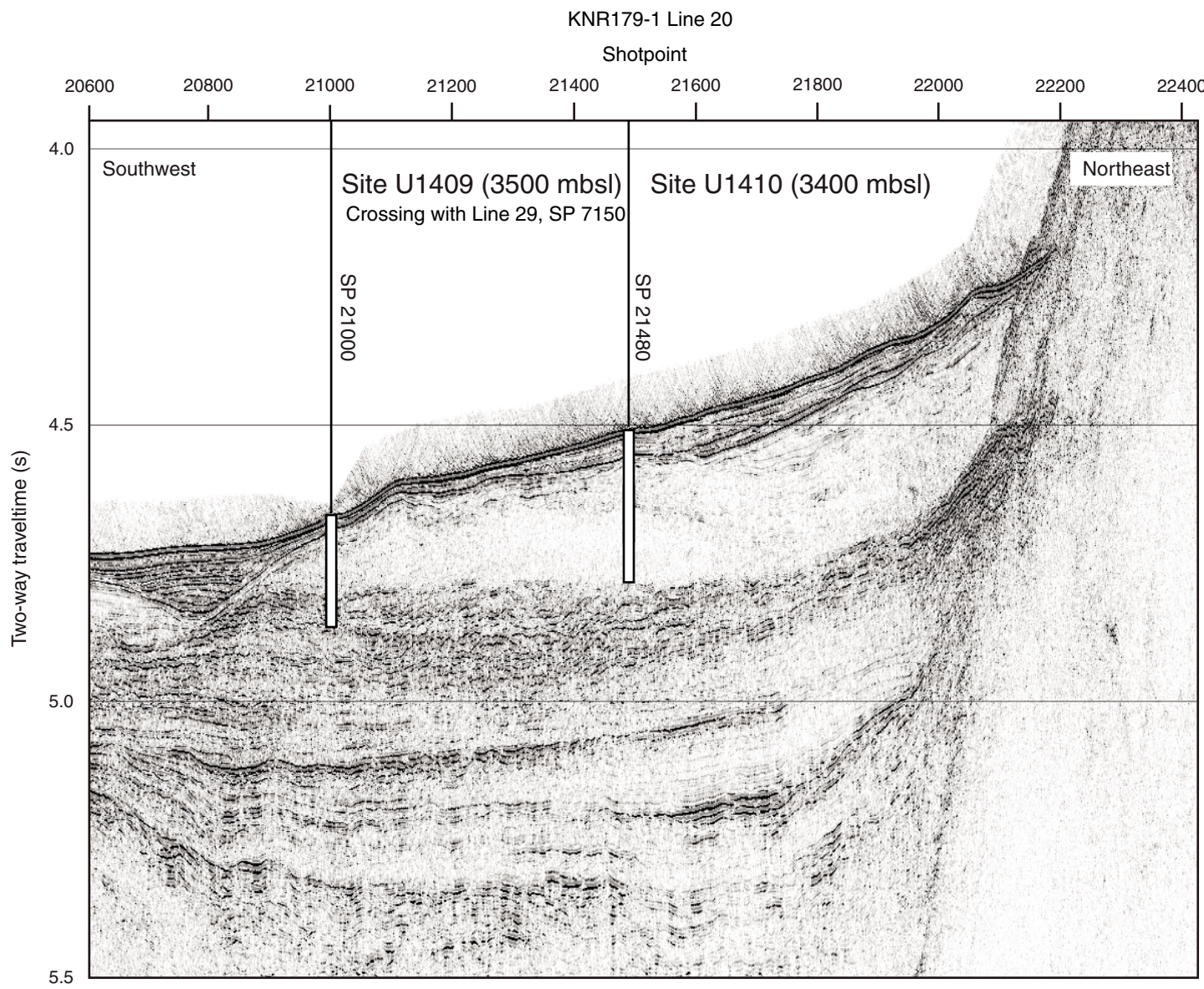


Figure F3. Single-channel seismic KNR179-1 Line 29. This is the northwest–southeast line passing southwest of Site U1410 (northeast of line crossing at shotpoint [SP] 21000). The record of the acoustically-transparent zone between ~4.7–4.8 s two-way traveltimes is thicker at Site U1410 than shown on KNR1970-1, Line 29, but the overall geometry of the sediment drift is similar.

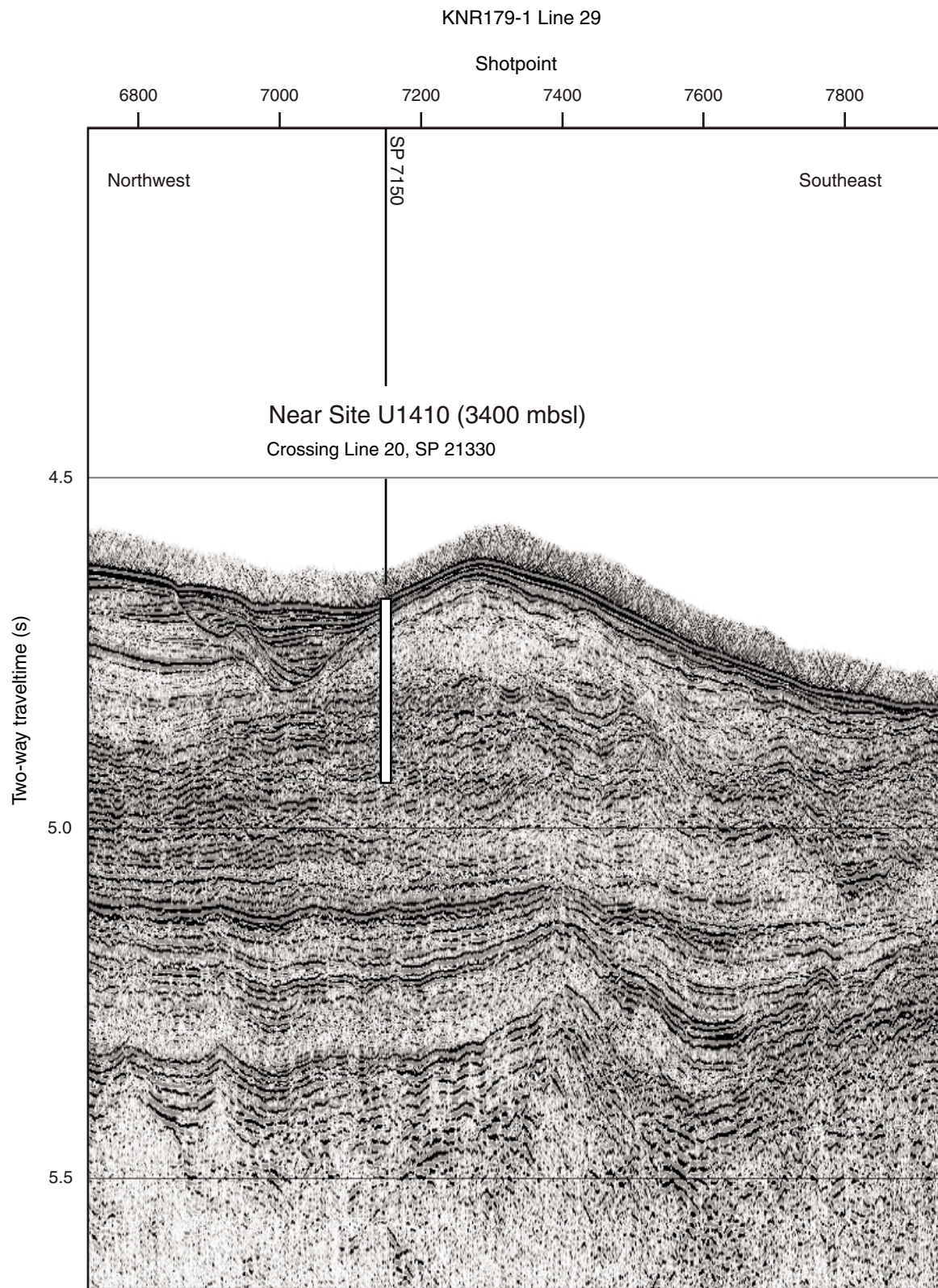


Figure F4. Lithostratigraphic summary, Site U1410. Typically the lighter colors reflect higher carbonate content. Note the green to pink/tan transition in the color data at the Unit III/IV boundary.

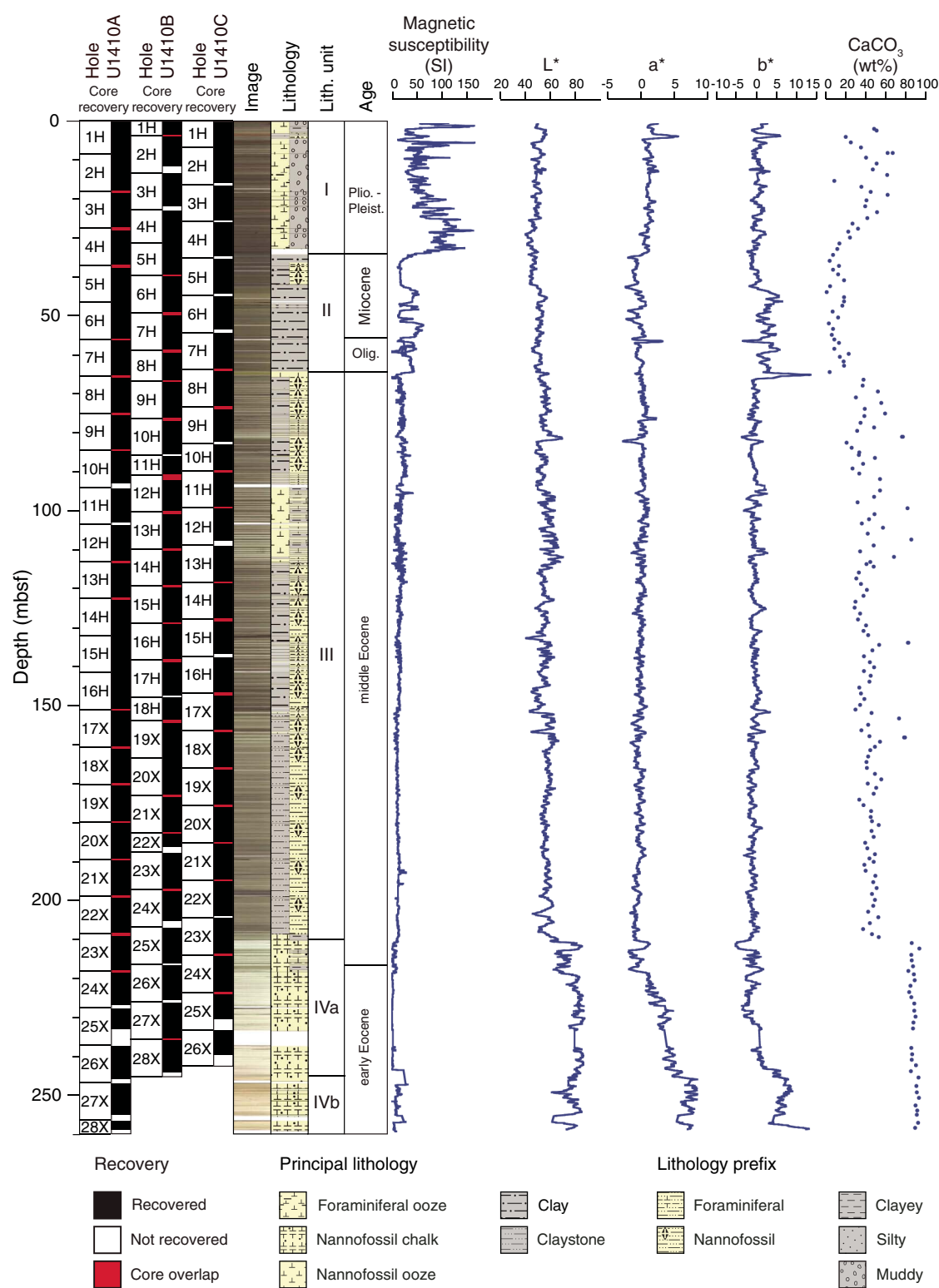


Figure F5. Core images from most common lithologies, Site U1410. A. Pleistocene silty clay, Unit I. B. Pleistocene muddy foraminiferal sand overlying reddish brown clay, Unit I. C. Miocene clay with nannofossils, Unit II. D. Oligocene clay with nannofossils, Unit II. E. Middle Eocene light gray nannofossil ooze (top) alternating with greenish gray nannofossil clay (bottom), Unit III. F. Early Eocene nannofossil chalk, Subunit IVa. G. Early Eocene chert (top) and nannofossil chalk (bottom), Subunit IVb.

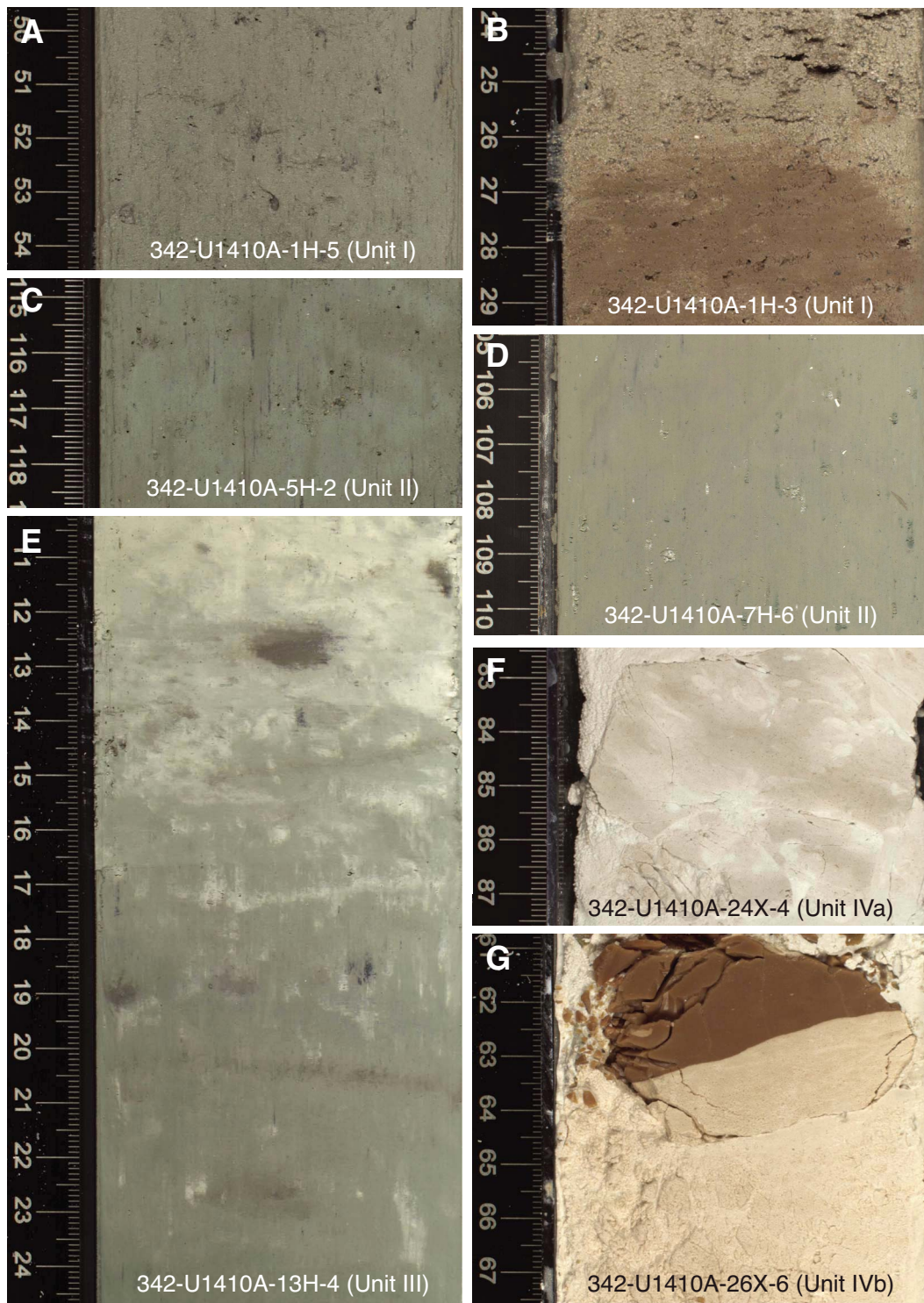


Figure F6. Photomicrographs of smear slides indicating the dominant lithologies of Units I–IV, Site U1410. A. Silty clay with nannofossils, Unit I. B. Clay with nannofossils, Unit II. C. Nannofossil ooze with foraminifers, Unit III. D. Nannofossil chalk with radiolarians, Unit IV.

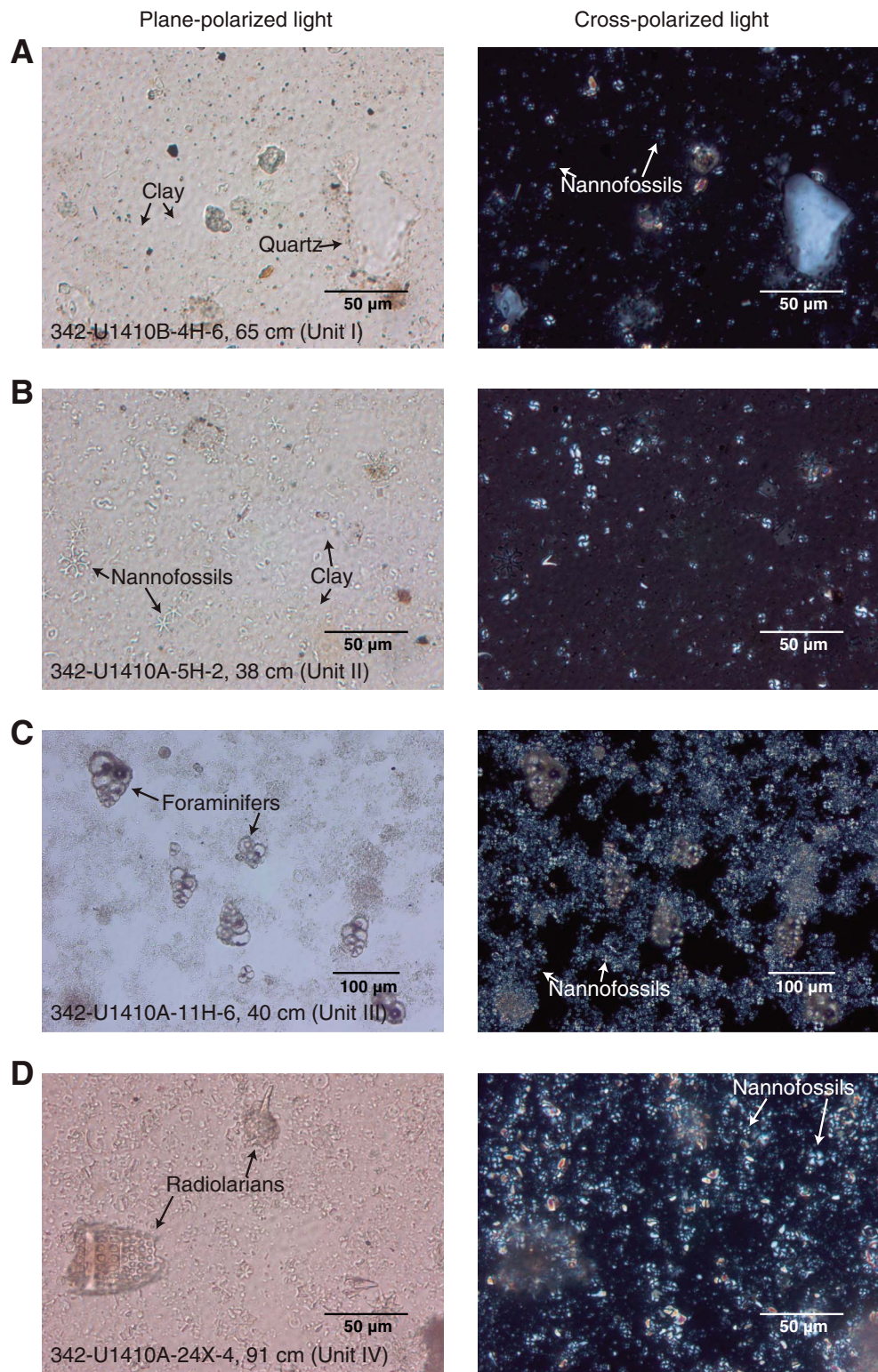


Figure F7. Plots of smear slide results of major biogenic and lithologic components and their relative abundance, Hole U1410A. VA = very abundant, A = abundant, C = common, F = few, P = present.

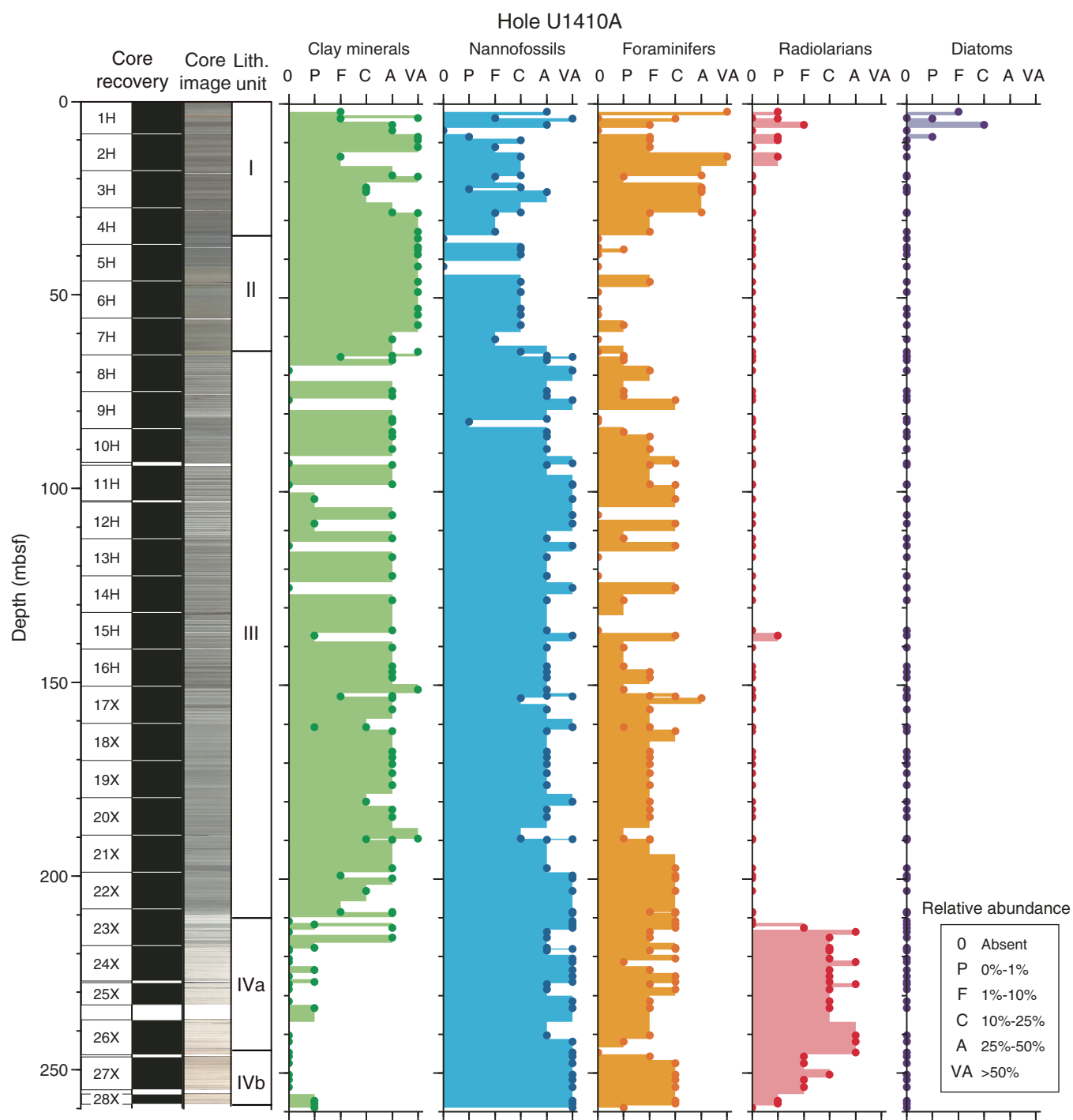


Figure F8. Plots of smear slide results of major biogenic and lithological components and their relative abundance, Hole U1410B. VA = very abundant, A = abundant, C = common, F = few, P = present.

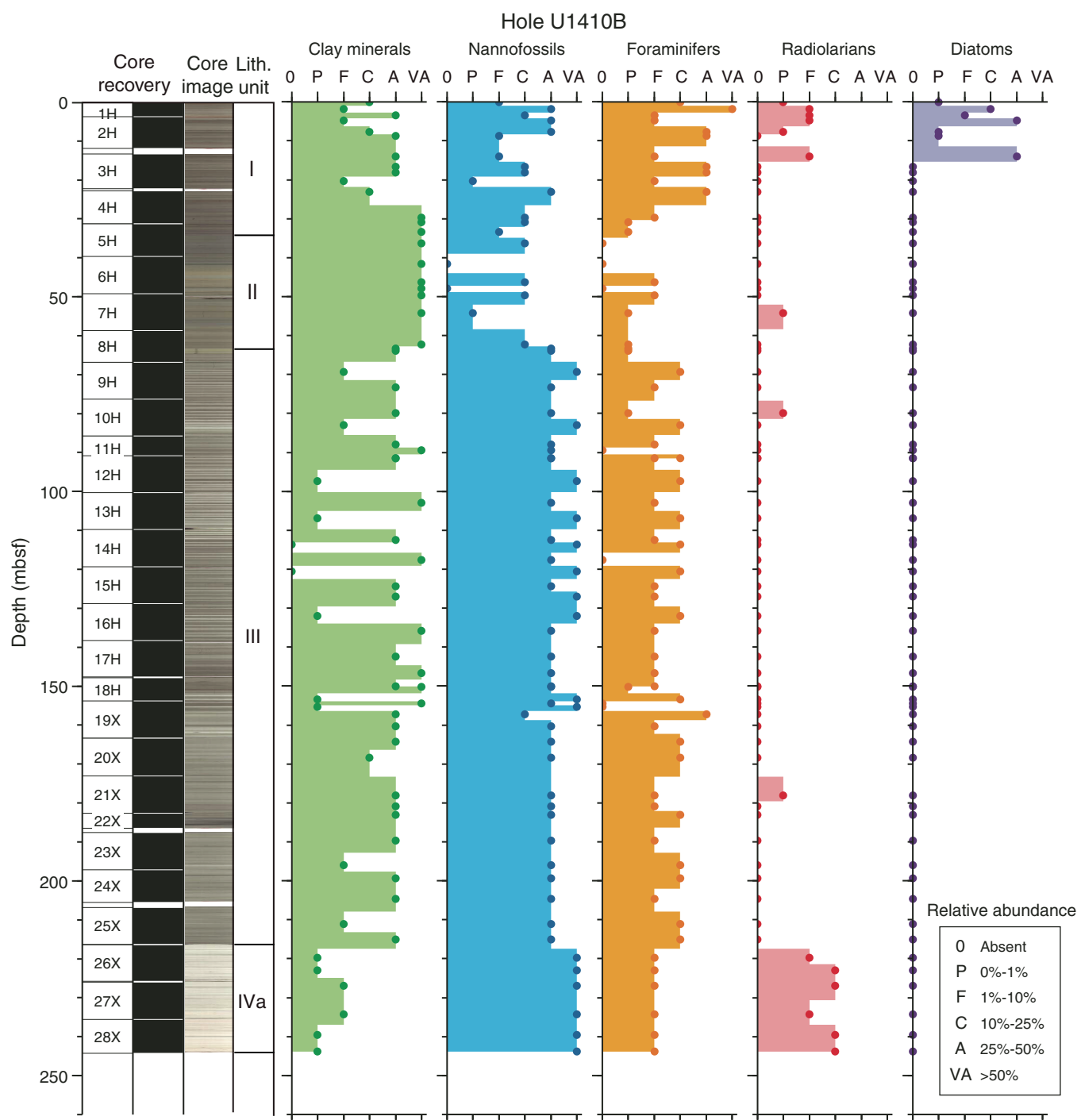


Figure F9. Plots of smear slide results of major biogenic and lithological components and their relative abundance, Hole U1410C. VA = very abundant, A = abundant, C = common, F = few, P = present.

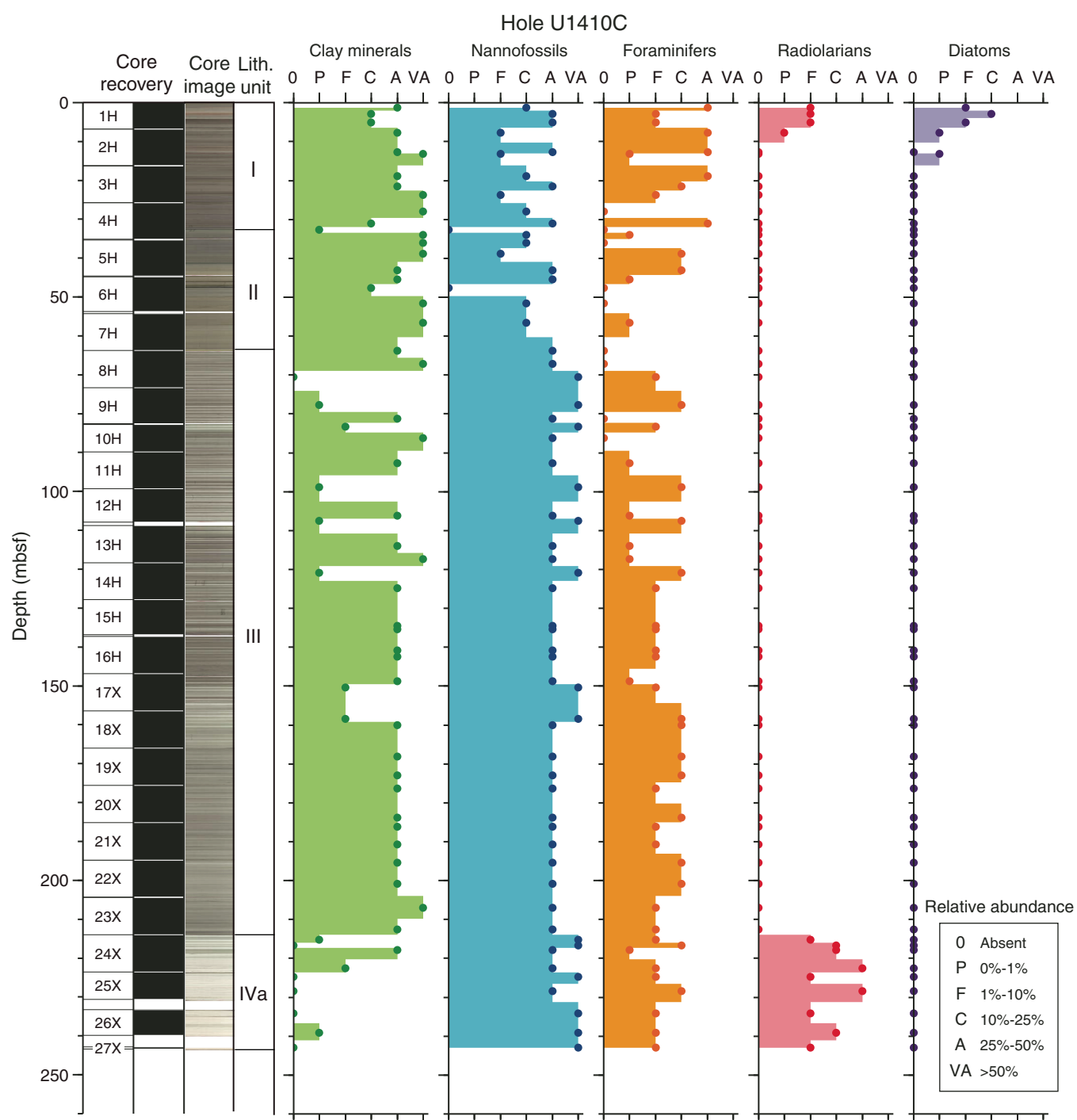


Figure F10. Core images of Miocene–Oligocene greenish gray nannofossil clay of Unit II showing dispersed quartz in (A) millimeter-scale patches/blebs and, more rarely, (B) a discontinuous lens, Site U1410. C. Mineralogy based on X-ray diffractometry of a sample of silt- to fine sand-sized white material. The clay and calcite peaks are from the background lithology within which the quartz occurs. D. Photomicrograph of smear slide showing angular quartz in coarse silt to very fine sand size range.

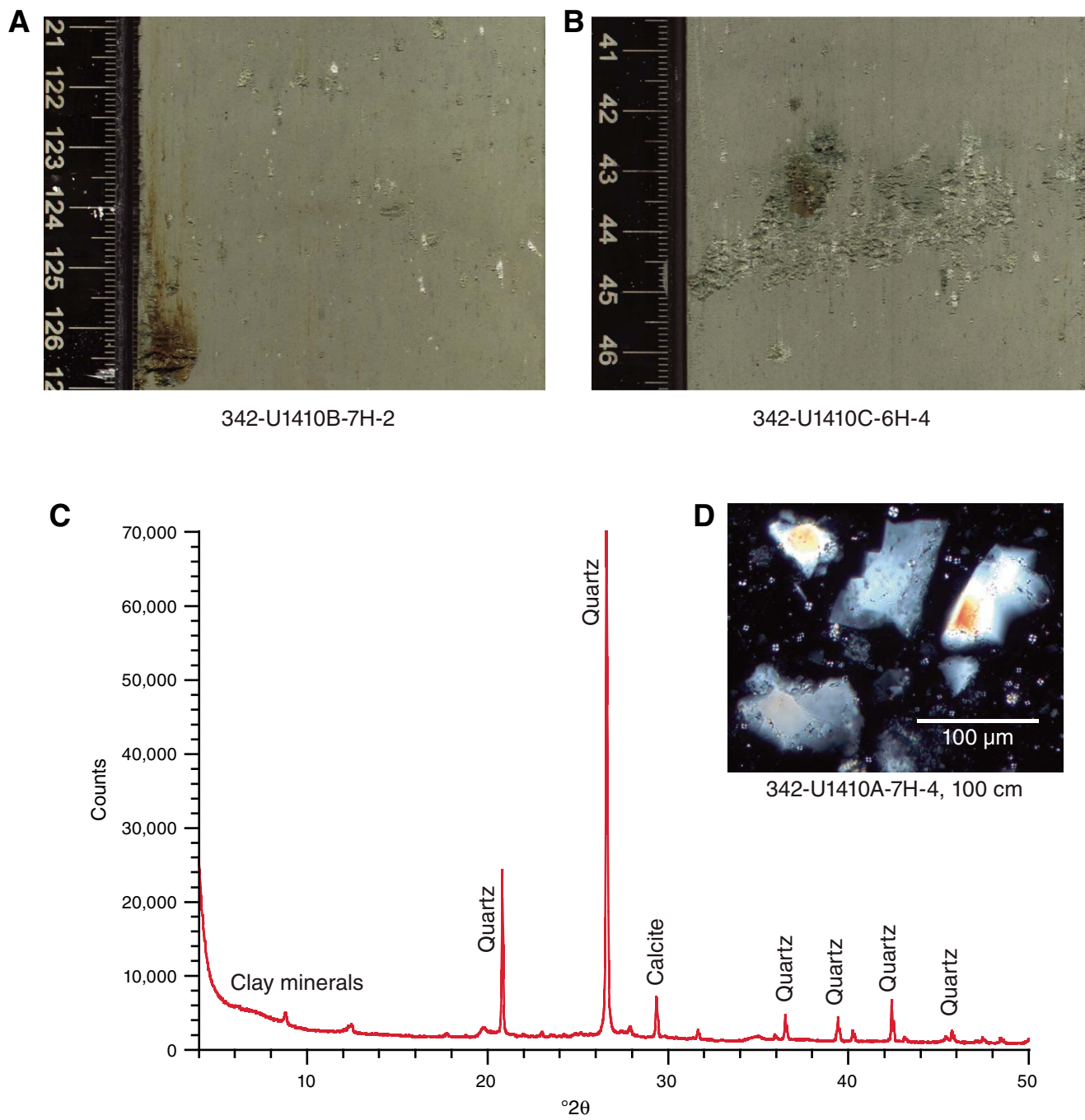


Figure F11. Core image and physical property data showing middle Eocene cyclicity in lithology, magnetic susceptibility, color reflectance (L^*) and natural gamma radiation (NGR), Core 342-U1410A-12H. All show well-expressed cyclicity over this interval (nannofossil Subzone NP16).

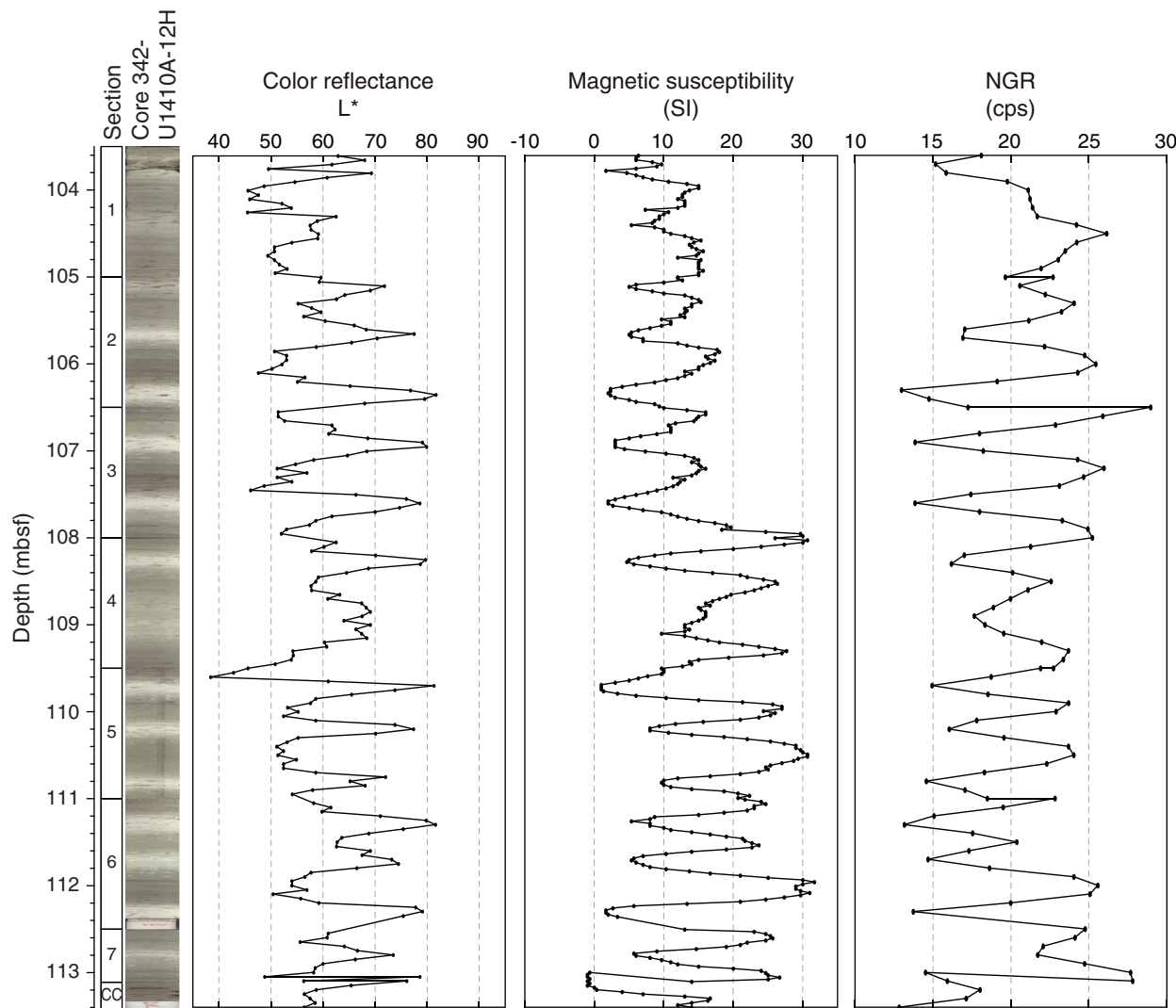


Figure F12. Core images of conglomerate with foraminiferal sand matrix bed in middle Eocene Unit III, Hole U1410A. Clasts are composed of nannofossil clay and clayey nannofossil ooze typical of Unit III. Calcareous nannofossil ages of a clast and the foraminiferal sand matrix are both Subzone NP15b.

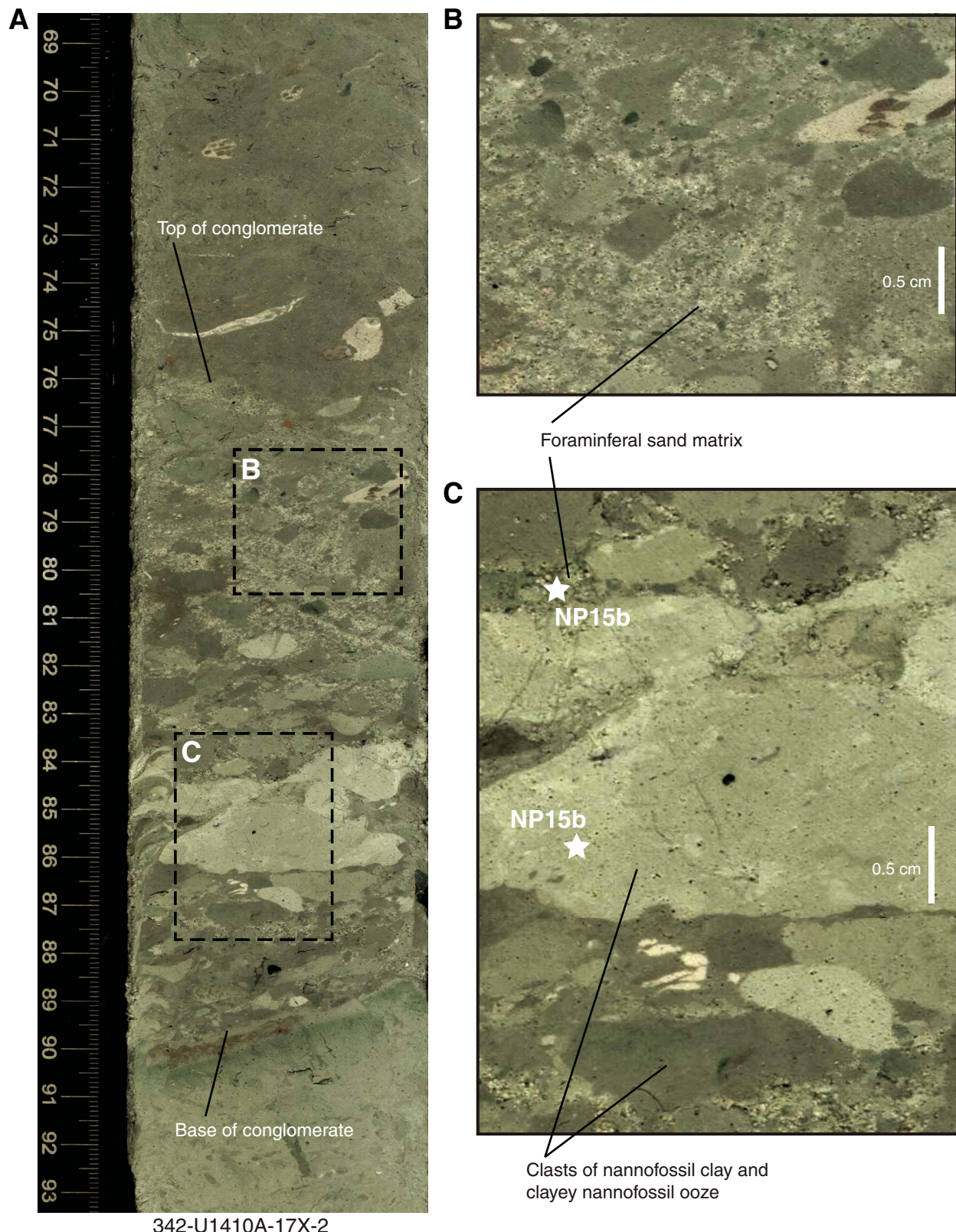


Figure F13. Integrated calcareous and siliceous microfossil biozonation, Site U1410.

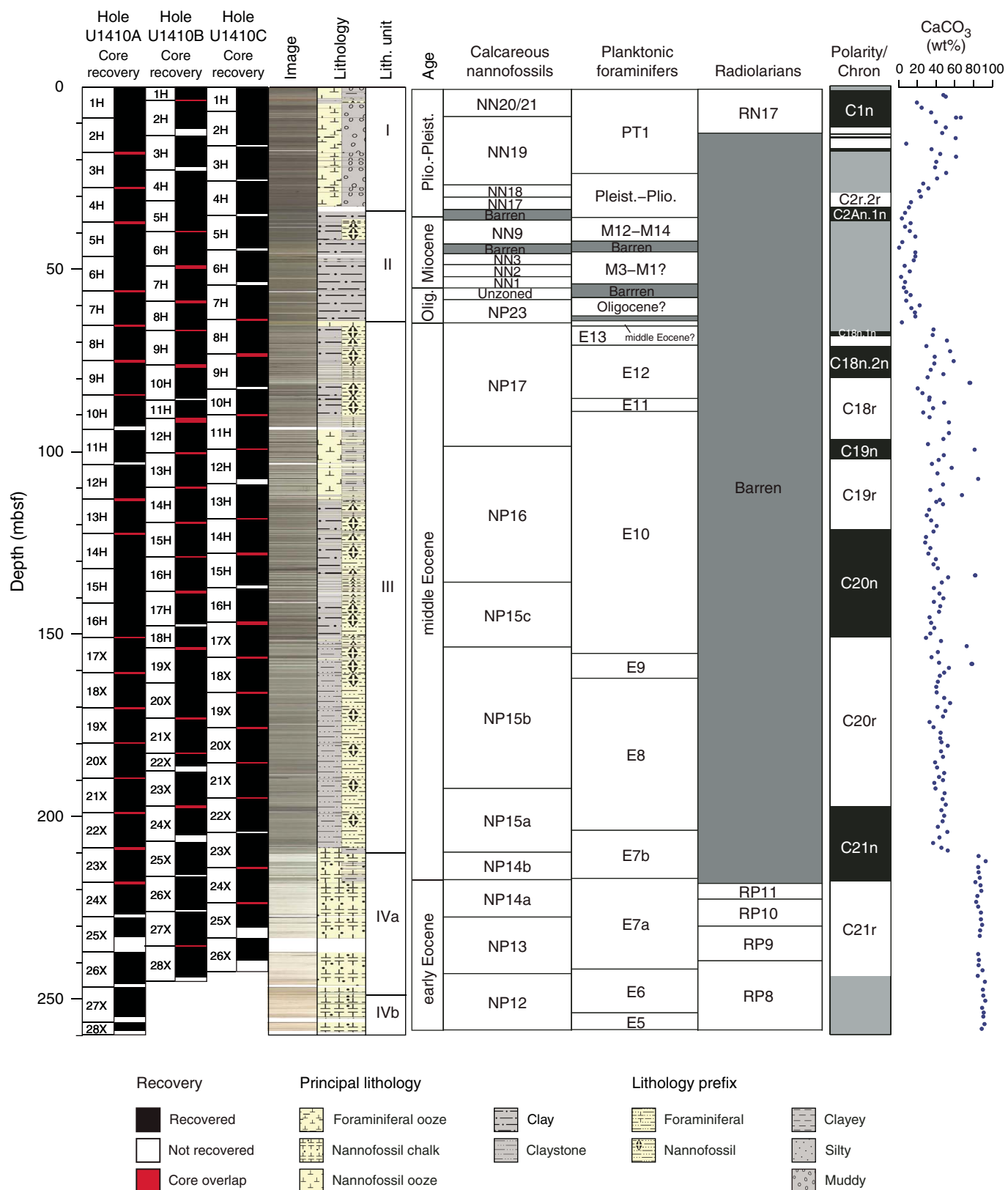


Figure F14. Group abundance and preservation of calcareous and siliceous microfossils, Site U1410. Abundance: B = barren, P = present, R = rare, F = few, C = common, A = abundant, D = dominant. Preservation: P = poor, M = moderate, G = good, VG = very good.

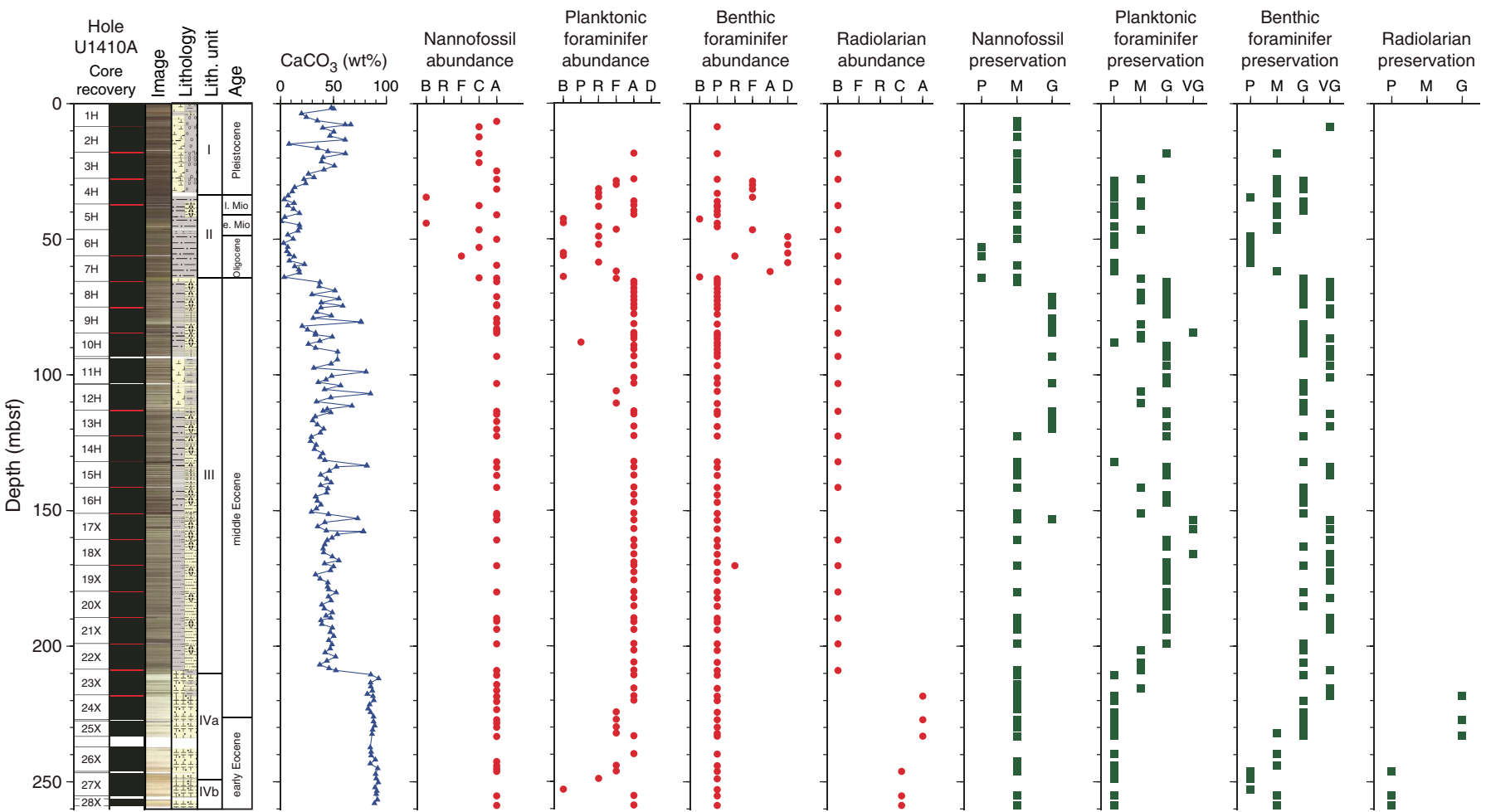


Figure F15. Plots of downhole variation of magnetic susceptibility and paleomagnetism data, Hole U1410A. Magnetization intensity, inclination, and declination are after 20 mT demagnetization. Only oriented advanced piston corer (APC) intervals show directions in geographic coordinates. Directions from extended core barrel (XCB) intervals are shown in sample coordinates. For discrete sample data, if the samples were analyzed by principal component analysis (PCA; Kirschvink, 1980), then directions are shown according to PCA declination and inclination. Otherwise, directions following 20 mT demagnetization are shown. Polarity: black = normal chron, white = reversed chron, gray = unidentified interval.

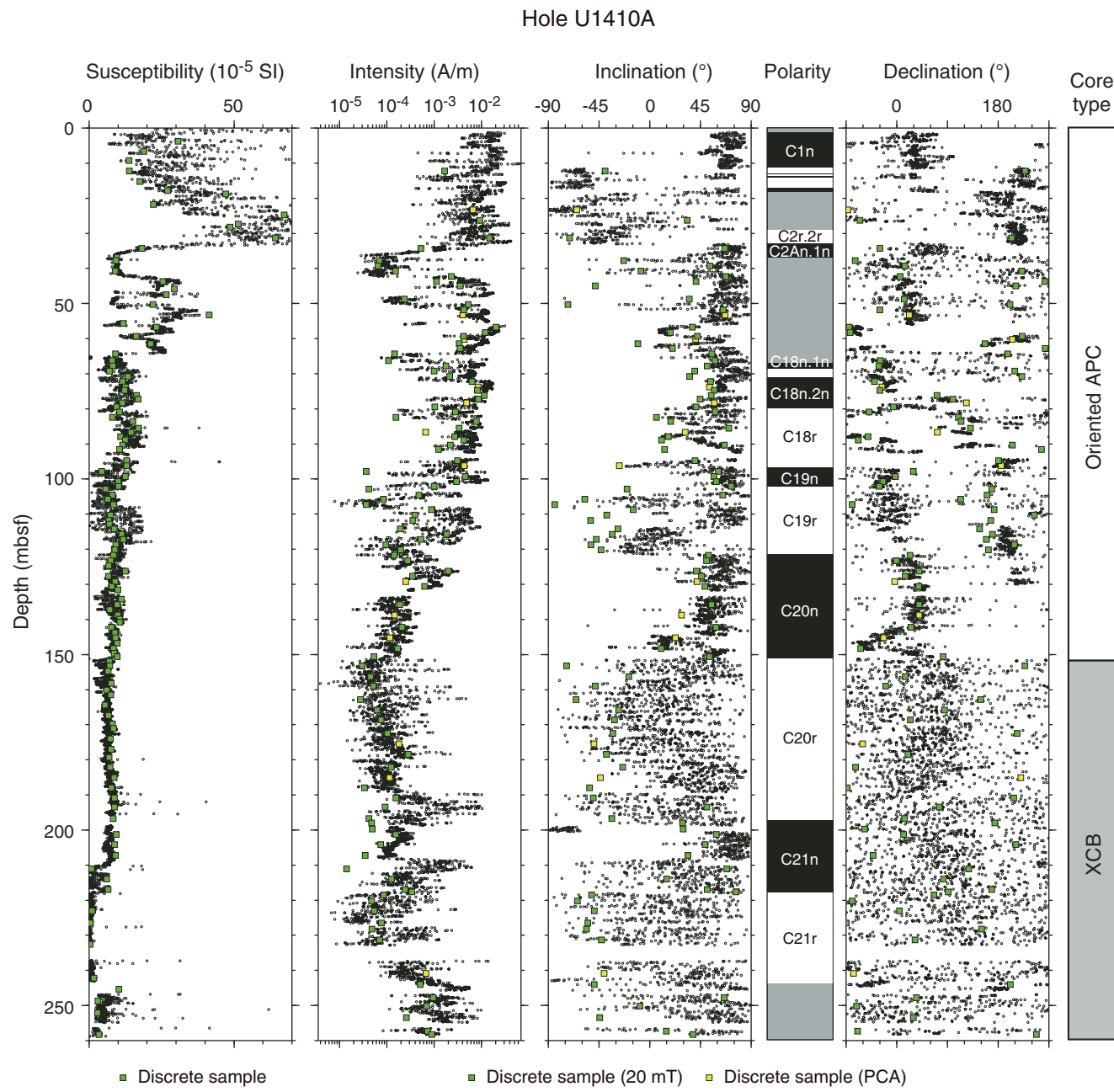


Figure F16. Plots of downhole variation of magnetic susceptibility and paleomagnetism data, Hole U1410B. Magnetization intensity, inclination, and declination are after 20 mT demagnetization. Directions are shown in geographic coordinates for the oriented advanced piston corer (APC) intervals. XCB = extended core barrel. Polarity: black = normal chron, white = reversed chron, gray = unidentified interval.

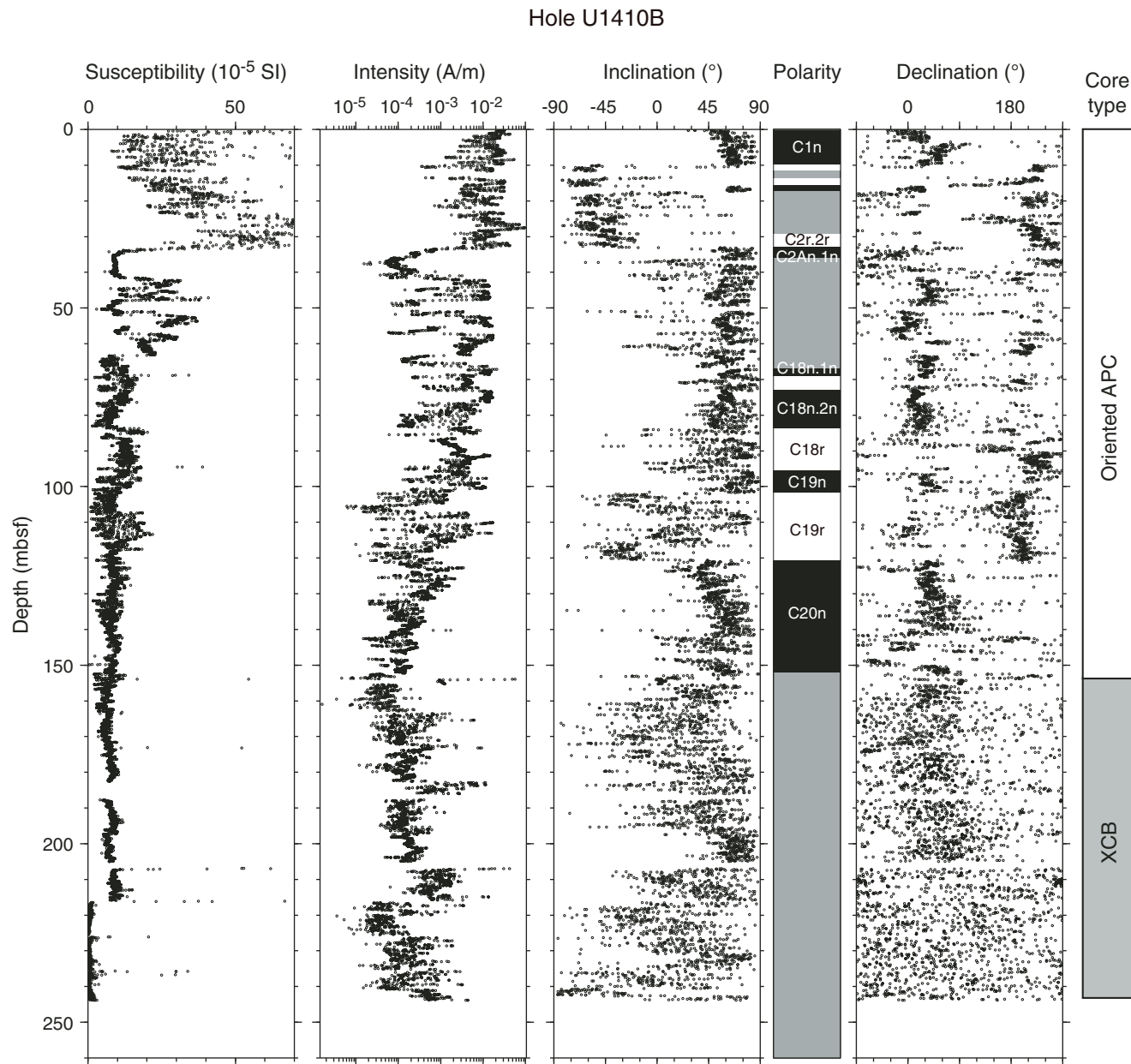


Figure F17. Plots of downhole variation of magnetic susceptibility and paleomagnetism data, Hole U1410C. Magnetization intensity, inclination, and declination are after 20 mT demagnetization. Directions are shown in sample coordinates. APC = advanced piston corer, XCB = extended core barrel. Polarity: black = normal chron, white = reversed chron, gray = unidentified interval.

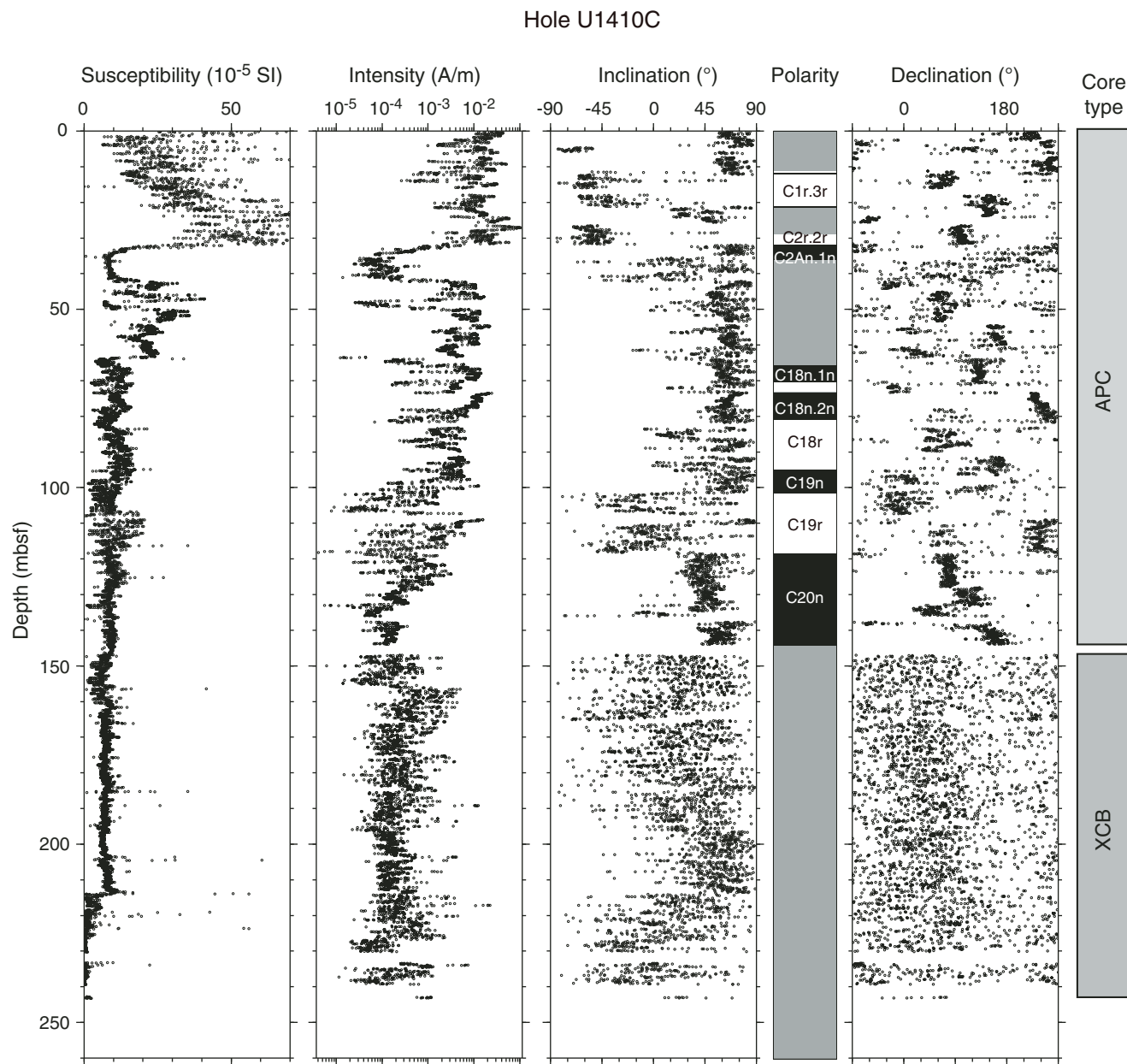


Figure F18. Plots of representative alternating field (AF) demagnetization results for discrete paleomagnetism samples, Site U1410. Upper plots show intensity variation with progressive demagnetization, and lower plots show vector endpoints of paleomagnetism directions on orthogonal vector diagrams (i.e., Zijderveld plots). Vector diagrams indicate reasonably resolved characteristic remanent magnetization (ChRM) directions for the (A) normal and (B) reversed chronos from the advanced piston corer intervals, whereas (C) some samples do not show stable component. Solid circles = horizontal projections, open circles = vertical projections, gray circles = data not used to calculate ChRM direction, black dashed line = ChRM direction. Inc = inclination, Dec = declination, MAD = maximum angle of deviation.

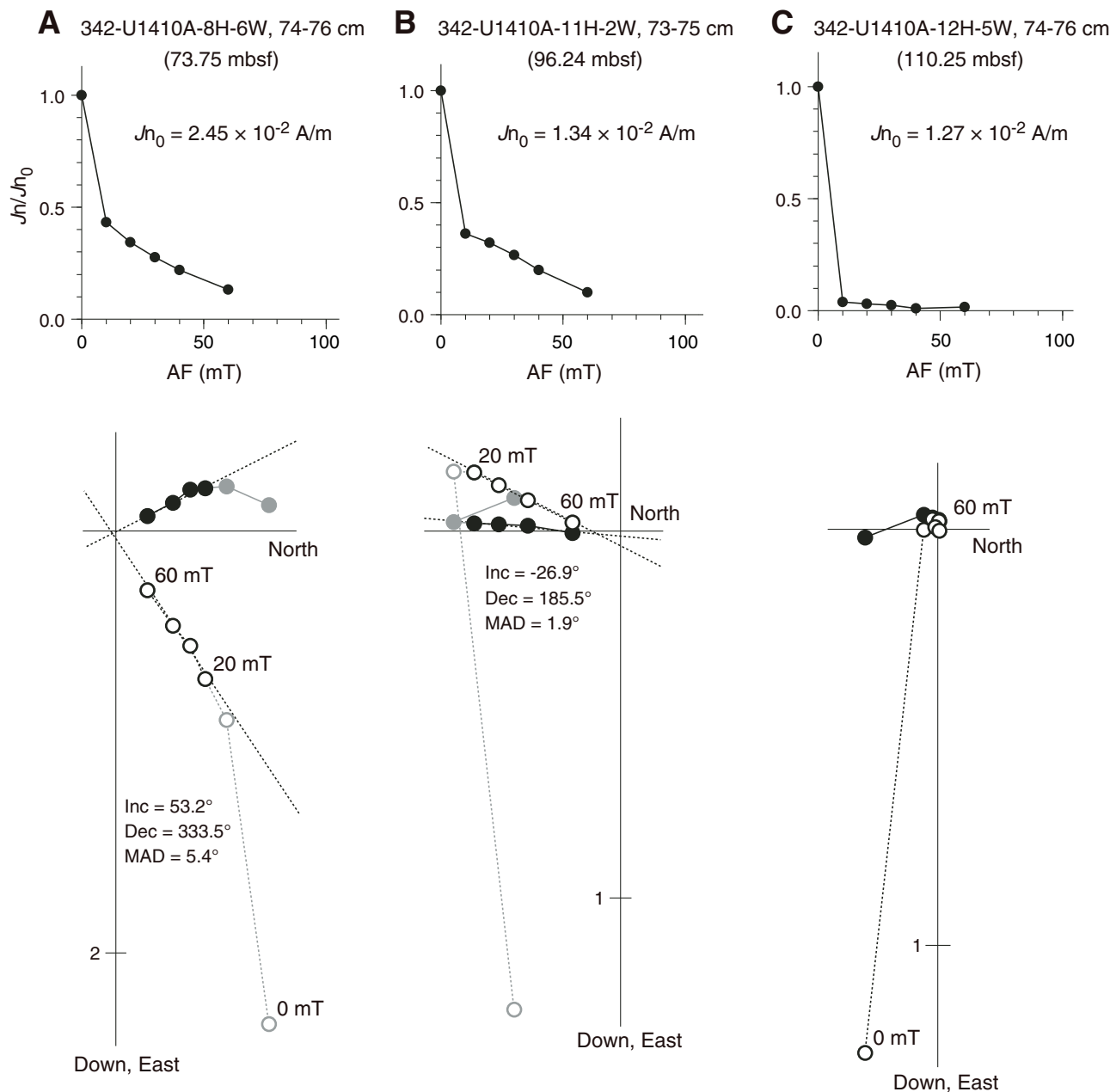


Figure F19. Illustration of magnetostratigraphy, Site U1410. Core recovery: black = recovered, white = not recovered, red = core overlap.

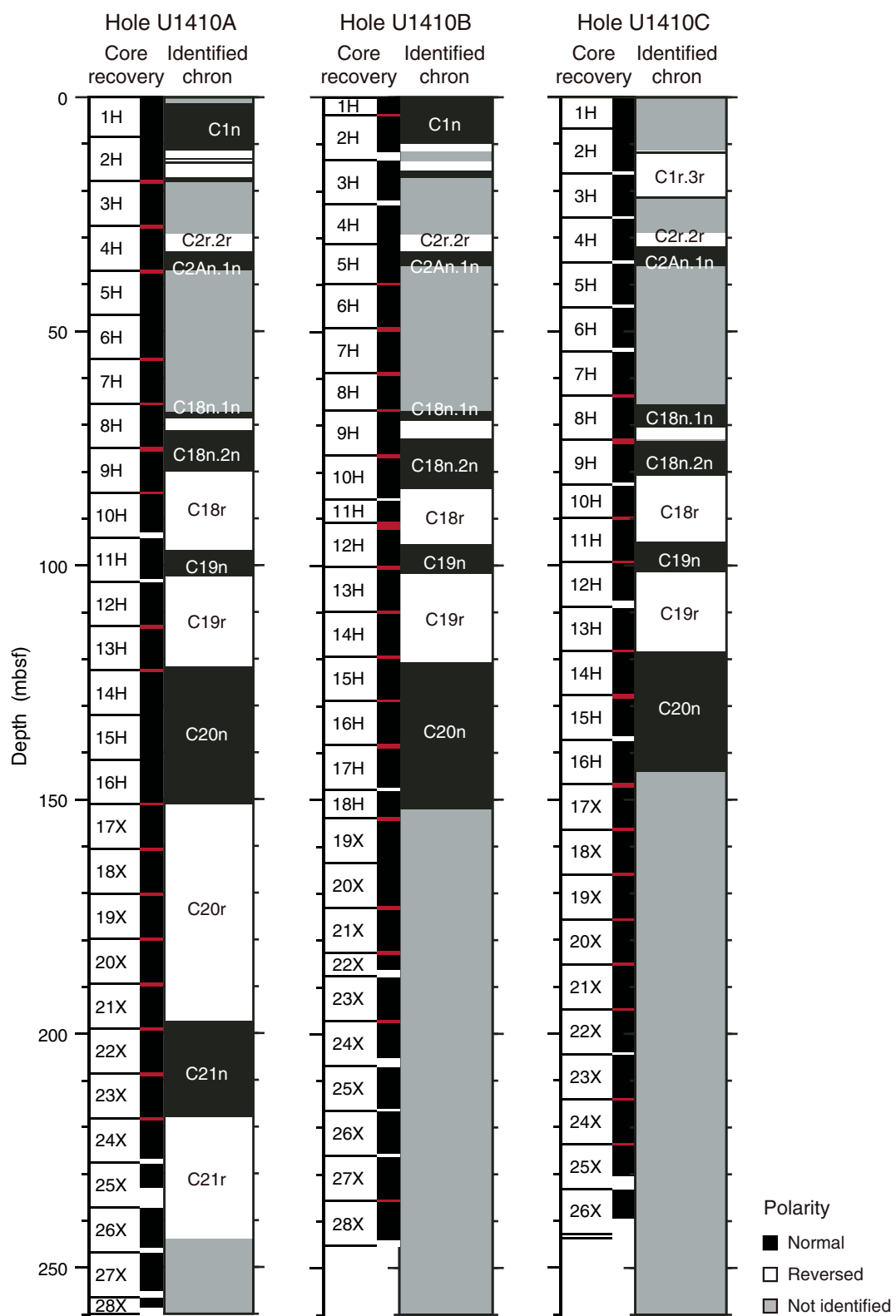


Figure F20. Plots of downhole variation of declination, inclination, and magnetization intensity after 20 mT demagnetization during the Chron C18n.1n–C18n.1r–C18n.2n geomagnetic field transitions in Hole U1410B and at Site U1408. Polarity: black = normal chron, white = reversed chron, gray = transitional period.

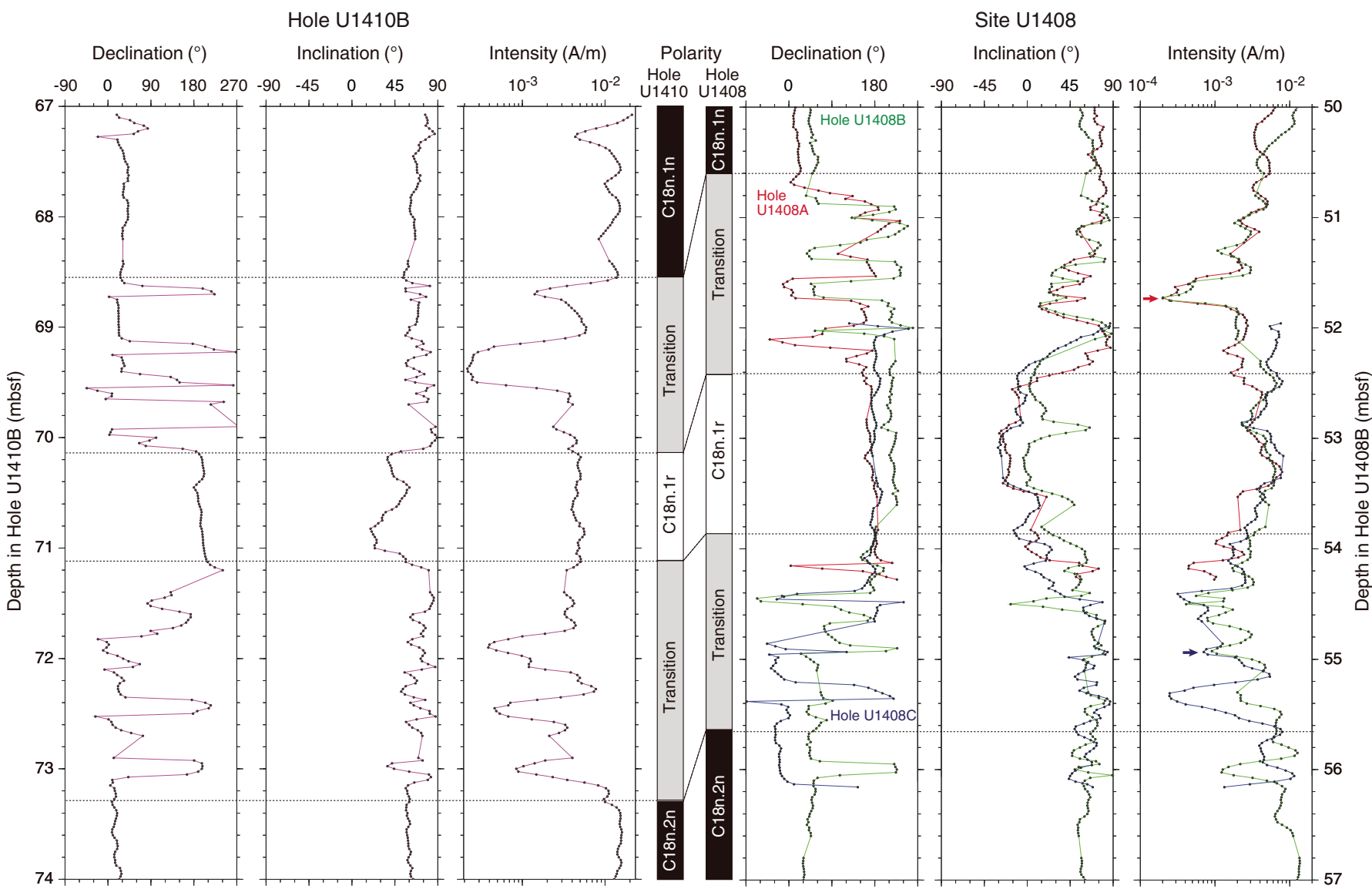


Figure F21. Plots of anisotropy of magnetic susceptibility vs. depth, Hole U1410A. Separation of eigenvalues is related to the shape and degree of the magnetic fabric (see “**Paleomagnetism**” in the “Methods” chapter [Norris et al., 2014a]). For example, if τ_1 and τ_2 are close or indistinguishable but distinct from τ_3 , then the bulk fabric is oblate. Lithostratigraphic units are described in “**Lithostratigraphy**.” Eigenvalues: τ_1 = maximum, τ_2 = intermediate, τ_3 = minimum. V_3 = minimum eigenvector, P = degree of anisotropy (τ_1/τ_3). APC = advanced piston corer, XCB = extended core barrel.

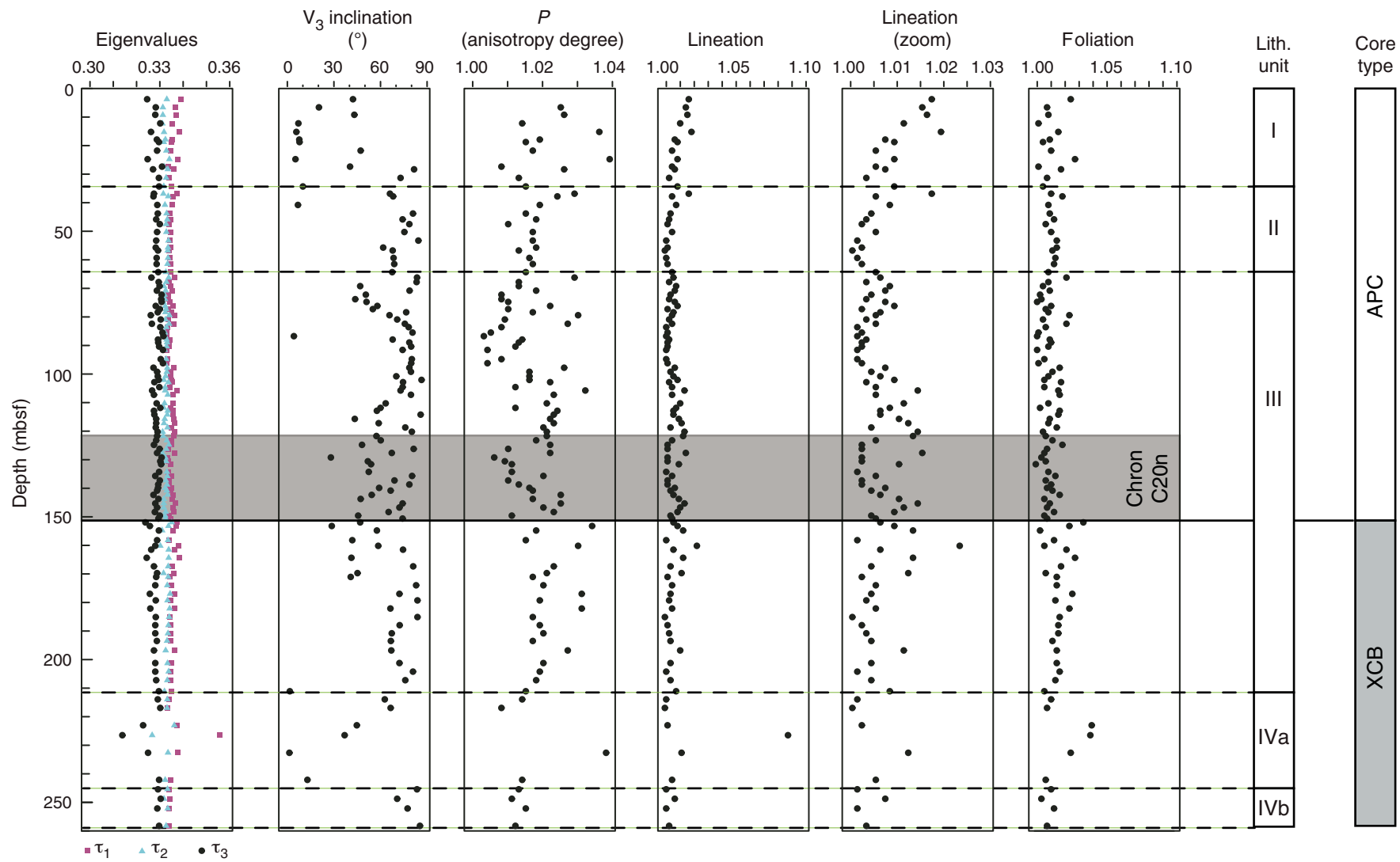


Figure F22. Age-depth model for Hole U1410A showing biostratigraphic and magnetostratigraphic datums. Also shown are estimated linear sedimentation rates for line segments based on the datums listed in Table T16.

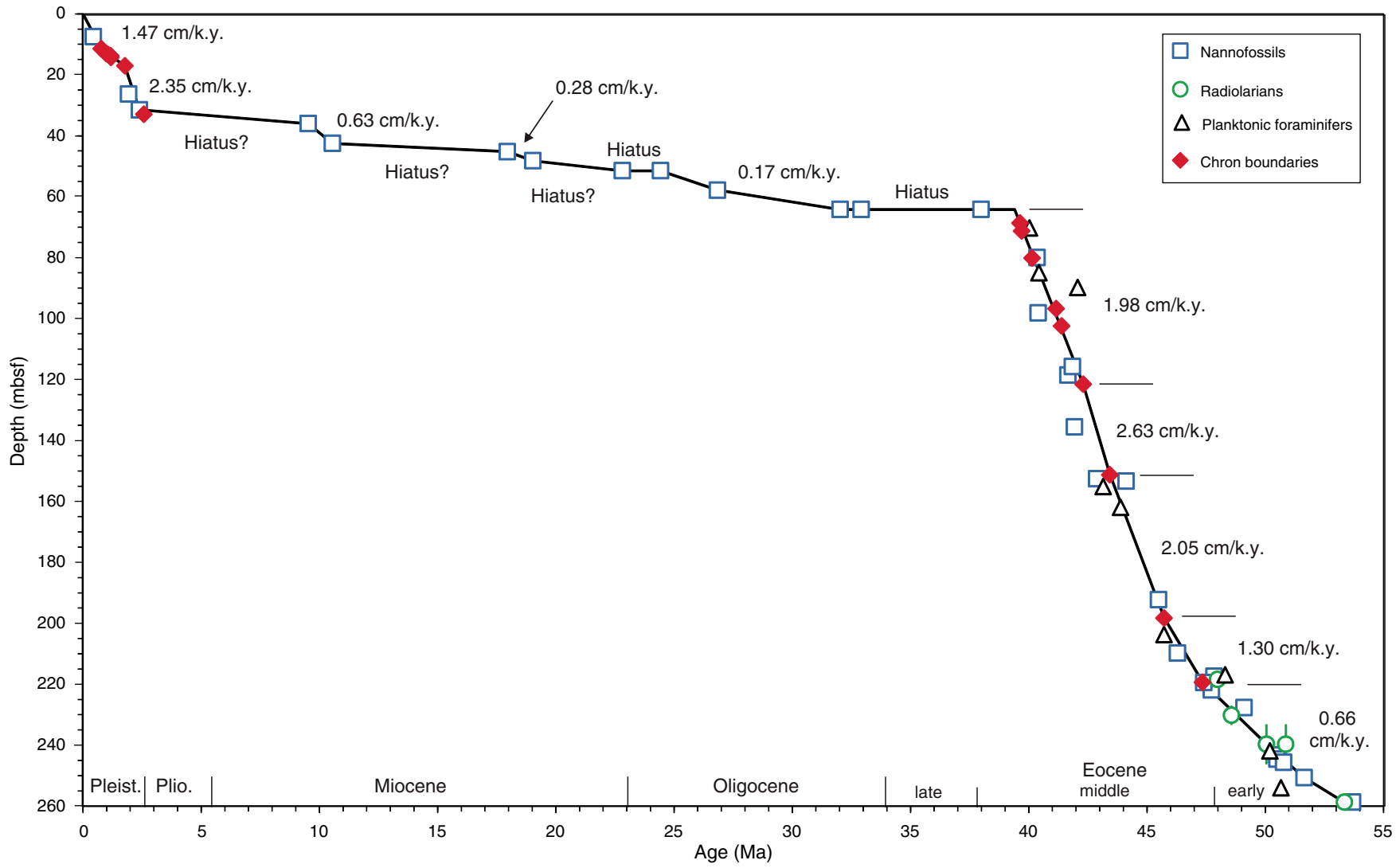


Figure F23. Linear sedimentation rate (LSR), dry bulk density (DBD), carbonate content, and mass accumulation rate (MAR) for carbonate and noncarbonate components at a time step of 200 k.y., Hole U1410A. Solid black diamonds show the inflection points in estimated LSR, DBD, and carbonate content. Geologic ages are on the GTS2012 timescale (Gradstein et al., 2012). CAR = carbonate mass accumulation rate, nCAR = noncarbonate mass accumulation rate.

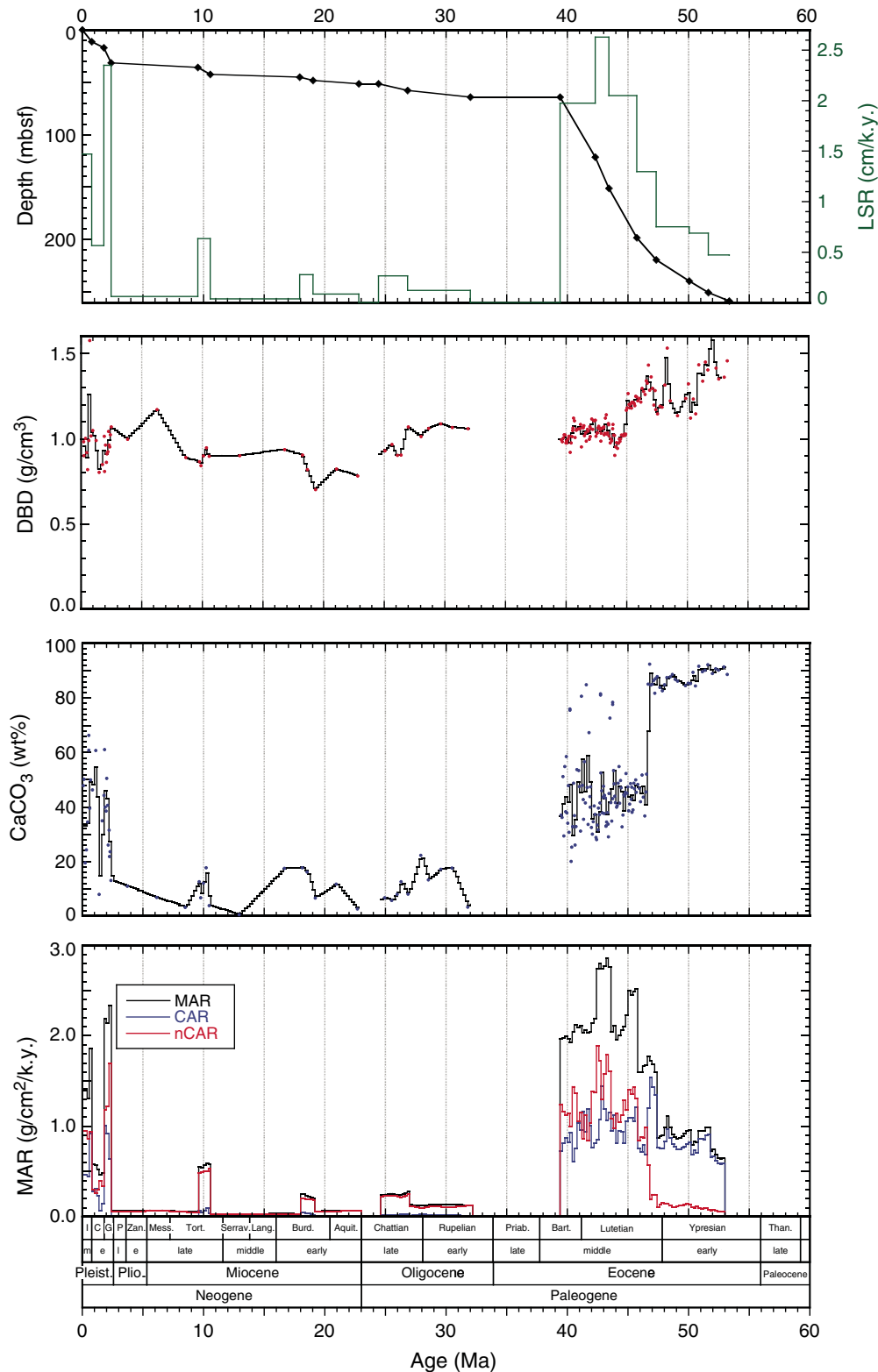


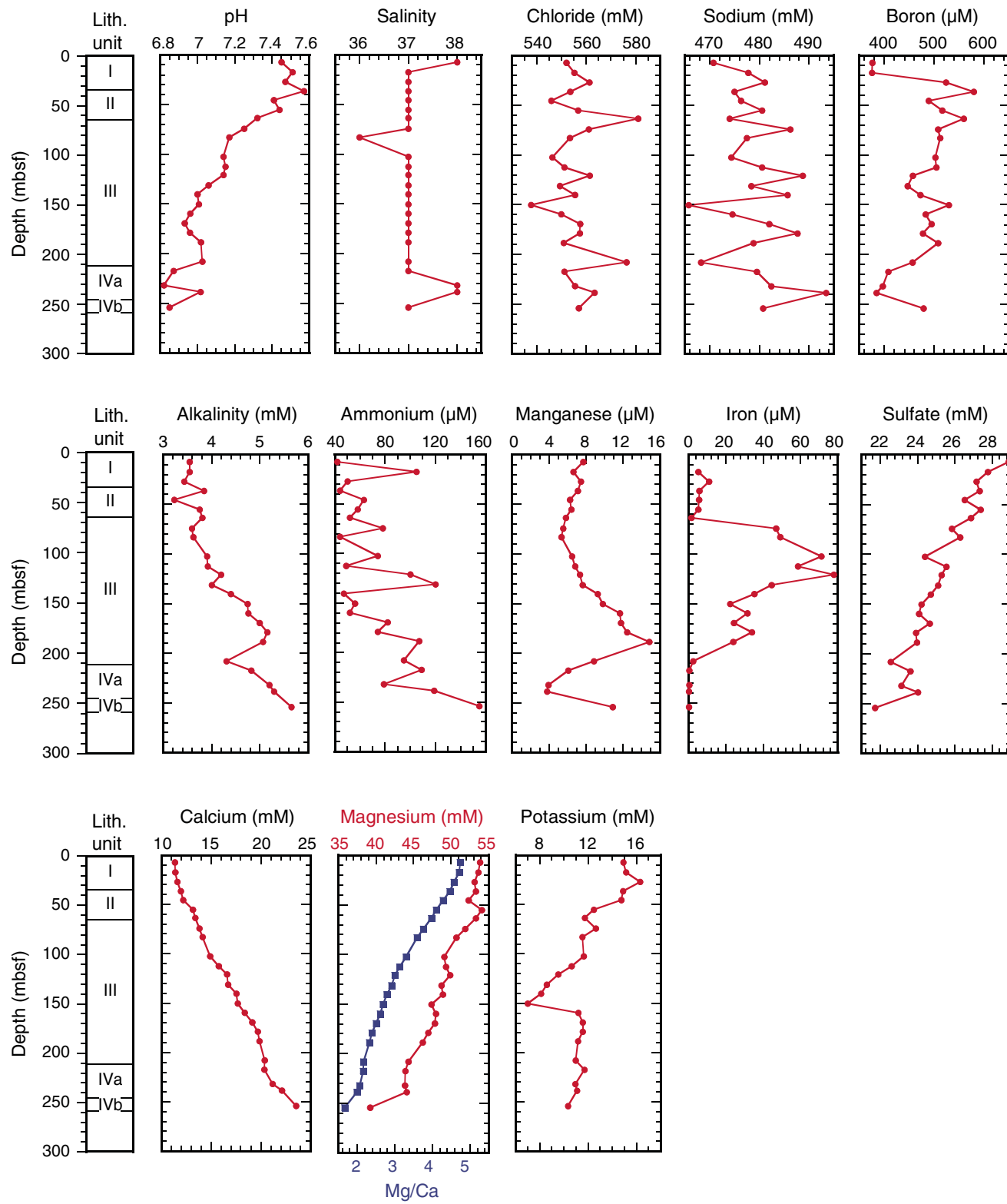
Figure F24. Plots of interstitial water constituent concentrations, Hole U1410A.

Figure F25. Plots of sedimentary carbonate, total organic carbon (TOC), and total nitrogen contents, Hole U1410A. Core recovery: black = recovered, white = not recovered, red = core overlap.

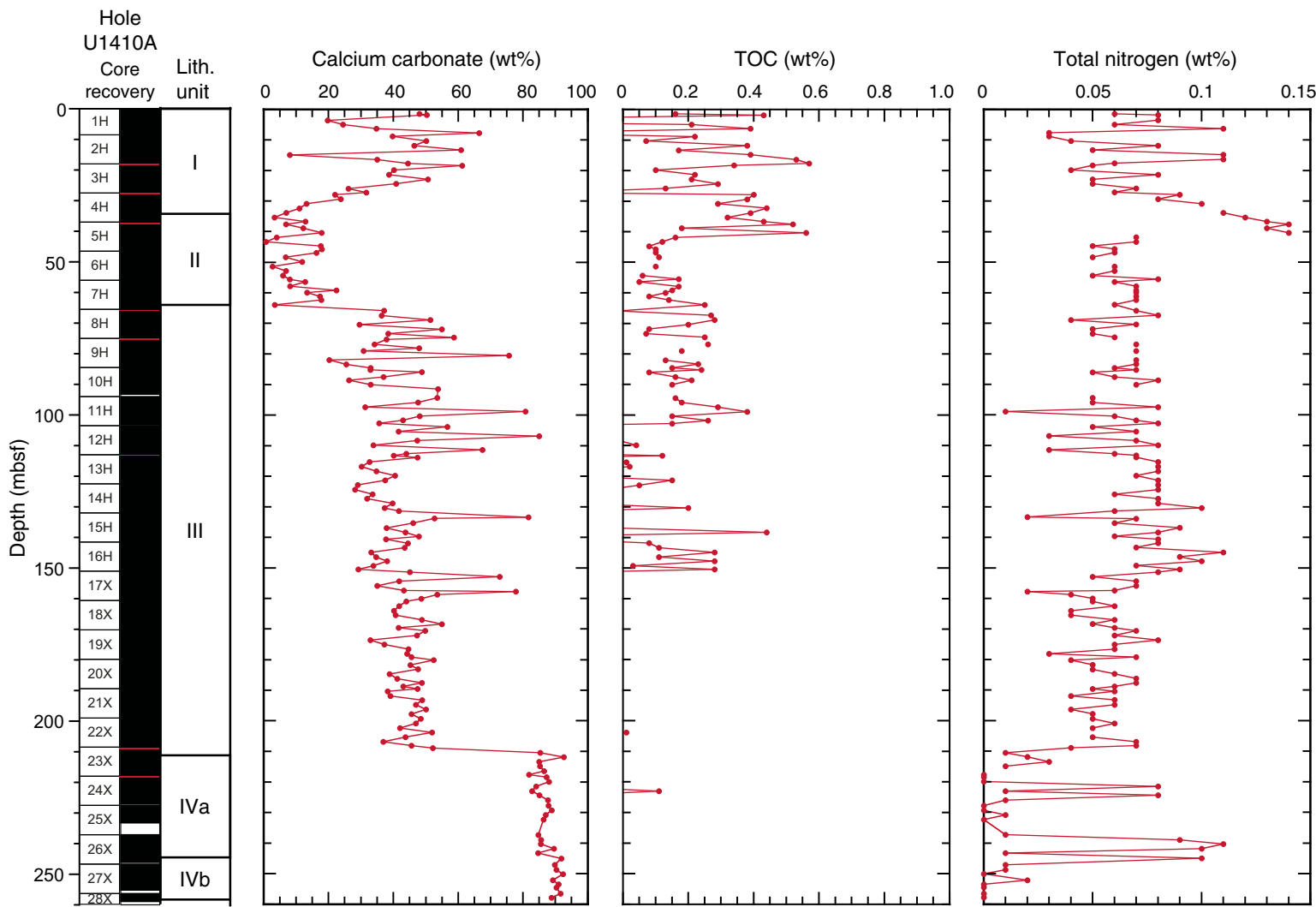


Figure F26. Plots of magnetic susceptibility (MS; truncated at 160 IU), bulk density, porosity, water content, and grain density, Site U1410. Core recovery: black = recovered, white = not recovered, red = core overlap. Bulk density: gray line = gamma ray attenuation bulk density from Whole-Round Multisensor Logger, black circles = moisture and density bulk density from discrete samples. Horizontal gray lines indicate lithostratigraphic unit boundaries (see “[Lithostratigraphy](#)”). APC = advanced piston corer, XCB = extended core barrel.

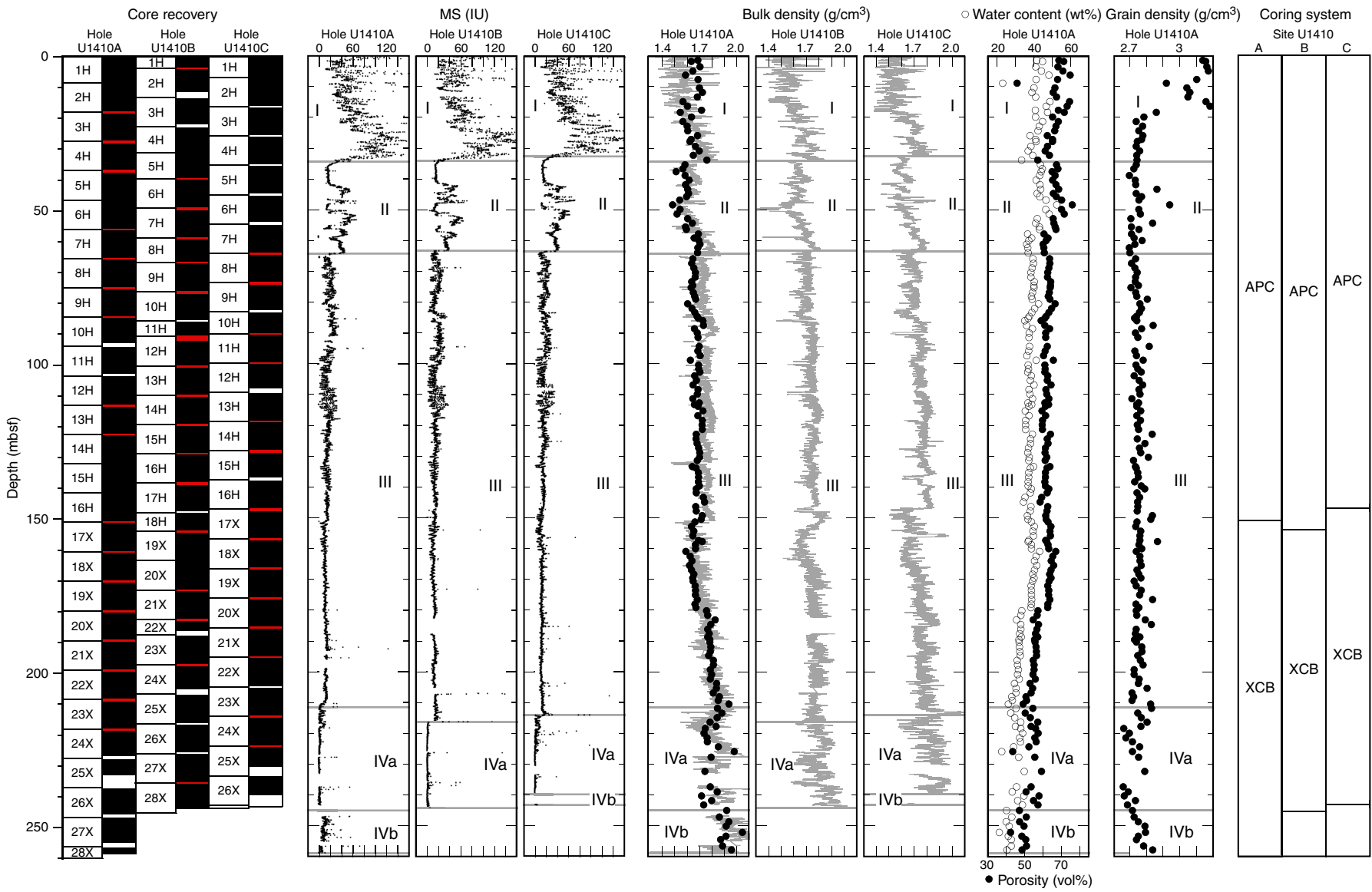


Figure F27. Plots of magnetic susceptibility (MS), *P*-wave velocity (gray line = *P*-wave logger data from whole-round sections, black circles = *P*-wave caliper data from section halves), and natural gamma radiation (NGR), Site U1410. Core recovery: black = recovered, white = not recovered, red = core overlap. Horizontal gray lines indicate lithostratigraphic unit boundaries (see “[Lithostratigraphy](#)”). APC = advanced piston corer, XCB = extended core barrel.

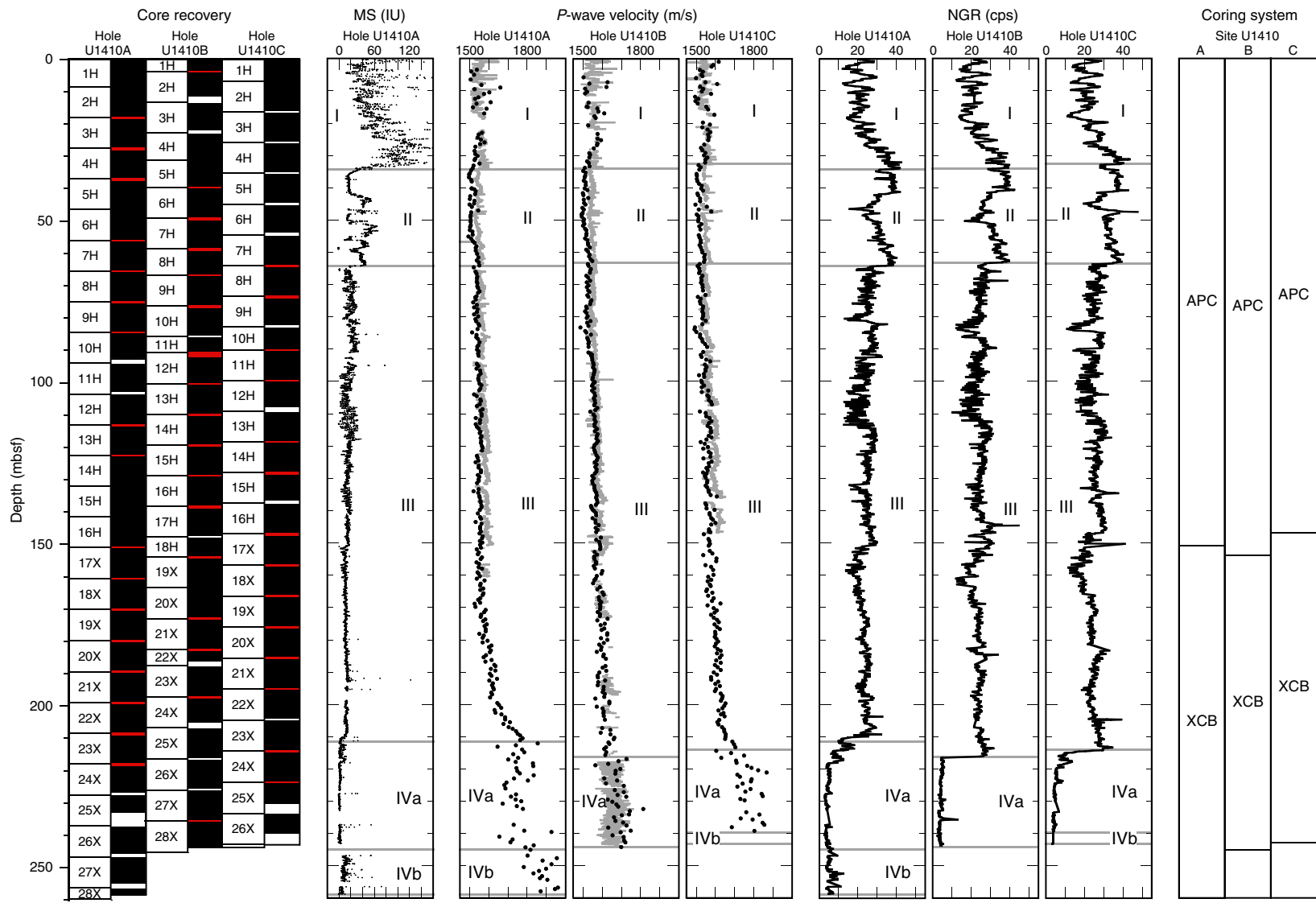


Figure F28. Plots of magnetic susceptibility (MS) and color reflectance (a^* , b^* , and L^*), Site U1410. Core recovery: black = recovered, white = not recovered, red = core overlap. Horizontal gray lines indicate lithostratigraphic unit boundaries (see “[Lithostratigraphy](#)”). APC = advanced piston corer, XCB = extended core barrel.

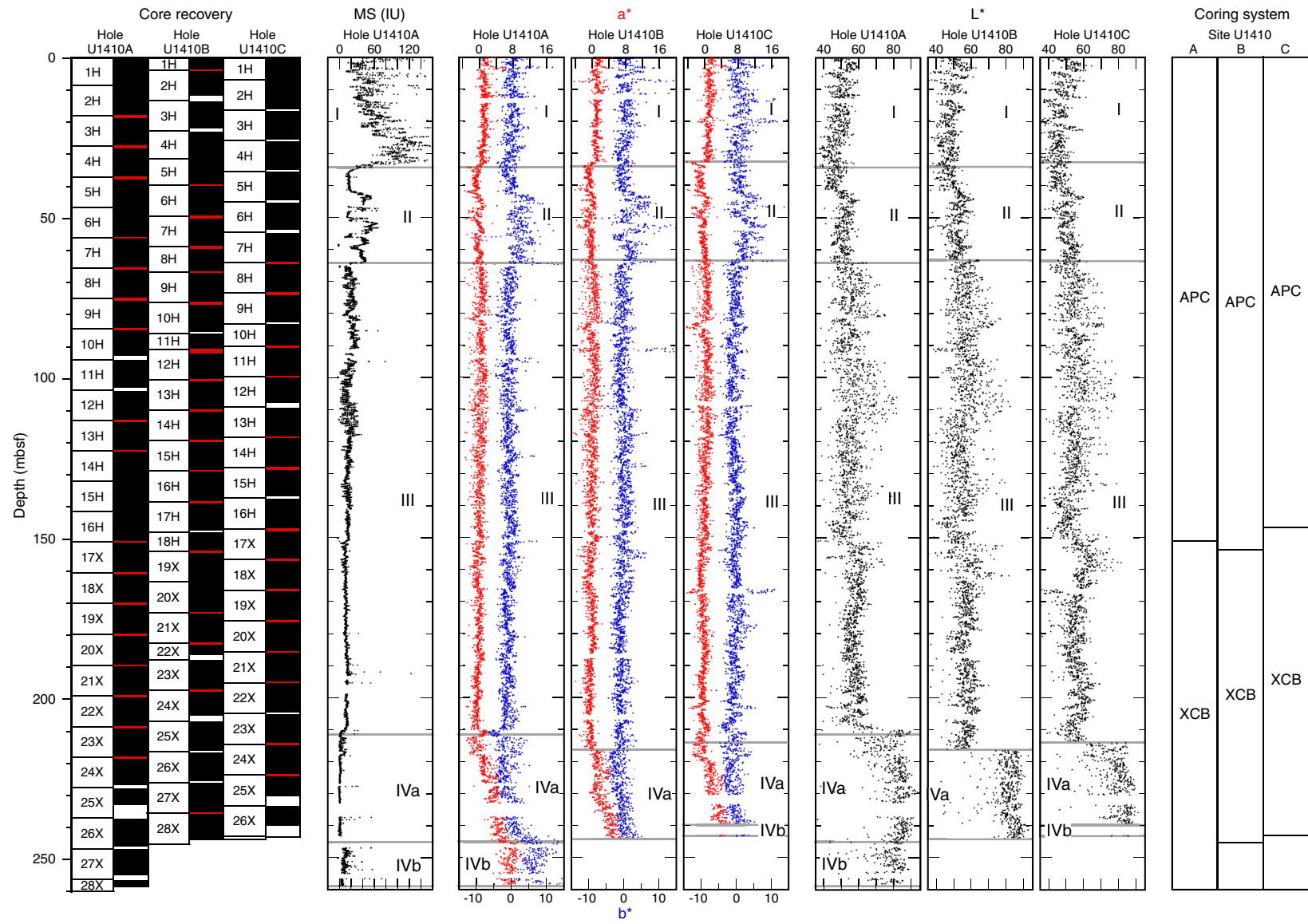


Figure F29. Plot of thermal conductivity measurements, Hole U1410A. Core recovery: black = recovered, white = not recovered, red = core overlap. Blue line is the smooth-curve fit for the data set. Horizontal gray lines indicate lithostratigraphic unit boundaries (see “[Lithostratigraphy](#)”).

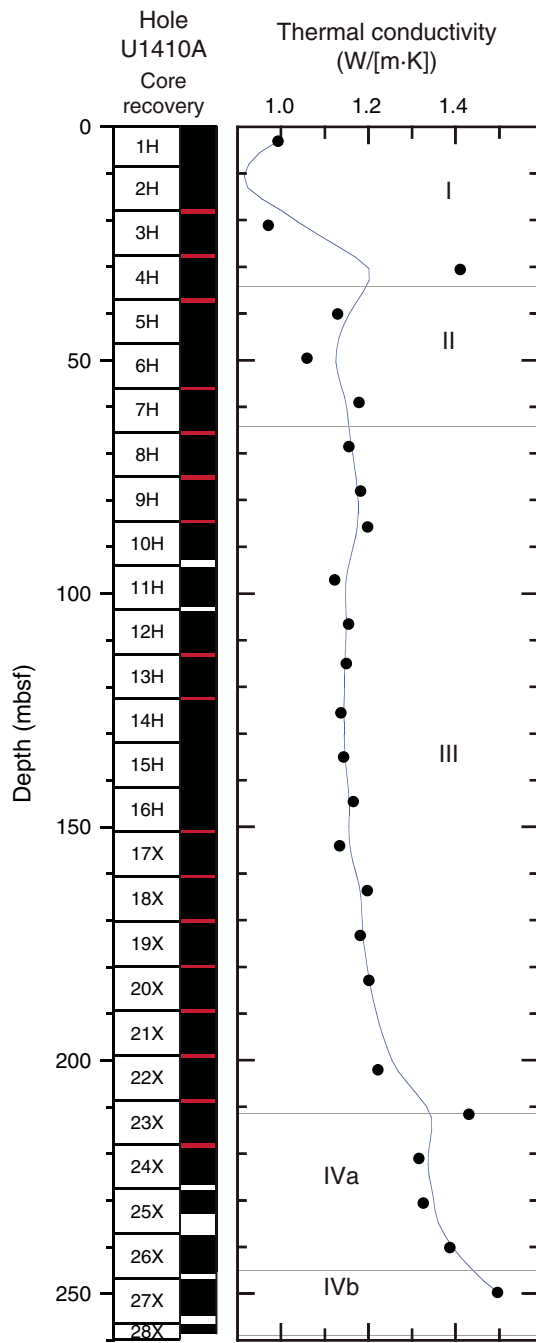


Figure F30. Plot of thermal conductivity vs. gamma ray attenuation (GRA) bulk density, Hole U1410A. Black line is the linear-curve fit for this data set, and R^2 is the correlation coefficient.

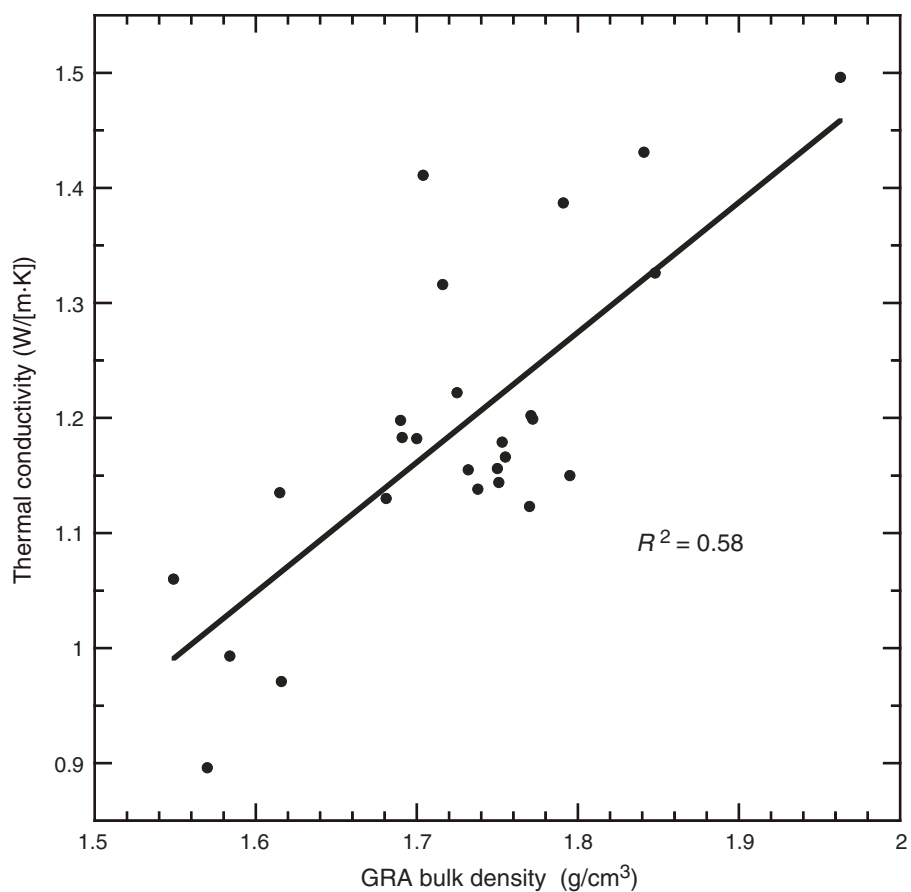


Figure F31. Plots of natural gamma radiation (NGR) data, Site U1410. Top panels show the spliced section for each interval of the splice. Bottom panels show all complete NGR records. Data from Holes U1410B and U1410C are offset by 25 and 50 cps, respectively, to aid visualization. Open circles indicate core tops, excluding culled data from disturbed intervals. A. 0–50 m CCSF. (Continued on next five pages.)

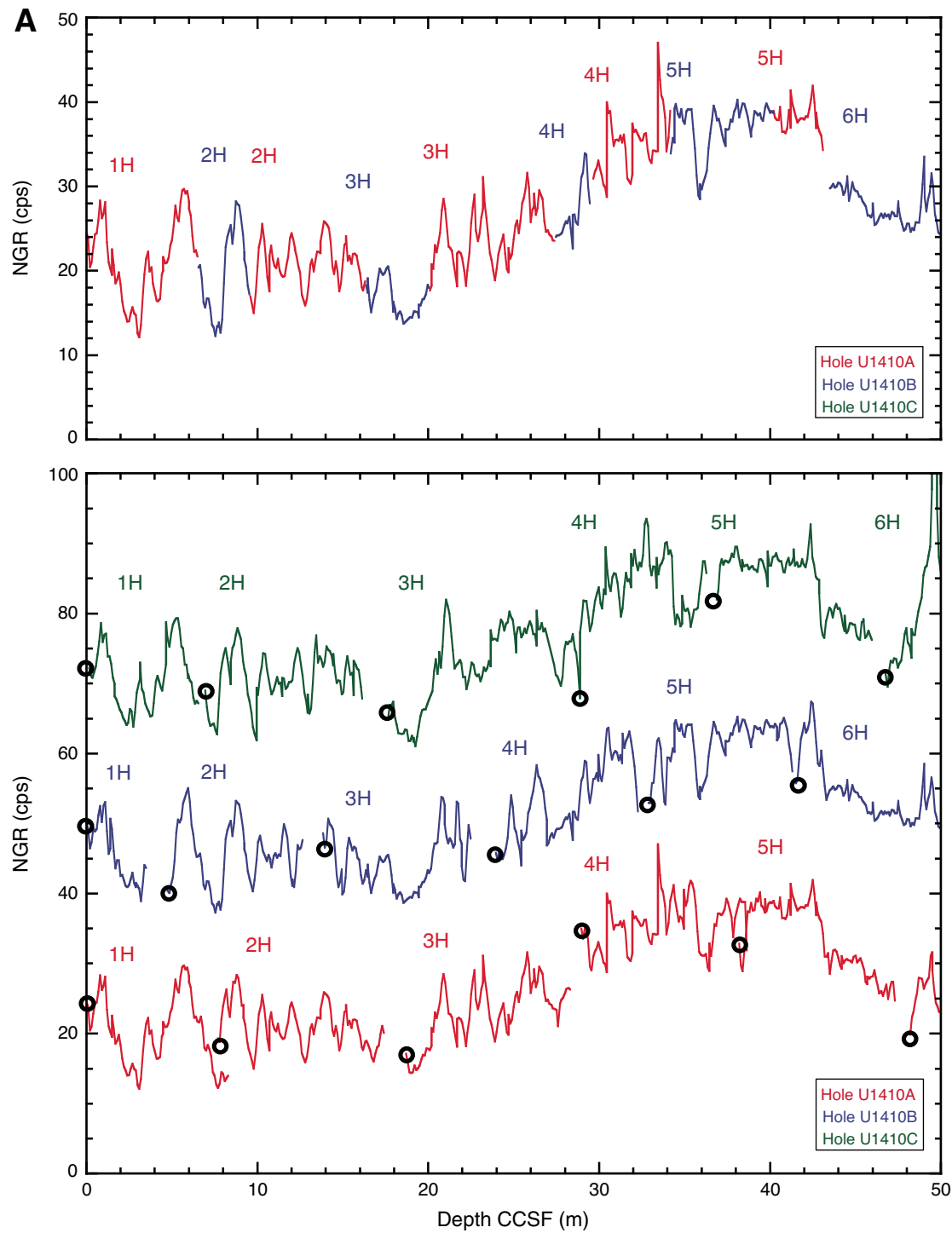


Figure F31 (continued). B. 50–100 m CCSF. (Continued on next page.)

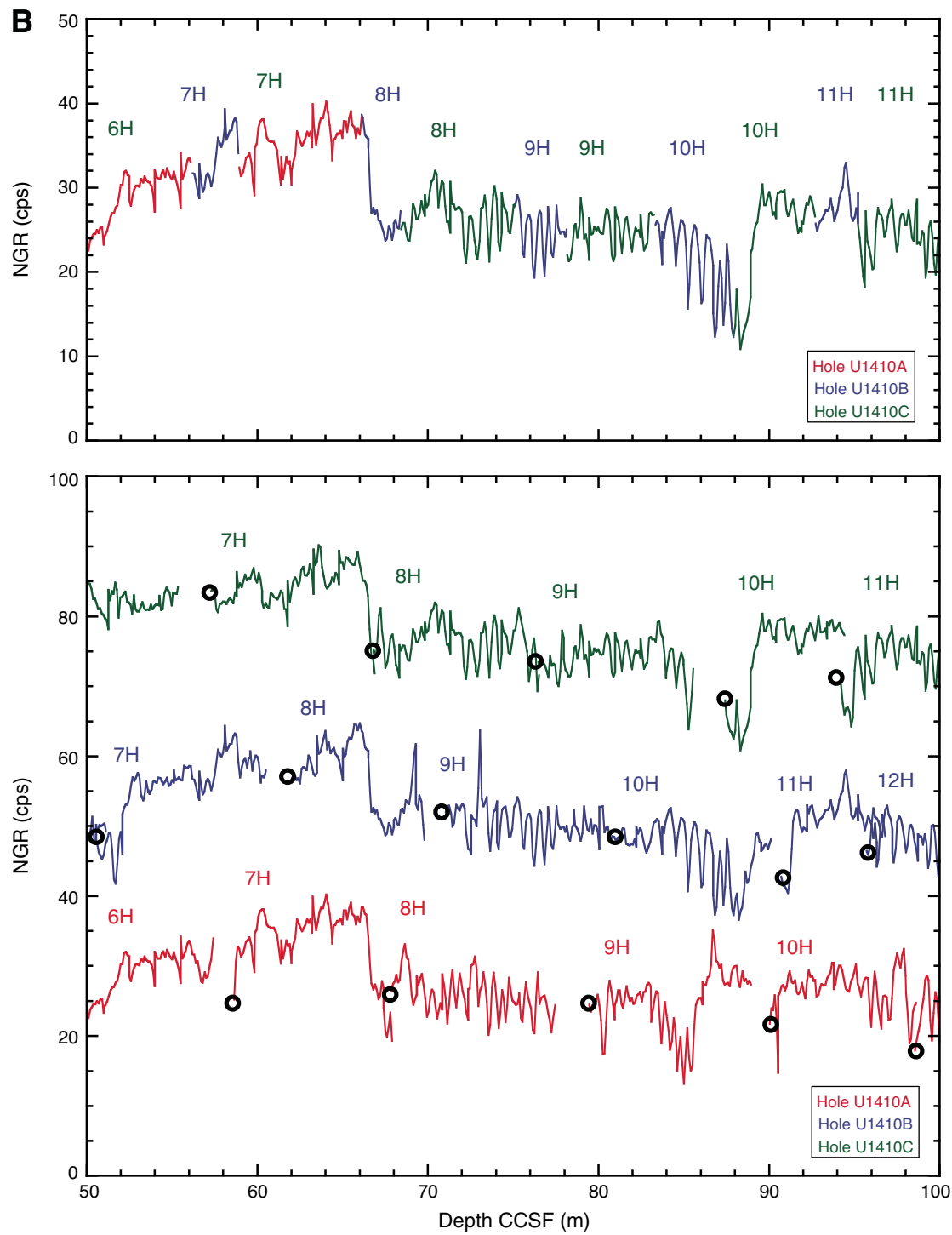


Figure F31 (continued). C. 100–150 m CCSF. (Continued on next page.)

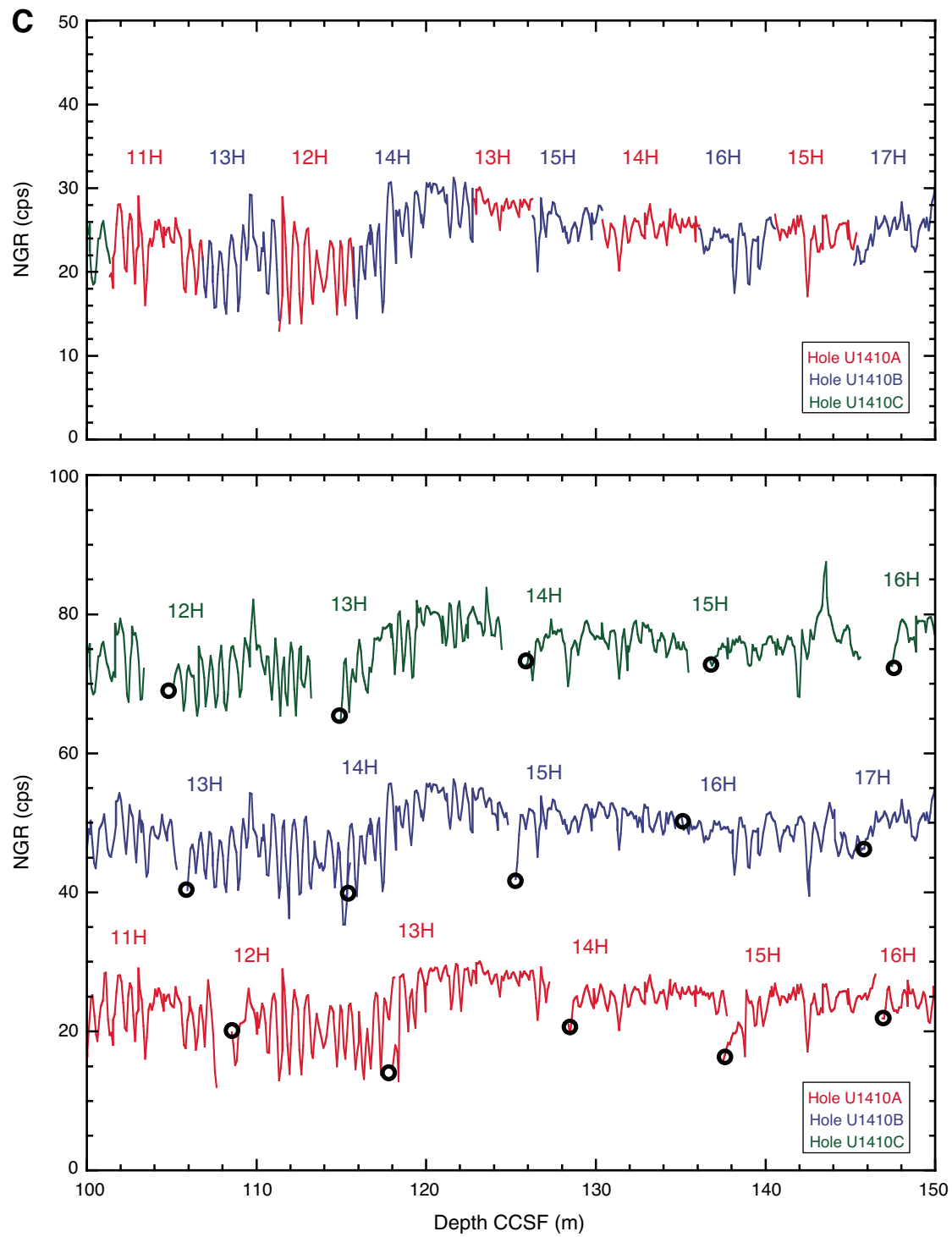


Figure F31 (continued). D. 150–200 m CCSF. (Continued on next page.)

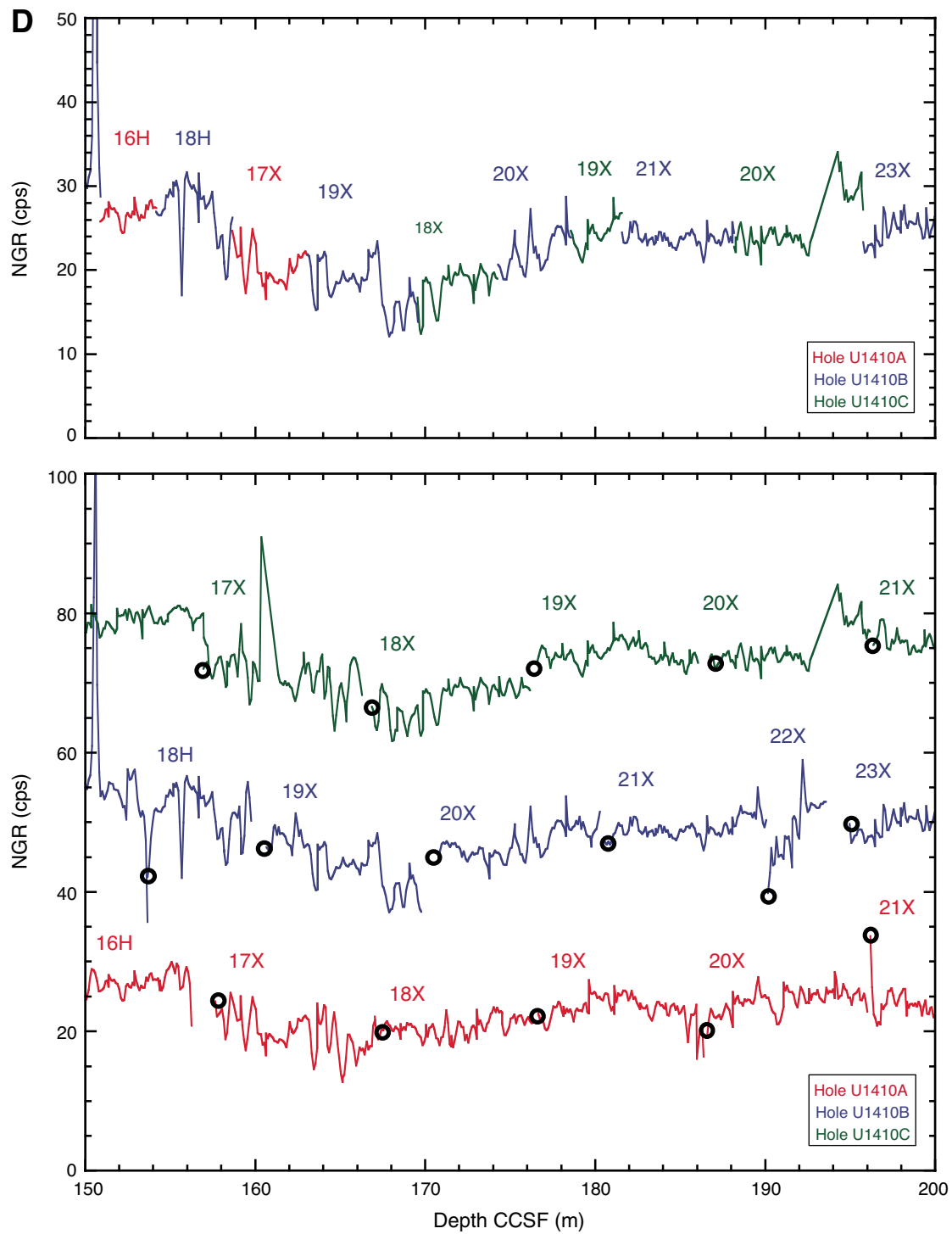


Figure F31 (continued). E. 200–250 m CCSF. (Continued on next page.)

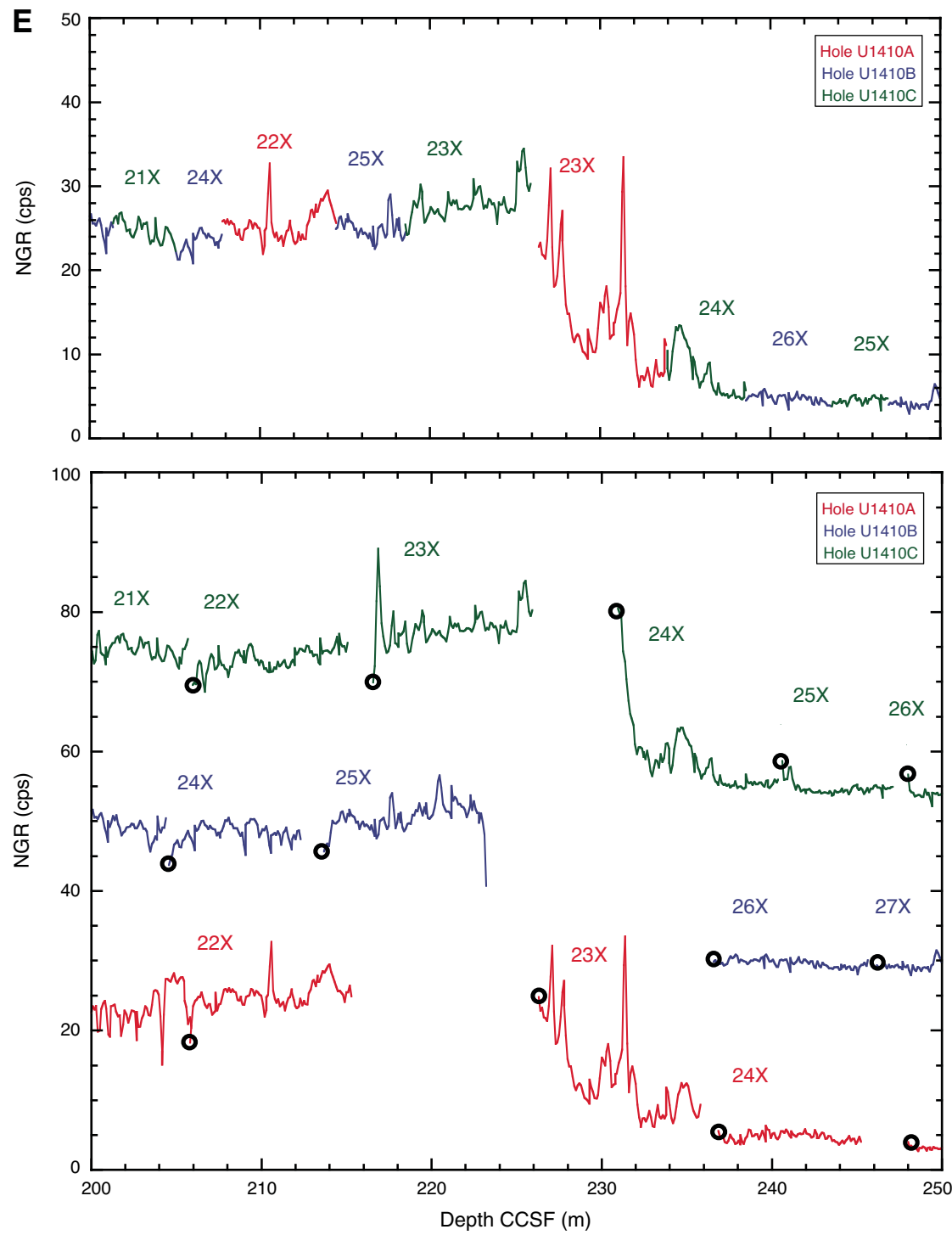


Figure F31 (continued). F. 250–280 m CCSF.

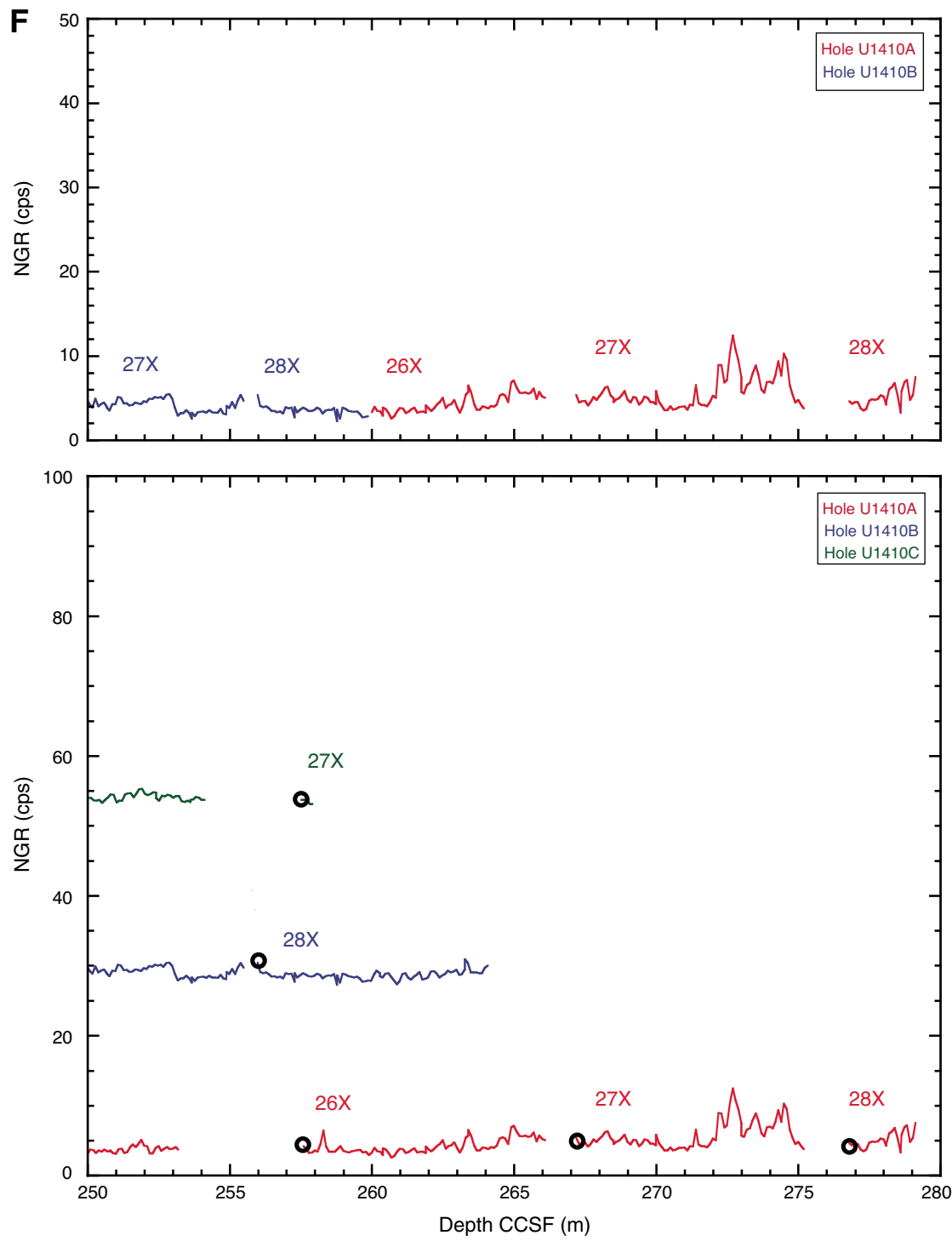


Figure F32. Plot of mbsf depth vs. CCSF depth, Site U1410. The growth factor is equal to the slope of the regression line.

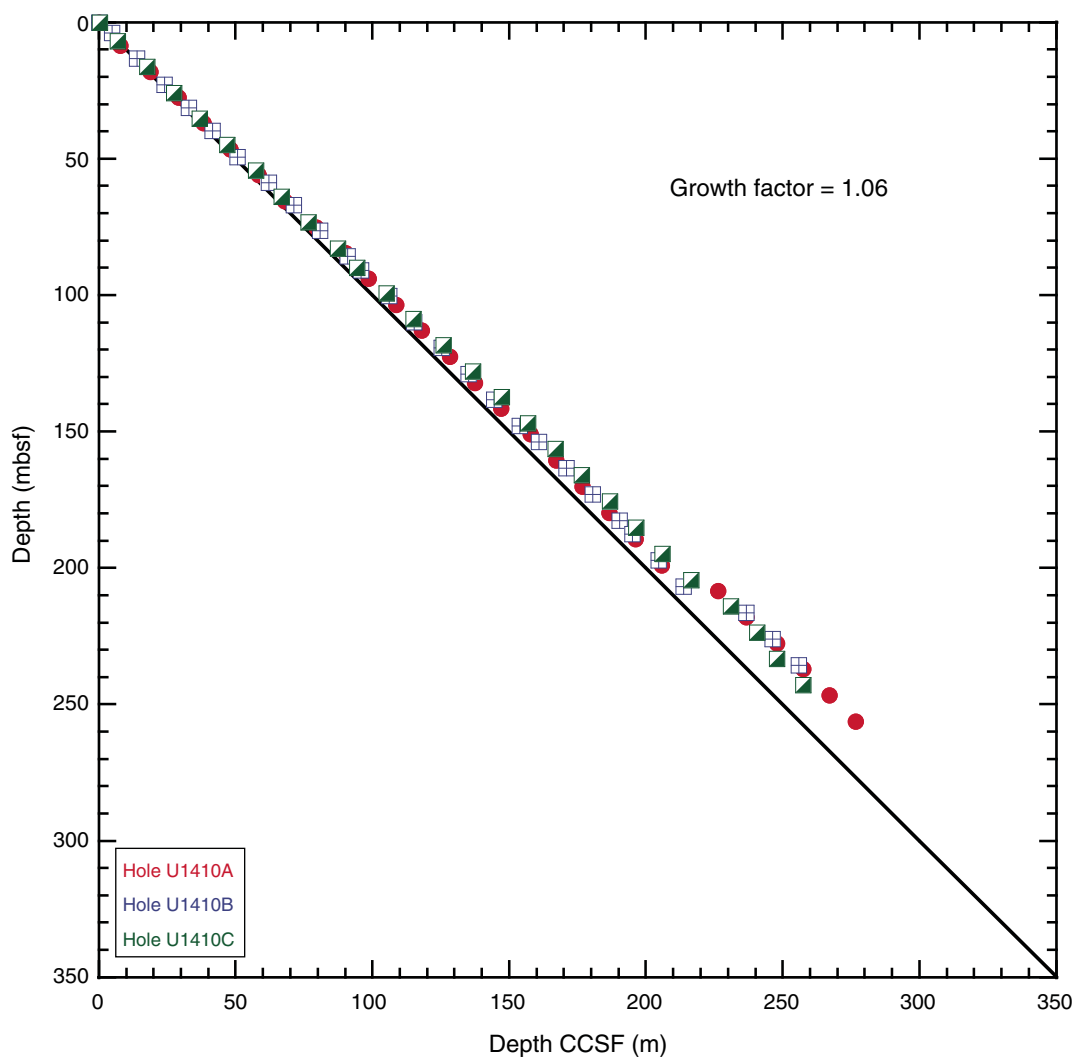


Table T1. Coring summary, Site U1410. (Continued on next page.)

Core	Date (2012)	Time UTC (h)	Depth DSF (m)				Depth CSF-A (m)			
			Top of cored interval	Bottom of cored interval	Interval cored (m)	Curated length (m)	Top of core	Bottom of core	Recovery (%)	Sections (N)
342-U1410A-										
1H	21 Jul	0010	0.0	8.5	8.5	8.53	0.00	8.53	100	7
2H	21 Jul	0120	8.5	18.0	9.5	9.91	8.50	18.41	104	8
3H	21 Jul	0205	18.0	27.5	9.5	9.91	18.00	27.91	104	8
4H	21 Jul	0255	27.5	37.0	9.5	10.07	27.50	37.57	106	8
5H	21 Jul	0345	37.0	46.5	9.5	9.50	37.00	46.50	100	8
6H	21 Jul	0440	46.5	56.0	9.5	9.74	46.50	56.24	103	8
7H	21 Jul	0525	56.0	65.5	9.5	9.71	56.00	65.71	102	8
8H	21 Jul	0625	65.5	75.0	9.5	9.94	65.50	75.44	105	8
9H	21 Jul	0725	75.0	84.5	9.5	9.61	75.00	84.61	101	8
10H	21 Jul	0815	84.5	94.0	9.5	8.71	84.50	93.21	92	8
11H	21 Jul	0945	94.0	103.5	9.5	9.21	94.00	103.21	97	8
12H	21 Jul	1035	103.5	113.0	9.5	9.92	103.50	113.42	104	8
13H	21 Jul	1145	113.0	122.5	9.5	9.62	113.00	122.62	101	8
14H	21 Jul	1235	122.5	132.0	9.5	9.54	122.50	132.04	100	7
15H	21 Jul	1340	132.0	141.5	9.5	9.52	132.00	141.52	100	7
16H	21 Jul	1500	141.5	151.0	9.5	9.60	141.50	151.10	101	7
17X	21 Jul	1635	151.0	160.6	9.6	9.84	151.00	160.84	103	8
18X	21 Jul	1740	160.6	170.2	9.6	9.75	160.60	170.35	102	8
19X	21 Jul	1845	170.2	179.8	9.6	9.81	170.20	180.01	102	8
20X	21 Jul	2020	179.8	189.4	9.6	9.84	179.80	189.64	103	8
21X	21 Jul	2125	189.4	199.0	9.6	9.75	189.40	199.15	102	8
22X	21 Jul	2235	199.0	208.5	9.5	9.95	199.00	208.95	105	8
23X	21 Jul	2330	208.5	218.0	9.5	9.95	208.50	218.45	105	8
24X	22 Jul	0025	218.0	227.5	9.5	9.08	218.00	227.08	96	7
25X	22 Jul	0115	227.5	237.1	9.6	5.73	227.50	233.23	60	5
26X	22 Jul	0215	237.1	246.7	9.6	9.03	237.10	246.13	94	7
27X	22 Jul	0355	246.7	256.3	9.6	8.50	246.70	255.20	89	7
28X	22 Jul	0555	256.3	259.8	3.5	2.61	256.30	258.91	75	3
Totals:				259.8	256.88			98	209	
342-U1410B-										
1H	22 Jul	0940	0.0	3.8	3.8	3.82	0.00	3.82	101	4
2H	22 Jul	1150	3.8	13.3	9.5	8.08	3.80	11.88	85	7
3H	22 Jul	1250	13.3	22.8	9.5	8.91	13.30	22.21	94	8
4H	22 Jul	1440	22.8	31.3	8.5	8.52	22.80	31.32	100	7
5H	22 Jul	1610	31.3	39.7	8.4	8.46	31.30	39.76	101	7
6H	22 Jul	1700	39.7	49.2	9.5	10.05	39.70	49.75	106	8
7H	22 Jul	1755	49.2	58.7	9.5	10.02	49.20	59.22	105	8
8H	22 Jul	1850	58.7	66.8	8.1	8.14	58.70	66.84	100	7
9H	22 Jul	1945	66.8	76.3	9.5	9.97	66.80	76.77	105	8
10H	22 Jul	2120	76.3	85.8	9.5	9.49	76.30	85.79	100	7
11H	22 Jul	2215	85.8	90.8	5.0	6.24	85.80	92.04	125	6
12H	22 Jul	2310	90.8	100.3	9.5	9.81	90.80	100.61	103	8
13H	23 Jul	0010	100.3	109.8	9.5	9.78	100.30	110.08	103	8
14H	23 Jul	0100	109.8	119.3	9.5	9.75	109.80	119.55	103	8
15H	23 Jul	0150	119.3	128.8	9.5	9.56	119.30	128.86	101	7
16H	23 Jul	0245	128.8	138.3	9.5	10.02	128.80	138.82	105	8
17H	23 Jul	0350	138.3	147.8	9.5	9.32	138.30	147.62	98	8
18H	23 Jul	0510	147.8	153.8	6.0	6.40	147.80	154.20	107	6
19X	23 Jul	0720	153.8	163.4	9.6	9.55	153.80	163.35	99	8
20X	23 Jul	0825	163.4	173.0	9.6	9.83	163.40	173.23	102	8
21X	23 Jul	0935	173.0	182.6	9.6	9.82	173.00	182.82	102	8
22X	23 Jul	1030	182.6	187.6	5.0	3.93	182.60	186.53	79	4
23X	23 Jul	1205	187.6	197.2	9.6	9.89	187.60	197.49	103	8
24X	23 Jul	1315	197.2	206.8	9.6	8.27	197.20	205.47	86	7
25X	23 Jul	1430	206.8	216.4	9.6	9.53	206.80	216.33	99	8
26X	23 Jul	1520	216.4	226.0	9.6	9.38	216.40	225.78	98	8
27X	23 Jul	1605	226.0	235.6	9.6	9.65	226.00	235.65	101	8
28X	23 Jul	1720	235.6	245.2	9.6	8.65	235.60	244.25	90	7
Totals:				245.2	244.84			100	204	
342-U1410C-										
1H	23 Jul	2010	0.0	6.8	6.8	6.82	0.00	6.82	100	6
2H	23 Jul	2230	6.8	16.3	9.5	9.39	6.80	16.19	99	8
3H	23 Jul	2325	16.3	25.8	9.5	9.48	16.30	25.78	100	8
4H	24 Jul	0055	25.8	35.3	9.5	9.31	25.80	35.11	98	7
5H	24 Jul	0140	35.3	44.8	9.5	9.31	35.30	44.61	98	8

Table T1 (continued).

Core	Date (2012)	Time UTC (h)	Depth DSF (m)				Depth CSF-A (m)			
			Top of cored interval	Bottom of cored interval	Interval cored (m)	Curated length (m)	Top of core	Bottom of core	Recovery (%)	Sections (N)
6H	24 Jul	0230	44.8	54.3	9.5	8.96	44.80	53.76	94	7
7H	24 Jul	0400	54.3	63.8	9.5	9.78	54.30	64.08	103	8
8H	24 Jul	0455	63.8	73.3	9.5	10.09	63.80	73.89	106	8
9H	24 Jul	0540	73.3	82.8	9.5	9.27	73.30	82.57	98	8
10H	24 Jul	0630	82.8	89.8	7.0	7.31	82.80	90.11	104	6
11H	24 Jul	0725	89.8	99.3	9.5	9.59	89.80	99.39	101	8
12H	24 Jul	0855	99.3	108.8	9.5	8.54	99.30	107.84	90	7
13H	24 Jul	0950	108.8	118.3	9.5	9.61	108.80	118.41	101	7
14H	24 Jul	1040	118.3	127.8	9.5	9.93	118.30	128.23	105	8
15H	24 Jul	1130	127.8	137.3	9.5	9.08	127.80	136.88	96	7
16H	24 Jul	1310	137.3	146.8	9.5	10.09	137.30	147.39	106	8
17X	24 Jul	1505	146.8	156.4	9.6	9.82	146.80	156.62	102	8
18X	24 Jul	1605	156.4	166.0	9.6	9.77	156.40	166.17	102	8
19X	24 Jul	1700	166.0	175.6	9.6	9.84	166.00	175.84	103	8
20X	24 Jul	1805	175.6	185.2	9.6	9.84	175.60	185.44	103	8
21X	24 Jul	1900	185.2	194.8	9.6	9.61	185.20	194.81	100	8
22X	24 Jul	2015	194.8	204.4	9.6	9.52	194.80	204.32	99	8
23X	24 Jul	2125	204.4	214.0	9.6	9.82	204.40	214.22	102	8
24X	24 Jul	2225	214.0	223.6	9.6	9.75	214.00	223.75	102	8
25X	24 Jul	2335	223.6	233.2	9.6	7.06	223.60	230.66	74	6
26X	25 Jul	0035	233.2	242.8	9.6	6.63	233.20	239.83	69	6
27X	25 Jul	0125	242.8	243.8	1.0	0.59	242.80	243.39	59	2
Totals:				243.8	238.81			97	197	
Site U1410 totals:				748.8	740.23			98	1008	

DSF = drilling depth below seafloor, CSF-A = core depth below seafloor, method A. H = advanced piston core, X = extended core barrel core.

Table T2. Lithostratigraphic unit intervals, Site U1410.

Lith. unit	Core, section, interval (cm)		Depth (mbfs)	
	Top	Bottom	Top	Bottom
342-U1410A-				
I	1H-1, 0	4H-5, 85	0.00	34.35
II	4H-5, 85	7H-7, 62	34.35	64.17
III	7H-7, 62	23X-1, 150	64.17	211.50
IVa	23X-2, 0	26X-6, 47	211.50	245.07
IVb	26X-6, 47	28X-CC, 58*	245.07	258.91
342-U1410B-				
I	1H-1, 0	5H-2, 135	0.00	34.15
II	5H-2, 135	8H-4, 7	34.15	63.27
III	8H-4, 7	25X-CC, 35	63.27	216.27
IVa	26X-1, 0	28X-CC, 32*	225.49	244.25
IVb	Not drilled			
342-U1410C-				
I	1H-1, 0	4H-5, 87	0.00	32.67
II	4H-5, 87	7H-7, 24	32.67	63.54
III	7H-7, 24	23X-CC, 37	63.54	214.22
IVa	24X-1, 0	26X-CC, 39	214.00	239.83
IVb	27X-1, 0	27X-1, 47*	242.80	243.27

* = end of hole.



Table T3. Biostratigraphic and magnetostratigraphic datums, Hole U1410A.

Datum tie point	Datum	Datum type	Zone/Subzone	Age (Ma)	Depth (mbsf)		
					Top	Bottom	Midpoint
	T <i>Pseudoemiliana lacunosa</i>	Calcareous nannofossil	NN20	0.44	6.56	8.48	7.52
	T <i>Discoaster brouweri</i>	Calcareous nannofossil	NN19	1.93	24.75	27.88	26.32
D03	T <i>Discoaster pentaradiatus</i>	Calcareous nannofossil	NN17	2.39	31.51	31.51	31.51
D04	T <i>Discoaster hamatus</i>	Calcareous nannofossil	NN10	9.53	34.50	37.57	36.04
D05	B <i>Discoaster hamatus</i>	Calcareous nannofossil	NN9	10.55	41.00	44.00	42.50
D06	Tc <i>Sphenolithus belemnos</i>	Calcareous nannofossil	NN4	17.95	44.00	46.45	45.23
D07	B <i>Sphenolithus belemnos</i>	Calcareous nannofossil		19.03	46.45	50.00	48.23
D08	B <i>Discoaster druggii</i>	Calcareous nannofossil	NN2	22.82	50.00	53.00	51.50
D09	T <i>Sphenolithus ciperoensis</i>	Calcareous nannofossil	NN1	24.43	50.00	53.00	51.50
D10	T <i>Sphenolithus distentus</i>	Calcareous nannofossil	NP25	26.84	56.20	59.55	57.88
D11	T <i>Reticulofenestra umbilicus</i> (>14 µm)	Calcareous nannofossil	NP23	32.02	64.17	64.25	64.21
	T <i>Coccolithus formosus</i>	Calcareous nannofossil	NP22	32.92	64.17	64.25	64.21
	T <i>Chiasmolithus grandis</i>	Calcareous nannofossil		37.98	64.17	64.25	64.21
	B <i>Dictyococcites bisectus</i> (>10 µm)	Calcareous nannofossil		40.36	79.23	80.85	80.04
	T <i>Sphenolithus furcatolithoides</i>	Calcareous nannofossil			82.95	83.71	83.33
	Tc <i>Chiasmolithus solitus</i>	Calcareous nannofossil	NP17	40.40	93.16	103.19	98.17
	B <i>Reticulofenestra reticulata</i>	Calcareous nannofossil		41.66	117.09	120.02	118.56
	T <i>Nannotetra</i> spp.	Calcareous nannofossil		41.85	114.47	117.09	115.78
	B <i>Reticulofenestra umbilicus</i> (>14 µm)	Calcareous nannofossil		41.94	134.07	137.09	135.58
	T <i>Nannotetra fulgens</i>	Calcareous nannofossil		42.87	151.75	153.36	152.56
	T <i>Chiasmolithus gigas</i>	Calcareous nannofossil	NP15c	44.12	153.36	153.37	153.37
	B <i>Sphenolithus furcatolithoides</i>	Calcareous nannofossil			170.33	179.98	175.16
	B <i>Chiasmolithus gigas</i>	Calcareous nannofossil	NP15b	45.49	190.74	193.75	192.25
	B <i>Nannotetra fulgens</i>	Calcareous nannofossil	NP15a	46.29	208.93	210.68	209.81
	B <i>Nannotetra cristata</i>	Calcareous nannofossil		47.73	220.43	223.34	221.89
	B <i>Blackites inflatus</i>	Calcareous nannofossil		47.84	216.28	218.45	217.37
	T <i>Discoaster lodoensis</i>	Calcareous nannofossil		47.41	218.45	220.43	219.44
	B <i>Discoaster sublodoensis</i> (5 rayed)	Calcareous nannofossil	NP14	49.11	227.06	228.26	227.66
	T <i>Trirachiatius orthostylus</i>	Calcareous nannofossil	NP13	50.50	242.45	244.00	243.23
	B <i>Dictyococcites/Reticulofenestra</i>	Calcareous nannofossil		50.50	244.00	245.16	244.58
	T <i>Toweius</i> spp.	Calcareous nannofossil		50.78	245.16	246.09	245.63
D18	B <i>Coccolithus crassus</i>	Calcareous nannofossil		51.64	246.09	255.14	250.62
	B <i>Discoaster lodoensis</i>	Calcareous nannofossil	NP12	53.70	258.69	258.69	258.69
	B <i>Dictyoprora mongolfieri</i>	Radiolarian	RP11	47.98	218.40	218.40	218.40
	B <i>Lithochytris vespertilio</i>	Radiolarian	RP10	48.57	227.10	233.20	230.15
D17	B <i>Lamptonium fabaeforme constrictum</i>	Radiolarian	RP9	50.05	233.20	246.10	239.65
	T <i>Buryella tetradica</i>	Radiolarian	RP8	50.87	233.20	246.10	239.65
D19	B <i>Buryella clinata</i>	Radiolarian	RP7	53.35	258.70	258.70	
	T <i>Orbulinoides bekmanni</i>	Planktonic foraminifer	E13/E12	40.03	69.61	71.11	70.36
	B <i>Orbulinoides bekmanni</i>	Planktonic foraminifer	E12/E11	40.43	84.56	85.46	85.01
	T <i>Guembelitrioides nuttalli</i>	Planktonic foraminifer	E11/E10	42.07	89.16	90.56	89.86
	T <i>Morozovella lehneri</i>	Planktonic foraminifer	Just above E10/E9	43.15	153.61	156.71	155.16
	B <i>Globigerinatheca kugleri</i>	Planktonic foraminifer	E9/E8	43.88	160.82	163.11	161.97
	B <i>Guembelitrioides nuttalli</i>	Planktonic foraminifer	E8/E7b	45.72	201.51	206.01	203.76
	B <i>Turborotalia frontosa</i>	Planktonic foraminifer	E7b/E7a	48.31	215.53	218.43	216.98
	B <i>Acarinina cuniacamerata</i>	Planktonic foraminifer	E7a/E6	50.20	239.75	244.08	241.92
	B <i>Morozovella subbotinae</i>	Planktonic foraminifer	E6/E5	50.67	252.83	255.14	253.99
D01	C1n (Brunhes)/C1r.1r (Matuyama)	Chron boundary		0.78			11.50
	C1r.1r (Matuyama)/C1r.1n (Jaramillo)	Chron boundary		0.99			13.00
	C1r.1n (Jaramillo)/C1r.2r	Chron boundary		1.07			13.48
	C1r.2r/C1r.2n (Cobb Mountain)	Chron boundary		1.17			13.79
D02	C1r.2n (Cobb Mountain)/C1r.3r	Chron boundary		1.19			14.33
	C1r.3r/C2n (Olduvai)	Chron boundary		1.78			17.13
	C2r.2r/C2An.1n (Gauss)	Chron boundary		2.58			32.95
	C18n.1n/C18n.1r	Chron boundary		39.63			68.68
	C18n.1r/C18n.2n	Chron boundary		39.70			71.25
	C18n.2n/C18r	Chron boundary		40.14			80.15
	C18r/C19n	Chron boundary		41.15			96.80
	C19n/C19r	Chron boundary		41.39			102.48
D13	C19r/C20n	Chron boundary		42.30			121.55
D14	C20n/C20r	Chron boundary		43.43			151.27
D15	C20r/C21n	Chron boundary		45.72			197.39
D16	C21n/C21r	Chron boundary		47.35			218.06

B = base, T = top, Tc = top common.



Table T4. Calcareous nannofossil datums, Site U1410.

Hole, core, section, interval (cm)	Top	Bottom	Age	Zone/ Subzone	Marker species	Age (Ma)	Depth (mbsf)				
							Top	Bottom	Midpoint	±	
342-	342-			Pleistocene							
U1410A-1H-5, 56	U1410A-1H-CC			NN20	T <i>Pseudoemiliania lacunosa</i>	0.44	6.56	8.48	7.52	0.96	
U1410A-3H-5, 75	U1410A-3H-CC			NN19	T <i>Discoaster brouweri</i>	1.93	24.75	27.88	26.32	1.57	
U1410A-4H-3, 100	U1410A-4H-3, 100			Pliocene	NN17	T <i>Discoaster pentaradiatus</i>	2.39	31.51	31.51	31.51	0.00
U1410A-4H-5, 100	U1410A-4H-CC			Miocene	NN10	T <i>Discoaster hamatus</i>	9.53	34.50	37.57	36.04	1.54
U1410A-5H-3, 100	U1410A-5H-5, 100				NN9	B <i>Discoaster hamatus</i>	10.55	41.00	44.00	42.50	1.50
U1410A-5H-5, 100	U1410A-5H-CC				NN4	Tc <i>Sphenolithus belemnos</i>	17.95	44.00	46.45	45.23	1.23
U1410A-5H-CC	U1410A-6H-3, 50					B <i>Sphenolithus belemnos</i>	19.03	46.45	50.00	48.23	1.77
U1410A-6H-3, 50	U1410A-6H-5, 50				NN2	B <i>Discoaster druggii</i>	22.82	50.00	53.00	51.50	1.50
U1410A-6H-3, 50	U1410A-6H-5, 50			Oligocene	NN1	T <i>Sphenolithus ciperoensis</i>	24.43	50.00	53.00	51.50	1.50
U1410A-6H-CC	U1410A-7H-3, 50				NP25	T <i>Sphenolithus distentus</i>	26.84	56.20	59.55	57.88	1.67
U1410A-7H-7, 62	U1410A-7H-7, 70				NP23	T <i>Reticulofenestra umbilicus</i> (>14 µm)	32.02	64.17	64.25	64.21	0.04
U1410A-7H-7, 62	U1410A-7H-7, 70				NP22	T <i>Coccoolithus formosus</i>	32.92	64.17	64.25	64.21	0.04
U1410A-7H-7, 62	U1410A-7H-7, 70			Eocene		T <i>Chiasmolithus grandis</i>	37.98	64.17	64.25	64.21	0.04
U1410A-9H-4, 58	U1410A-9H-5, 70					B <i>Dictyococcites bisectus</i> (>10 µm)*	40.36	79.23	80.85	80.04	0.81
U1410A-9H-6, 130	U1410A-9H-7, 56					T <i>Sphenolithus furcatolithoides</i>		82.95	83.71	83.33	0.38
U1410A-10H-CC	U1410A-11H-CC				NP17	Tc <i>Chiasmolithus solitus</i>	40.40	93.16	103.185	98.17	5.01
U1410A-13H-4, 62	U1410A-13H-6, 62					B <i>Reticulofenestra reticulata</i>	41.66	117.09	120.02	118.56	1.46
U1410A-13H-2, 100	U1410A-13H-4, 62					T <i>Nannotetraena</i> spp.	41.85	114.47	117.09	115.78	1.31
U1410A-15H-2, 58	U1410A-15H-4, 60					B <i>Reticulofenestra umbilicus</i> (>14 µm)	41.94	134.07	137.09	135.58	1.51
U1410A-17X-1, 75	U1410A-17X-2, 86					T <i>Nannotetraena fulgens</i>	42.87	151.75	153.36	152.56	0.81
U1410A-17X-2, 86	U1410A-17X-2, 87				NP15c	T <i>Chiasmolithus gigas</i>	44.12	153.36	153.37	153.37	0.00
U1410A-18X-CC	U1410A-19X-CC					B <i>Sphenolithus furcatolithoides</i>		170.33	179.98	175.16	4.82
U1410A-21X-2, 70	U1410A-21X-4, 75				NP15b	B <i>Chiasmolithus gigas</i>	45.49	190.74	193.75	192.25	1.50
U1410A-22X-CC	U1410A-23X-2, 67				NP15a	B <i>Nannotetraena fulgens</i>	46.29	208.93	210.68	209.81	0.88
U1410A-24X-2, 84	U1410A-24X-4, 84					B <i>Nannotetraena cristata</i>	47.73	220.43	223.34	221.89	1.45
U1410A-23X-6, 108	U1410A-23X-CC					B <i>Blackites inflatus</i>	47.84	216.28	218.45	217.37	1.08
U1410A-23X-CC	U1410A-24X-2, 84					T <i>Discoaster lodoensis</i>	47.41	218.45	220.43	219.44	0.99
U1410A-24X-CC	U1410A-25X-1, 76			NP14		B <i>Discoaster sublodoensis</i> (5 rayed)	49.11	227.06	228.26	227.66	0.60
U1410A-26X-4, 85	U1410A-26X-5, 90			NP13		T <i>Tribrachiatus orthostylus</i>	50.50	242.45	244.00	243.23	0.78
U1410A-26X-5, 90	U1410A-26X-6, 56					B <i>Dictyococcites/Reticulofenestra</i>	50.50	244.00	245.16	244.58	0.58
U1410A-26X-6, 56	U1410A-26X-CC					T <i>Toweius</i> spp. [†]	50.78	245.16	246.09	245.63	0.47
U1410A-26X-CC	U1410A-27X-CC					B <i>Coccoolithus crassus</i> [†]	51.64	246.09	255.14	250.62	4.52
U1410A-28X-CC	U1410A-28X-CC			NP12		B <i>Discoaster lodoensis</i>	53.70	258.69	258.69	258.69	0.00

* = from Fornaciari et al. (2010) recalibrated to GTS2012. † = from Agnini et al. (2006) recalibrated to GTS2012. B = base, Bc = base common, T = top, Tc = top common.



Table T5. Stratigraphic distribution of selected nannofossils, Site U1410. This table available in an [oversized format](#).**Table T6.** Radiolarian datums, Site U1410.

Core, section		Age	Zone	Marker species	Age (Ma)	Depth (mbsf)			
Top	Bottom					Top	Bottom	Midpoint	±
342-U1410A-	342-U1410A-	Eocene	RP11	B <i>Dictyoprora mongolfieri</i>	47.98	0.00	218.40	218.40	
23X-CC	23X-CC		RP10	B <i>Lithochytris vespertilio</i>	48.57	227.10	233.20	230.15	3.05
25X-CC	25X-CC		RP9	B <i>Lamptonium fabaeforme constrictum</i>	50.05	233.20	246.10	239.65	6.45
25X-CC	26X-CC			T <i>Buryella tetradica</i>	50.87	233.20	246.10	239.65	6.45
26X-CC			RP8	B <i>Buryella clinata</i>	53.35	258.70		258.70	
28X-CC									

B = base, T = top.



**Table T7.** Radiolarian distribution, U1410.

Core, section	Depth (mbsf)	Age	Zone	Preservation	Abundance	<i>Amphicaspedum gracilis</i>	<i>Amphicaspedum murayanum</i>	<i>Amphicaspedum prolixum</i>	<i>Amphiperis alamedaeensis</i>	<i>Amphisphaera coronata</i>	<i>Amphisphaera goruna</i>	<i>Amphisphaera aff. goruna</i>	<i>Amphisphaera macrospheara</i>	<i>Astrophaeus linkiaformis</i>	<i>Axoprumum pierinae</i>	<i>Buryella clinata</i>	<i>Buryella pentadica</i>	<i>Buryella tetradica</i>	<i>Calocyclus hispida</i>	<i>Calocyclus costum</i>	<i>Clathrocyclus universa</i>	<i>Cryptocarpium ornatum</i>	<i>Dendrosprysis golii</i>	<i>Dictyopora amphora</i>	<i>Dictyopora mongolfieri</i>	<i>Dictyopora urceolus</i>	<i>Diplodiscus bicorona bicorona</i>	<i>Dorcadopsis platycantha</i>	<i>Lamptoniump tabaeforme chaunothorax</i>	<i>Lamptoniump tabaeforme constictum</i>	<i>Lipmanella</i> sp.	<i>Lithochrytis archaea</i>	<i>Lithochrytis vespertilio</i>	<i>Lophocrytis jacchia</i>	<i>Lophocrytis klyodus</i>	<i>Lophocrytis semipolita</i> gr.	<i>Lophocrytis? sphaerula</i>	<i>Lophocrytis auxilla</i>	<i>Lophocrytis bellum</i>	<i>Lophocrytis? triplidium</i>	<i>Middoumum regulans</i>
342-U1410A-																																									
23X-CC	218.40	early Eocene	RP11	G	A	F	P	P	F	R	P	P	P	P	P	P	P	P	P	P	P	P	P	P	P	P	P	P	P	P	P	F	F								
24X-CC	227.10	early Eocene	RP10	G	A	C	C	P	F	F	R	R	R	R	R	R	R	R	R	R	R	R	R	R	R	R	R	R	R	R	R	R									
25X-CC	233.20	early Eocene	RP9	G	A	C	C	P	F	F	R	R	R	R	R	R	R	R	R	R	R	R	R	R	R	R	R	R	R	R	R	R									
26X-CC	246.10	early Eocene	RP8	P	C	P	C	C	P	C	P	R	R	R	R	R	R	R	R	R	R	R	R	R	R	R	R	R	R	R	R	R									
27X-CC	255.10	early Eocene	RP8	P	C	F		C	P	R	R	R	R	R	R	R	R	R	R	R	R	R	R	R	R	R	R	R	R	R	R	R	R								
28X-CC	258.70	early Eocene	RP8	P	C																																				

Preservation: G = good, P = poor. Abundance: A = abundant, C = common, F = few, R = rare. See “[Biostratigraphy](#)” in the “Methods” chapter (Norris et al., 2014a) for preservation and abundance definitions.

Core, section	Depth (mbsf)	Age	Zone	Preservation	Abundance	<i>Periphæna decora</i>	<i>Periphæna heliasteriscus</i>	<i>Periphæna tripyramis triangula</i>	<i>Periphæna tripyramis tripyramis</i>	<i>Phormocrytis ligulata</i>	<i>Phormocrytis striata exquisita</i>	<i>Podocrytis stria striata</i>	<i>Podocrytis acelles</i>	<i>Podocrytis diamesa</i>	<i>Podocrytis papalis</i>	<i>Podoconchus sinuosus</i>	<i>Pterocodon tenellus</i>	<i>Rhopalosyringium ornatum</i>	<i>Saturnalis circularis</i>	<i>Sedocrytis babylonis</i>	<i>Siphonocystis didacta</i>	<i>Spongatractus pachysylus</i>	<i>Spongistratis bivalvis</i>	<i>Syllophocystis nitidus</i>	<i>Thecoctys antarctica</i>	<i>Thecoctys plesionacasta</i>	<i>Thecoctys phyzella</i>	<i>Thecoctys aff. phyzella</i>	<i>Thecoctyle cryocephala</i>	<i>Thecoctyle nigritiae</i>	<i>Thecoctylissa flocs</i>	<i>Thecoctylissa histria</i>	<i>Thecoctylissa thysdona</i>	<i>Thecoctylissa leesa</i>	<i>Zelithidium daodecum</i>
342-U1410A-																																			
23X-CC	218.40	early Eocene	RP11	G	A	R	P	P	R	P	R	F	R	R	R	R	P	P	F	R	R	R	R	R	P	P	R	F	R	P	R	P			
24X-CC	227.10	early Eocene	RP10	G	A	C	P	C	R	P	R	R	F	R	R	R	P	P	R	P	P	P	P	P	P	R	F	R	P	R	P				
25X-CC	233.20	early Eocene	RP9	G	A	P	C	C	P	R	R	R	F	R	R	R	P	P	P	R	R	R	R	P	P	R	F	R	P	R	P				
26X-CC	246.10	early Eocene	RP8	P	C	P	C	C	P	R	R	R	F	R	R	R	P	P	P	R	R	R	R	P	P	R	F	R	P	R	P				
27X-CC	255.10	early Eocene	RP8	P	C	F		C	P	R	R	R	F	R	R	R	P	P	P	R	R	R	R	P	P	R	F	R	P	R	P				
28X-CC	258.70	early Eocene	RP8	P	C																														

Table T8. Planktonic foraminifer datums, Site U1410.

Core, section, interval (cm)		Age	Zone/ Subzone	Marker event	Age (Ma)	Depth (mbsf)			
Top	Bottom					Top	Bottom	Midpoint	±
342-U1410A-8H-3, 110–112	342-U1410A-8H-4, 110–112	middle Eocene	E13/E12	T <i>Orbulinoides bekmanni</i>	40.03	69.61	71.11	70.36	0.75
9H-CC	10H-2, 45–47	middle Eocene	E12/E11	B <i>Orbulinoides bekmanni</i>	40.43	84.56	85.46	85.01	0.45
10H-5, 90–92	10H-6, 90–92	middle Eocene	E11/E10	T <i>Guembelitrioides nuttalli</i>	42.07	89.16	90.56	89.86	0.70
17X-2, 110–112	17X-4, 120–122	middle Eocene	Just above E10/E9	T <i>Morozovella lehneri</i>	43.15	153.61	156.71	155.16	1.55
17X-CC	18X-2, 100–102	middle Eocene	E9/E8	B <i>Globigerinatheka kugleri</i>	43.88	160.82	163.11	161.97	1.15
22X-2, 100–102	22X-5, 100–102	middle Eocene	E8/E7b	B <i>Guembelitrioides nuttalli</i>	45.70	201.5	206.01	203.76	2.25
23X-5, 102–104	23X-CC	early Eocene	E7b/E7a	B <i>Turborotalia frontosa</i>	48.30	215.53	218.43	216.98	1.45
26X-2, 114–115	26X-5, 97–98	early Eocene	E7a/E6	B <i>Acarinina cuniacamerata</i>	50.20	239.75	244.08	241.92	2.17
27X-5, 12–13	27X-CC	early Eocene	E6/E5	B <i>Morozovella subbotinae</i>	50.67	252.83	255.14	253.99	1.15

T = top, B = base.

Table T9. Planktonic foraminifer distribution, Site U1410. This table is available in an [oversized format](#).

Table T10. Benthic foraminifer distribution, Site U1410. (Continued on next page.)

Core, section	Depth (mbsf)	Preservation	Abundance	<i>Abyssammina quadrata</i>	<i>Alabamina dissimilata</i>	<i>Alabamina</i> sp.	<i>Anomalina</i> sp.	<i>Anomalinoides semisulcatus</i>	<i>Argonautinoides</i> sp.	<i>Asteclina</i> sp.	<i>Bathylypon</i> sp.	<i>Buliminina</i> sp.	<i>Buliminina</i> sp.?	<i>Buliminina</i> sp.	<i>Cassidulina subglobosa</i>	<i>Chilostomella</i> sp.	<i>Chrysalogonium</i> sp.	<i>Cibicidoides aff. laurisae</i>	<i>Cibicidoides cf. havanensis</i>	<i>Cibicidoides eocenensis</i>	<i>Cibicidoides globulosus</i>	<i>Cibicidoides subspiratus</i>	<i>Cibicidoides grimsdalei</i>	<i>Dentatula</i> sp.	<i>Dorothia trachoides</i>	<i>Ellipsidion hina</i> spp.	<i>Epsomitella umbonifera</i> ?	<i>Gaudryina pacifica</i>	<i>Gaudryina pacifica</i> as sp.	<i>Gaudryina austalis</i>	<i>Kalymene</i> sp.	<i>Lagena</i> sp.	<i>Lagena</i> sp. <i>paperata</i>	<i>Lenticularia</i> sp. <i>determinate</i>
342-U1410A-																																		
1H-CC	8.48	VG	P																															
2H-CC	18.36	M	P																															
3H-CC	27.88	M	P																															
4H-CC	37.52	G	P																															
5H-CC	46.45	M	F																															
6H-CC	56.20	P	R																															
7H-CC	65.66	VG	P	F	F	A																												
8H-CC	75.39	VG	P	F	F	F																												
9H-CC	84.56	G	P	F	F	F																												
10H-CC	93.16	VG	P																															
11H-CC	103.18	G	P																															
12H-CC	113.37	G	P																															
13H-CC	122.57	G	P																															
14H-7	131.98	G	P																															
15H-7	141.45	G	P																															
16H-7	150.99	G	P																															
17X-CC	160.82	VG	P	P	F	F																												
18X-CC	170.33	G	R	F	P	F	F																											
19X-CC	179.98	G	P	F	F	F																												
20X-CC	189.62	VG	P	P	F	A	F																											
21X-CC	199.13	G	P	A																														
22X-CC	208.93	VG	P	A	F	F	F																											
23X-CC	218.43	VG	P																															
24X-CC	227.06	G	P																															
25X-CC	233.19	G	P																															
26X-CC	246.09	P	P																															
27X-CC	255.14	M	P																															
28X-CC	258.69	M	P	A	F																													

Preservation: VG = very good, G = good, M = moderate, P = poor. Abundance: P = present, R = rare, F = few, A = abundant. See “**Biostratigraphy**” in the “Methods” chapter (Norris et al., 2014a) for preservation and abundance definitions.

Table T10 (continued).

Core, section	Depth (mbsf)	Taxa										Others Vascular plants?	Fungi Lichen spores?
		Tulipa sp.	Leptostoma sp.	Trichomanes sp.	Thelypteris sp.	Urticales sp.	Urticariales sp.						
342-U1410A-													
1H-CC	8.48	VG	P	F	P	P	A	F	P	P	A	F	P
2H-CC	18.36	M	P	F		P	A	F	P	P	F	P	P
3H-CC	27.88	M	P		P	F	A	P	P	P	P	P	P
4H-CC	37.52	G	P		P	F	A	F	P	P	F	P	F
5H-CC	46.45	M	F		P	P	P	P	P	P	F	P	F
6H-CC	56.20	P	R		P	F	P	F	P	P	F	P	F
7H-CC	65.66	VG	P	F	P	A	P	F	P	P	F	P	F
8H-CC	75.39	VG	P		P	A	P	F	P	P	F	P	F
9H-CC	84.56	G	P		P	F	P	F	P	P	F	P	F
10H-CC	93.16	VG	P	P	P	A	A	F	P	P	F	P	F
11H-CC	103.18	G	P		P	A	P	A	F	P	F	P	F
12H-CC	113.37	G	P	P	P	A	A	A	F	P	F	P	F
13H-CC	122.57	G	P		P	A	F	A	F	P	F	P	F
14H-7	131.98	G	P		P	A	P	P	P	P	F	P	F
15H-7	141.45	G	P		P	F	A	P	P	P	F	P	F
16H-7	150.99	G	P		P	F	A	P	F	P	F	P	F
17X-CC	160.82	VG	P	P	P	F	F	A	P	P	F	P	F
18X-CC	170.33	G	R		P	F	A	P	F	P	F	P	F
19X-CC	179.98	G	P		P	A	A	F	P	P	F	P	F
20X-CC	189.62	VG	P		P	A	A	F	P	P	F	P	F
21X-CC	199.13	G	P		P	A	A	F	P	P	F	P	F
22X-CC	208.93	VG	P		P	A	A	F	P	P	F	P	F
23X-CC	218.43	VG	P	P	P	F	A	F	P	P	A	A	F
24X-CC	227.06	G	P	A	P	A	F	F	P	P	A	A	P
25X-CC	233.19	G	P	F	P	F	F	P	P	P	F	P	P
26X-CC	246.09	P	P		P	P	P	P	P	P	P	P	P
27X-CC	255.14	M	P	F		A	P	P	P	P	P	P	P
28X-CC	258.69	M	P										P



Table T11. Abundance and preservation of benthic foraminifers, Site U1410. (Continued on next page.)

Core, section, interval (cm)	Depth (mbsf)	Preservation	Abundance
342-U1410A-			
4H-1W, 100–102	28.51	G F	
4H-2W, 100–102	30.01	M F	
4H-3W, 100–102	31.51	G F	
4H-4W, 100–102	33.01	M P	
4H-5W, 100–102	34.51	P F	
4H-6W, 100–102	36.01	G P	
5H-1W, 100–102	38.01	M P	
5H-2W, 100–102	39.51	G P	
5H-3W, 100–102	41.01	M P	
5H-4W, 100–102	42.51	B	
5H-5W, 100–102	44.01	P	
5H-6W, 90–92	45.41	M P	
6H-2W, 100–102	49.01	P D	
6H-4W, 100–102	52.01	P D	
6H-6W, 100–102	55.01	P D	
7H-2W, 100–102	58.53	P D	
7H-5W, 100–102	61.90	M A	
7H-7W, 28–30	63.84	B	
7H-7W, 100–102	64.56	G P	
8H-1W, 110–112	66.61	G P	
8H-2W, 110–112	68.11	VG P	
8H-3W, 110–112	69.61	G P	
8H-4W, 110–112	71.11	VG P	
8H-5W, 110–112	72.61	G P	
8H-6W, 110–112	74.11	G P	
9H-2W, 110–112	77.61	VG P	
9H-5W, 110–112	81.26	G P	
10H-2W, 45–47	85.46	G P	
10H-3W, 90–92	86.59	VG P	
10H-4W, 90–92	88.06	G P	
10H-5W, 90–92	89.16	G P	
10H-6W, 90–92	90.56	VG P	
10H-7W, 90–92	91.97	G P	
11H-2W, 100–102	96.51	VG P	
11H-5W, 105–107	101.06	VG P	
12H-2W, 100–102	106.01	G P	
12H-5W, 100–102	110.51	G P	
13H-2W, 100–102	114.48	VG P	
13H-5W, 100–102	118.98	VG P	
15H-2W, 58–60	134.07	VG P	
15H-4W, 60–62	137.09	VG P	
16H-2W, 120–122	144.21	G P	
16H-4W, 94–96	146.95	G P	
17X-2W, 110–112	153.61	VG P	
17X-4W, 120–122	156.71	VG P	
18X-2W, 100–102	163.11	G P	
18X-4W, 100–102	166.11	VG P	
18X-6W, 100–102	169.11	VG P	
19X-2W, 100–102	172.71	VG P	
19X-4W, 100–102	175.71	VG P	
20X-2W, 100–102	182.31	VG P	
20X-4W, 100–102	185.31	G P	
21X-2W, 100–102	191.05	VG P	
21X-4W, 100–102	194.01	VG P	
22X-2W, 100–102	201.51	G P	
22X-5W, 100–102	206.01	G P	
23X-2W, 67–69	210.68	G P	
23X-5W, 102–104	215.53	VG P	
24X-2W, 52–54	220.03	G P	
24X-5W, 37–38	224.38	G P	



Table T11 (continued).

Core, section, interval (cm)	Depth (mbsf)	Preservation	Abundance
25X-2W, 86–88	229.87	G	P
25X-4W, 13–15	232.14	M	P
26X-2W, 114–115	239.75	M	P
26X-5W, 97–98	244.08	M	P
27X-2W, 71–72	248.92	P	P
27X-5W, 12–13	252.83	P	P

Preservation: VG = very good, G = good, M = moderate, P = poor. Abundance: D = dominant, A = abundant, F = few, P = present, B = barren.

Table T12. Core orientation data, Site U1410.

Hole U1410A		Hole U1410B	
Core	MTF (°)	Core	MTF (°)
342-U1410A-		342-U1410B-	
1H	129	1H	158
2H	198	2H	140
3H	311	3H	158
4H	34	4H	119
5H	273	5H	118
6H	342	6H	359
7H	228	7H	216
8H	211	8H	42
9H	144	9H	293
10H	288	10H	39
11H	159	11H	225
12H	317	12H	133
13H	52	13H	356
14H	123	14H	259
15H	7	15H	41
16H	330	16H	104
		17H	166
		18H	96

MTF = magnetic tool face orientation from geomagnetic north.



Table T13. Summary of AF demagnetization results for discrete samples, Hole U1410A. (Continued on next page.)

Core, section, interval (cm)	Depth (mbsf)	Declination 20 mT or PCA (°)	Inclination 20 mT or PCA (°)	PCA MAD (°)	PCA range (mT)	NRM 20 mT (A/m)	Measurement error (%)
342-U1410A-							
2H-3W, 75–77	12.26	227.9	-39.6			1.68E-03	3.3
3H-4W, 75–77	23.26	-87.1	-64.8	5.3	20–60	6.60E-03	4.7
3H-6W, 75–77	26.26	-65.5	33.2			9.16E-03	5.6
4H-3W, 75–77	31.26	203.9	-71.1			1.49E-02	3.5
4H-5W, 75–77	34.26	-30.0	66.7			5.31E-04	3.7
5H-1W, 75–77	37.76	-73.6	-23.1			6.99E-05	14.6
5H-2W, 75–77	39.26	14.6	53.4			6.53E-05	7.8
5H-3W, 75–77	40.76	222.0	-7.8			1.53E-04	12.3
5H-4W, 75–77	42.26	6.3	67.6			2.31E-03	4.2
5H-5W, 75–77	43.76	262.9	41.2			1.12E-03	4.5
5H-6W, 50–52	45.01	211.1	-48.4			3.58E-03	5.5
6H-2W, 75–77	48.76	13.3	35.2			2.37E-04	4.2
6H-3W, 75–77	50.26	201.1	-72.5			5.26E-03	3.7
6H-4W, 75–77	51.76	-30.3	65.1			4.26E-03	2.8
6H-5W, 75–77	53.26	21.9	66.9	5.4	10–40	4.04E-03	2.5
7H-1W, 74–76	56.75	-84.5	37.9			2.03E-02	3.7
7H-2W, 74–76	58.27	-83.0	18.2			1.19E-02	3.5
7H-3W, 28–30	59.34	222.9	42.2			4.21E-03	4.7
7H-4W, 54–56	60.22	204.9	40.8	4.1	20–60	4.30E-03	4.7
7H-5W, 54–56	61.44	156.5	-10.5			3.39E-03	6.7
7H-6W, 74–76	62.78	263.2	20.0			3.54E-03	3.1
7H-7W, 74–76	64.30	196.5	55.3			1.47E-04	6.4
8H-1W, 72–74	66.23	-29.4	58.0			1.09E-04	4.3
8H-2W, 74–76	67.75	-31.6	51.1			1.78E-03	5.6
8H-3W, 74–76	69.25	209.6	40.0			1.01E-03	4.7
8H-4W, 74–76	70.75	221.9	35.4			2.13E-03	4.1
8H-5W, 74–76	72.25	-39.4	54.0			6.34E-03	4.9
8H-6W, 74–76	73.75	-26.5	53.2	5.4	20–60	8.44E-03	4.7
8H-7W, 20–22	74.71	-29.9	57.3			8.24E-03	4.7
9H-1W, 119–121	76.20	71.2	54.7			1.15E-02	4.1
9H-2W, 74–76	77.25	99.3	44.8			8.67E-03	4.8
9H-3W, 32–34	78.33	123.7	57.4	0.7	30–60	4.84E-03	3.9
9H-4W, 74–76	79.40	-5.9	41.1			1.04E-03	3.9
9H-5W, 74–76	80.90	-49.2	58.2			2.82E-03	4.2
9H-6W, 74–76	82.40	109.1	6.1			1.57E-04	11.1
9H-7W, 41–43	83.57	113.9	18.7			7.85E-03	6.1
10H-2W, 49–51	85.50	130.5	70.1			3.37E-03	3.2
10H-3W, 99–101	86.68	71.7	31.5	7.6	20–60	6.64E-04	5.7
10H-4W, 77–79	87.93	-50.7	16.4			2.73E-03	4.3
10H-5W, 65–67	88.91	-68.5	10.4			4.28E-03	4.6
10H-6W, 65–67	90.31	205.1	66.3			2.21E-03	3.5
10H-7W, 50–52	91.57	257.0	13.2			1.24E-03	7.0
11H-1W, 74–76	94.75	180.5	40.3			3.14E-03	3.3
11H-2W, 73–75	96.24	185.5	-26.9	1.9	20–60	4.32E-03	3.3
11H-3W, 82–84	97.83	29.5	61.0			3.66E-05	25.4
11H-4W, 74–76	99.25	-2.1	56.9			4.53E-03	3.5
11H-5W, 74–76	100.75	-24.7	59.2			2.98E-03	3.9
11H-6W, 57–59	102.08	-31.3	72.3			9.98E-04	3.8
11H-7W, 26–28	102.88	168.4	-20.1			4.19E-05	16.0
12H-1W, 110–112	104.61	159.9	64.7			4.80E-04	3.2
12H-2W, 74–76	105.75	113.2	-57.5			8.47E-05	8.8
12H-3W, 74–76	107.25	-79.3	-84.2			3.69E-05	21.1
12H-4W, 74–76	108.75	173.0	-14.8			8.82E-04	4.7
12H-5W, 74–76	110.25	244.3	-38.2			3.95E-04	12.3
12H-6W, 80–82	111.81	167.0	-52.7			3.56E-04	4.6
13H-2W, 74–76	114.22	146.7	-28.1			1.93E-04	4.1
13H-3W, 74–76	115.72	169.7	-33.3			1.84E-03	5.9
13H-4W, 74–76	117.22	159.0	-47.4			5.27E-04	4.5
13H-5W, 74–76	118.72	208.8	-52.1			9.58E-05	9.7
13H-6W, 74–76	120.22	162.3	-43.3			1.96E-04	5.1
13H-7W, 74–76	121.72	23.7	52.3			1.43E-04	6.9
14H-1W, 74–76	123.25	-0.5	50.5			2.79E-04	4.5
14H-3W, 74–76	126.25	39.8	41.4			2.01E-03	4.9
14H-4W, 68–70	127.69	14.7	45.9			3.48E-04	5.6
14H-5W, 74–76	129.25	-3.6	42.1	8.4	20–60	2.50E-04	5.7



Table T13 (continued).

Core, section, interval (cm)	Depth (mbsf)	Declination 20 mT or PCA (°)	Inclination 20 mT or PCA (°)	PCA MAD (°)	PCA range (mT)	NRM 20 mT (A/m)	Measurement error (%)
14H-6W, 54–56	130.55	38.8	48.9			6.30E–04	5.9
15H-3W, 75–77	135.74	39.8	54.8			1.87E–04	2.1
15H-5W, 75–77	138.74	39.7	28.1	10.0	20–60	1.45E–04	3.3
16H-1W, 75–77	142.26	25.4	58.8			2.09E–04	2.5
16H-3W, 75–77	145.26	–23.5	22.8	5.2	10–60	1.17E–04	7.1
16H-5W, 75–77	148.26	–64.0	10.1			1.70E–04	10.7
16H-7W, 25–27	150.62	81.9	53.0			5.34E–05	6.8
17X-2W, 70–72	153.21	227.4	–73.9			3.04E–05	15.1
17X-4W, 75–77	156.26	14.8	–18.5			4.54E–05	1.0
17X-6W, 52–54	159.03	–19.8	–48.4			5.16E–05	12.7
18X-2W, 75–77	162.86	148.8	–65.5			2.79E–05	16.3
18X-4W, 75–77	165.86	84.6	–27.7			6.26E–05	7.5
18X-6W, 55–57	168.66	24.0	–31.3			7.59E–05	9.9
19X-2W, 75–77	172.46	213.4	–32.6			1.04E–04	9.1
19X-4W, 75–77	175.46	–60.3	–49.5	7.6	10–60	1.80E–04	6.1
19X-6W, 75–77	178.46	19.7	–38.3			2.84E–04	4.4
20X-2W, 81–83	182.12	–73.3	–24.2			1.25E–04	9.2
20X-4W, 77–79	185.08	220.2	–43.9	8.0	20–40	1.14E–04	5.3
20X-6W, 65–67	187.96	–88.0	–53.5			3.40E–05	11.0
21X-2W, 77–79	190.82	207.3	–50.2			1.57E–04	5.2
21X-4W, 42–44	193.43	75.7	50.6			9.21E–05	2.3
21X-6W, 90–92	196.78	14.0	–33.7			4.22E–05	15.6
21X-7W, 62–64	198.00	174.1	29.2			4.80E–05	11.1
22X-1W, 74–76	199.75	–57.1	29.7			4.96E–05	19.3
22X-2W, 76–78	201.27	11.8	59.1			1.57E–04	6.6
22X-4W, 67–69	204.18	211.2	49.1			7.46E–05	11.3
22X-6W, 72–74	207.23	–42.2	33.8			3.47E–05	17.0
23X-2W, 109–111	211.10	128.0	68.4			1.41E–05	26.3
23X-4W, 93–95	213.94	82.6	15.1			1.26E–04	1.7
23X-6W, 92–94	216.93	168.3	51.0			2.45E–04	3.4
23X-7W, 9–11	217.60	91.5	76.4			3.36E–04	3.8
24X-1W, 51–53	218.52	66.2	–51.7			8.62E–05	4.9
24X-2W, 75–77	220.26	–79.0	–64.1			4.78E–05	18.2
24X-4W, 52–54	223.03	4.7	–49.3			5.45E–05	11.0
24X-6W, 97–99	226.48	–89.7	–54.9			7.75E–05	13.2
25X-1W, 67–69	228.18	150.6	–56.0			4.85E–05	13.5
25X-3W, 84–86	231.35	32.1	–43.0			7.12E–05	14.3
26X-3W, 69–71	240.80	–76.8	–40.6	2.1	20–40	6.79E–04	6.7
26X-5W, 95–97	244.06	201.8	–49.1			5.13E–04	4.8
27X-1W, 104–106	247.75	34.8	65.9			9.51E–04	1.1
27X-3W, 46–48	250.17	–71.3	–8.9			6.95E–04	8.5
27X-5W, 74–76	253.45	29.2	–44.5			2.58E–04	4.0
28X-1W, 96–98	257.27	–69.8	14.6			7.30E–04	6.9
28X-2W, 41–43	258.22	248.1	38.3			8.90E–04	4.4

Declinations for Cores 2H to 16H are in geographic coordinates. PCA = principal component analysis, MAD = maximum angle of deviation, NRM = natural remanent magnetism.



Table T14. Magnetostratigraphic tie points, Site U1410.

Chron boundary	Age (Ma)	Top		Bottom		Midpoint (mbsf)
		Core, section, interval (cm)	Depth (mbsf)	Core, section, interval (cm)	Depth (mbsf)	
Hole U1410A						
C1n (Brunhes)/C1r.1r (Matuyama)	0.781	2H-2, 140.0	11.4	2H-3, 10.0	11.6	11.50
C1r.1r (Matuyama)/C1r.1n (Jaramillo)	0.988	2H-3, 140.0	12.90	2H-4, 10.0	13.10	13.00
C1r.1n (Jaramillo)/C1r.2r	1.072	2H-4, 42.5	13.43	2H-4, 55.0	13.53	13.48
C1r.2r/C1r.2n (Cobb Mountain)	1.173	2H-4, 72.5	13.73	2H-4, 85.0	13.85	13.79
C1r.2n (Cobb Mountain)/C1r.3r	1.185	2H-4, 125.0	14.25	2H-4, 140.0	14.40	14.33
C1r.3r/C2n (Olduvai)	1.778	2H-6, 100.0	17.00	2H-6, 126.0	17.25	17.13
C2n (Olduvai)/C2r.1r	1.945	NI	NI	NI	NI	NI
C2r.1r/C2r.1n (Reunion)	2.128	NI	NI	NI	NI	NI
C2r.1n (Reunion)/C2r.2r	2.148	NI	NI	NI	NI	NI
C2r.2r/C2An.1n (Gauss)	2.581	4H-4, 65.0	32.65	4H-4, 122.5	33.25	32.95
C18n.1n/C18n.1r	39.627	8H-2, 110.0	68.10	8H-3, 75.0	69.25	68.68
C18n.1r/C18n.2n	39.698	8H-4, 75.0	70.25	8H-5, 75.0	72.25	71.25
C18n.2n/C18r	40.145	9H-4, 75.0	79.40	9H-5, 75.0	80.90	80.15
C18r/C19n	41.154	11H-2, 120.0	96.70	11H-2, 140.0	96.90	96.80
C19n/C19r	41.390	11H-6, 58.0	102.08	11H-7, 27.0	102.88	102.48
C19r/C20n	42.301	13H-7, 40.0	121.37	13H-7, 75.0	121.72	121.55
C20n/C20r	43.432	16H-7, 26.0	150.62	17X-1, 92.0	151.92	151.27
C20r/C21n	45.724	21X-6, 91.0	196.78	21X-7, 63.0	198.00	197.39
C21n/C21r	47.349	23X-7, 10.0	217.60	24X-1, 52.0	218.52	218.06
Hole U1410B						
C1n (Brunhes)/C1r.1r (Matuyama)	0.781	2H-5, 10.0	9.90	2H-5, 25.0	10.05	9.98
C1r.1r (Matuyama)/C1r.1n (Jaramillo)	0.988	NI	NI	NI	NI	NI
C1r.1n (Jaramillo)/C1r.2r	1.072	NI	NI	NI	NI	NI
C1r.2r/C1r.2n (Cobb Mountain)	1.173	NI	NI	NI	NI	NI
C1r.2n (Cobb Mountain)/C1r.3r	1.185	NI	NI	NI	NI	NI
C1r.3r/C2n (Olduvai)	1.778	3H-2, 122.5	15.64	3H-3, 10.0	16.01	15.83
C2n (Olduvai)/C2r.1r	1.945	NI	NI	NI	NI	NI
C2r.1r/C2r.1n (Reunion)	2.128	NI	NI	NI	NI	NI
C2r.1n (Reunion)/C2r.2r	2.148	NI	NI	NI	NI	NI
C2r.2r/C2An.1n (Gauss)	2.581	5H-1, 127.5	32.58	5H-2, 32.5	33.13	32.86
C18n.1n/C18n.1r	39.627	9H-2, 22.5	68.25	9H-3, 35.0	70.15	69.20
C18n.1r/C18n.2n	39.698	9H-3, 132.5	71.13	9H-6, 40.0	74.70	72.92
C18n.2n/C18r	40.145	10H-5, 132.5	83.63	10H-6, 17.5	83.98	83.81
C18r/C19n	41.154	12H-3, 55.0	94.35	12H-4, 115.0	96.45	95.40
C19n/C19r	41.390	13H-1, 130.0	101.60	13H-2, 35.0	102.15	101.88
C19r/C20n	42.301	15H-1, 120.0	120.50	15H-2, 12.5	120.93	120.72
C20n/C20r	43.432	NI	NI	NI	NI	NI
C20r/C21n	45.724	NI	NI	NI	NI	NI
C21n/C21r	47.349	NI	NI	NI	NI	NI
Hole U1410C						
C1n (Brunhes)/C1r.1r (Matuyama)	0.781	NI	NI	NI	NI	NI
C1r.1r (Matuyama)/C1r.1n (Jaramillo)	0.988	NI	NI	NI	NI	NI
C1r.1n (Jaramillo)/C1r.2r	1.072	NI	NI	NI	NI	NI
C1r.2r/C1r.2n (Cobb Mountain)	1.173	2H-4, 22.5	11.53	2H-4, 40.0	11.70	11.62
C1r.2n (Cobb Mountain)/C1r.3r	1.185	2H-4, 77.5	12.08	2H-4, 87.5	12.18	12.13
C1r.3r/C2n (Olduvai)	1.778	3H-4, 22.5	21.03	3H-4, 42.5	21.23	21.13
C2n (Olduvai)/C2r.1r	1.945	NI	NI	NI	NI	NI
C2r.1r/C2r.1n (Reunion)	2.128	NI	NI	NI	NI	NI
C2r.1n (Reunion)/C2r.2r	2.148	NI	NI	NI	NI	NI
C2r.2r/C2An.1n (Gauss)	2.581	4H-4, 140.0	31.70	4H-5, 10.0	31.90	31.80
C18n.1n/C18n.1r	39.627	8H-4, 140.0	69.70	8H-4, 10.0	71.40	70.55
C18n.1r/C18n.2n	39.698	NI	NI	NI	NI	NI
C18n.2n/C18r	40.145	9H-5, 137.5	80.68	9H-6, 20.0	81.00	80.84
C18r/C19n	41.154	11H-4, 52.5	94.79	11H-4, 72.5	94.88	94.84
C19n/C19r	41.390	12H-2, 10.0	100.90	12H-2, 140.0	102.20	101.55
C19r/C20n	42.301	13H-7, 50.0	118.20	14H-1, 15.0	118.45	118.33
C20n/C20r	43.432	NI	NI	NI	NI	NI
C20r/C21n	45.724	NI	NI	NI	NI	NI
C21n/C21r	47.349	NI	NI	NI	NI	NI

Ages from Gradstein et al. (2012). NI = not identified.



Table T15. Summary of anisotropy of magnetic susceptibility of discrete samples, Hole U1410A. (Continued on next two pages.)

Core, section, interval (cm)	Depth (mbsf)	τ_3	V ₃ (°)		V ₂ (°)		V ₁ (°)		Declination	Inclination	Declination	Inclination	Declination	Inclination	susceptibility (SI)	Anisotropy (%)	<i>P</i>	<i>L</i>	<i>F</i>
			Declination	Inclination	Declination	Inclination	Declination	Inclination											
342-U1410A-																			
1H-3W, 75-77	3.76	0.3257	343.5	44.1	0.3342	245.8	7.8	0.3402	148.0	44.8	3.07E-04	1.4	1.045	1.018	1.026				
1H-5W, 60-62	6.61	0.3295	180.5	22.2	0.3325	89.4	2.7	0.3379	352.8	67.6	1.90E-04	0.8	1.026	1.016	1.009				
2H-1W, 75-77	9.26	0.3293	178.1	45.0	0.3325	271.4	3.3	0.3381	4.7	44.8	1.38E-04	0.9	1.027	1.017	1.010				
2H-3W, 75-77	12.26	0.3313	249.3	8.9	0.3323	76.3	81.1	0.3364	339.5	1.1	1.39E-04	0.5	1.015	1.012	1.003				
2H-5W, 75-77	15.26	0.3274	134.9	7.7	0.3330	30.4	61.6	0.3396	228.9	27.1	1.74E-04	1.2	1.037	1.020	1.017				
2H-7W, 35-37	17.86	0.3299	82.2	9.6	0.3336	348.2	22.8	0.3364	193.5	65.1	2.70E-04	0.6	1.020	1.008	1.011				
3H-1W, 75-77	18.76	0.3308	173.3	9.7	0.3329	263.4	0.5	0.3362	356.0	80.3	4.71E-04	0.5	1.016	1.010	1.006				
3H-3W, 75-77	21.76	0.3300	167.2	49.0	0.3340	76.6	0.6	0.3360	346.1	41.0	2.21E-04	0.6	1.018	1.006	1.012				
3H-5W, 75-77	24.76	0.3259	242.9	7.1	0.3353	141.8	57.1	0.3388	337.3	32.0	6.73E-04	1.3	1.040	1.010	1.029				
3H-7W, 35-37	27.36	0.3321	179.3	42.3	0.3330	78.0	12.2	0.3349	335.5	45.2	5.15E-04	0.3	1.009	1.006	1.003				
4H-1W, 75-77	28.26	0.3283	133.1	83.5	0.3346	280.3	5.5	0.3372	10.6	3.5	4.87E-04	0.9	1.027	1.008	1.019				
4H-3W, 75-77	31.26	0.3308	100.1	74.8	0.3339	240.5	11.8	0.3353	332.5	9.4	6.43E-04	0.5	1.014	1.004	1.009				
4H-5W, 75-77	34.26	0.3309	85.8	11.9	0.3329	217.9	72.5	0.3361	353.1	12.6	1.82E-04	0.5	1.016	1.010	1.006				
4H-7W, 35-37	36.86	0.3287	90.3	67.9	0.3327	273.2	22.0	0.3386	182.8	1.0	9.59E-05	1.0	1.030	1.018	1.012				
5H-1W, 75-77	37.76	0.3284	230.9	70.0	0.3348	58.9	19.9	0.3368	328.0	2.6	9.17E-05	0.8	1.025	1.006	1.020				
5H-3W, 75-77	40.76	0.3301	229.9	8.7	0.3334	338.9	64.8	0.3365	136.1	23.5	8.93E-05	0.6	1.020	1.009	1.010				
5H-5W, 75-77	43.76	0.3303	90.9	82.8	0.3341	264.2	7.1	0.3356	354.3	0.8	2.54E-04	0.5	1.016	1.005	1.011				
5H-7W, 25-27	45.87	0.3297	218.3	76.0	0.3344	335.0	6.4	0.3359	66.4	12.4	2.94E-04	0.6	1.019	1.004	1.014				
6H-1W, 100-102	47.51	0.3312	180.5	80.4	0.3339	298.8	4.6	0.3350	29.5	8.5	2.66E-04	0.4	1.011	1.003	1.008				
6H-3W, 75-77	50.26	0.3300	119.3	77.2	0.3340	294.2	12.8	0.3360	24.5	1.1	2.20E-04	0.6	1.018	1.006	1.012				
6H-5W, 75-77	53.26	0.3296	191.1	86.3	0.3349	306.6	1.6	0.3355	36.7	3.3	4.14E-04	0.6	1.018	1.002	1.016				
6H-7W, 28-30	55.70	0.3295	102.4	63.6	0.3347	3.8	4.3	0.3358	271.7	26.0	1.18E-04	0.6	1.019	1.003	1.016				
7H-1W, 74-76	56.75	0.3304	114.7	69.6	0.3346	10.7	5.1	0.3350	278.9	19.7	2.33E-04	0.5	1.014	1.001	1.013				
7H-3W, 28-30	59.34	0.3298	135.4	70.2	0.3347	267.2	13.5	0.3355	0.7	14.2	1.62E-04	0.6	1.017	1.002	1.015				
7H-5W, 54-56	61.44	0.3298	119.4	70.7	0.3345	250.1	12.9	0.3357	343.4	14.1	2.13E-04	0.6	1.018	1.003	1.014				
7H-7W, 74-76	64.30	0.3305	167.9	69.5	0.3338	289.7	11.2	0.3357	23.2	17.0	9.06E-05	0.5	1.016	1.006	1.010				
8H-1W, 72-74	66.23	0.3276	125.1	85.3	0.3350	302.7	4.7	0.3374	32.7	0.2	7.92E-05	1.0	1.030	1.007	1.023				
8H-2W, 74-76	67.75	0.3307	15.4	85.0	0.3340	198.5	5.0	0.3353	108.5	0.3	8.11E-05	0.5	1.014	1.004	1.010				
8H-3W, 74-76	69.25	0.3311	145.4	48.9	0.3330	307.4	39.7	0.3359	45.0	9.0	6.97E-05	0.5	1.014	1.009	1.006				
8H-4W, 74-76	70.75	0.3299	198.2	80.6	0.3337	82.8	4.1	0.3364	352.2	8.5	1.34E-04	0.6	1.019	1.008	1.011				
8H-5W, 74-76	72.25	0.3319	101.9	52.4	0.3332	339.8	22.3	0.3349	236.9	28.6	1.15E-04	0.3	1.009	1.005	1.004				
8H-6W, 74-76	73.75	0.3317	74.1	45.6	0.3334	263.7	44.0	0.3348	169.0	4.9	1.25E-04	0.3	1.009	1.004	1.005				
8H-7W, 20-22	74.71	0.3319	149.0	52.8	0.3327	332.1	37.2	0.3354	241.0	1.5	1.23E-04	0.4	1.011	1.008	1.002				
9H-1W, 119-121	76.20	0.3295	234.9	59.9	0.3335	43.8	29.6	0.3370	136.5	4.8	1.63E-04	0.7	1.023	1.010	1.012				
9H-2W, 74-76	77.25	0.3312	227.1	57.0	0.3339	14.6	28.7	0.3349	112.9	14.9	1.69E-04	0.4	1.011	1.003	1.008				
9H-3W, 32-34	78.33	0.3303	54.2	78.4	0.3336	281.9	7.9	0.3361	190.7	8.5	1.14E-04	0.6	1.018	1.007	1.010				
9H-4W, 74-76	79.40	0.3273	215.6	67.6	0.3353	120.6	2.0	0.3374	29.8	22.3	9.39E-05	1.0	1.031	1.006	1.025				
9H-5W, 74-76	80.90	0.3316	51.2	72.7	0.3336	219.8	17.0	0.3349	310.8	3.2	1.05E-04	0.3	1.010	1.004	1.006				
9H-6W, 74-76	82.40	0.3278	159.5	77.6	0.3352	260.5	2.4	0.3371	351.1	12.2	8.03E-05	0.9	1.028	1.006	1.023				
9H-7W, 41-43	83.57	0.3314	199.6	80.0	0.3340	33.9	9.7	0.3345	303.5	2.4	1.50E-04	0.3	1.009	1.002	1.008				
10H-2W, 49-51	85.50	0.3323	173.2	82.5	0.3334	295.4	4.0	0.3343	25.9	6.4	1.70E-04	0.2	1.006	1.003	1.003				
10H-3W, 99-101	86.68	0.3327	289.1	6.2	0.3334	24.3	39.4	0.3340	191.7	49.9	1.45E-04	0.1	1.004	1.002	1.002				
10H-4W, 77-79	87.93	0.3304	120.4	69.8	0.3341	270.4	17.6	0.3354	3.4	9.5	1.09E-04	0.5	1.015	1.004	1.011				
10H-5W, 65-67	88.91	0.3305	97.9	80.4	0.3343	339.8	4.6	0.3352	249.1	8.5	1.24E-04	0.5	1.014	1.003	1.012				
10H-6W, 65-67	90.31	0.3309	245.9	81.6	0.3341	59.1	8.4	0.3350	149.2	1.0	1.15E-04	0.4	1.013	1.003	1.010				
10H-7W, 50-52	91.57	0.3326	20.8	76.0	0.3333	145.9	8.1	0.3341	237.5	11.3	1.06E-04	0.2	1.005	1.002	1.002				
11H-1W, 74-76	94.75	0.3316	70.3	82.1	0.3339	281.9	6.7	0.3345	191.5	4.1	1.30E-04	0.3	1.009	1.002	1.007				
11H-2W, 73-75	96.24	0.3325	127.9	81.6	0.3333	281.5	7.6	0.3342	12.0	3.7	1.29E-04	0.2	1.005	1.003	1.003				
11H-3W, 82-84	97.83	0.3284	310.7	80.4	0.3344	107.2	8.9	0.3372	197.8	3.8	4.28E-05	0.9	1.027	1.008	1.018				

Table T15 (continued). (Continued on next page.)

Core, section, interval (cm)	Depth (mbsf)	τ_3	V ₃ (°)		V ₂ (°)		V ₁ (°)		Bulk susceptibility (SI)	Anisotropy (%)	P	L	F		
			Declination	Inclination	Declination	Inclination	Declination	Inclination							
11H-4W, 74–76	99.25	0.3300	239.1	81.5	0.3342	353.8	3.6	0.3358	84.3	7.7	1.25E-04	0.6	1.017	1.005	1.013
11H-5W, 74–76	100.75	0.3303	222.7	72.0	0.3337	100.4	9.9	0.3360	7.7	14.9	9.98E-05	0.6	1.017	1.007	1.010
11H-6W, 57–59	102.08	0.3307	99.7	88.3	0.3330	269.1	1.7	0.3363	359.1	0.3	1.01E-04	0.6	1.017	1.010	1.007
11H-7W, 26–28	102.88	0.3288	164.4	76.5	0.3349	27.5	9.9	0.3364	295.9	9.0	5.77E-05	0.8	1.023	1.004	1.019
12H-1W, 110–112	104.61	0.3310	355.5	76.1	0.3335	254.1	2.8	0.3355	163.4	13.7	8.07E-05	0.4	1.013	1.006	1.007
12H-2W, 74–76	105.75	0.3279	293.8	74.8	0.3335	113.7	15.2	0.3386	203.7	0.0	6.46E-05	1.1	1.033	1.015	1.017
12H-3W, 74–76	107.25	0.3287	119.8	81.5	0.3346	271.5	7.5	0.3367	2.0	4.0	8.35E-05	0.8	1.024	1.006	1.018
12H-5W, 74–76	110.25	0.3298	357.7	65.2	0.3332	205.8	22.2	0.3370	111.5	10.6	7.34E-05	0.7	1.022	1.012	1.010
12H-6W, 80–82	111.81	0.3314	93.4	61.9	0.3329	222.7	18.7	0.3357	319.9	20.2	6.75E-05	0.4	1.013	1.009	1.004
12H-7W, 35–37	112.86	0.3286	160.8	59.5	0.3346	339.5	30.5	0.3368	69.8	0.6	7.04E-05	0.8	1.025	1.007	1.018
13H-2W, 74–76	114.22	0.3288	94.9	87.7	0.3344	213.6	1.1	0.3367	303.6	2.0	8.61E-05	0.8	1.024	1.007	1.017
13H-3W, 74–76	115.72	0.3296	105.4	45.4	0.3333	329.6	35.2	0.3371	221.7	23.6	1.12E-04	0.8	1.023	1.011	1.011
13H-4W, 74–76	117.22	0.3296	229.6	60.6	0.3330	48.9	29.4	0.3374	139.1	0.3	1.18E-04	0.8	1.024	1.013	1.010
13H-5W, 74–76	118.72	0.3294	49.2	77.8	0.3345	236.3	12.1	0.3362	146.0	1.5	9.18E-05	0.7	1.021	1.005	1.016
13H-6W, 74–76	120.22	0.3302	239.9	82.1	0.3324	66.9	7.9	0.3374	336.8	1.0	8.88E-05	0.7	1.022	1.015	1.006
13H-7W, 74–76	121.72	0.3300	267.9	59.2	0.3327	107.7	29.3	0.3373	12.8	8.7	8.42E-05	0.7	1.022	1.014	1.008
14H-1W, 74–76	123.25	0.3297	133.0	62.0	0.3342	286.1	25.4	0.3361	21.4	11.1	7.43E-05	0.6	1.019	1.006	1.013
14H-2W, 74–76	124.75	0.3286	286.5	50.0	0.3351	34.9	14.9	0.3363	136.1	36.2	6.73E-05	0.8	1.023	1.003	1.020
14H-3W, 74–76	126.25	0.3311	79.9	83.2	0.3340	255.1	6.8	0.3349	345.1	0.6	1.25E-04	0.4	1.011	1.003	1.009
14H-4W, 68–70	127.69	0.3300	249.3	69.2	0.3323	104.1	17.3	0.3377	10.6	11.2	6.62E-05	0.8	1.023	1.016	1.007
14H-5W, 74–76	129.25	0.3320	273.4	30.0	0.3336	5.9	4.4	0.3344	103.3	59.6	8.93E-05	0.2	1.007	1.003	1.005
14H-6W, 54–56	130.55	0.3313	250.0	53.8	0.3339	116.9	26.5	0.3348	14.9	22.7	7.76E-05	0.3	1.010	1.003	1.008
14H-7W, 30–32	131.53	0.3318	87.3	55.8	0.3322	275.8	33.9	0.3359	183.1	4.0	9.93E-05	0.4	1.012	1.011	1.001
15H-2W, 75–77	134.24	0.3309	86.7	54.2	0.3342	242.8	33.4	0.3349	340.5	11.4	1.11E-04	0.4	1.012	1.002	1.010
15H-3W, 75–77	135.74	0.3293	66.9	82.3	0.3344	276.5	6.7	0.3363	186.1	3.8	9.65E-05	0.7	1.021	1.006	1.015
15H-4W, 75–77	137.24	0.3312	42.0	70.9	0.3338	158.7	8.8	0.3350	251.4	16.8	7.17E-05	0.4	1.011	1.003	1.008
15H-5W, 75–77	138.74	0.3305	83.7	80.5	0.3343	284.6	8.9	0.3352	194.1	3.3	9.91E-05	0.5	1.014	1.003	1.012
15H-6W, 40–42	139.89	0.3304	48.4	61.1	0.3335	185.7	22.1	0.3361	283.2	17.7	1.06E-04	0.6	1.017	1.008	1.009
15H-7W, 30–32	140.80	0.3300	77.9	68.4	0.3342	266.7	21.4	0.3358	175.5	3.0	1.06E-04	0.6	1.018	1.005	1.013
16H-1W, 75–77	142.26	0.3285	123.5	56.2	0.3345	253.8	23.4	0.3370	354.3	23.0	7.67E-05	0.8	1.026	1.007	1.018
16H-2W, 75–77	143.76	0.3306	65.2	49.2	0.3329	227.3	39.4	0.3365	324.7	9.0	8.83E-05	0.6	1.018	1.011	1.007
16H-3W, 75–77	145.26	0.3293	292.5	76.1	0.3329	93.9	13.2	0.3378	184.9	4.3	9.08E-05	0.9	1.026	1.015	1.011
16H-4W, 75–77	146.76	0.3300	194.7	74.1	0.3329	292.3	2.2	0.3370	22.9	15.8	9.69E-05	0.7	1.021	1.012	1.009
16H-5W, 75–77	148.26	0.3291	16.5	67.2	0.3337	106.5	0.0	0.3372	196.5	22.8	8.44E-05	0.8	1.024	1.010	1.014
16H-6W, 60–62	149.61	0.3312	315.2	47.5	0.3335	76.6	25.5	0.3353	183.5	31.4	8.67E-05	0.4	1.012	1.005	1.007
16H-7W, 25–27	150.62	0.3306	76.0	76.2	0.3337	202.1	8.3	0.3357	293.7	11.0	9.70E-05	0.5	1.015	1.006	1.009
17X-1W, 91–93	151.92	0.3250	250.2	48.9	0.3363	95.2	38.3	0.3386	355.0	12.6	6.97E-05	1.4	1.042	1.007	1.035
17X-2W, 70–72	153.21	0.3269	220.3	30.4	0.3349	12.8	56.5	0.3382	122.7	12.7	7.14E-05	1.1	1.035	1.010	1.025
17X-3W, 75–77	154.76	0.3308	312.3	59.6	0.3322	218.5	2.2	0.3370	127.2	30.3	6.48E-05	0.6	1.019	1.014	1.004
17X-5W, 119–121	158.20	0.3300	78.7	43.7	0.3347	272.1	45.5	0.3353	175.2	6.7	7.53E-05	0.5	1.016	1.002	1.014
17X-7W, 23–25	160.15	0.3292	275.7	60.4	0.3314	178.2	4.2	0.3394	85.9	29.2	6.11E-05	1.0	1.031	1.024	1.007
18X-1W, 90–92	161.51	0.3275	250.1	76.3	0.3350	58.1	13.4	0.3375	148.8	2.8	7.46E-05	1.0	1.030	1.007	1.023
18X-3W, 75–77	164.36	0.3255	288.2	43.1	0.3350	107.0	47.0	0.3395	197.6	0.6	5.44E-05	1.4	1.043	1.014	1.029
18X-5W, 75–77	167.36	0.3287	119.7	82.9	0.3348	341.8	5.3	0.3366	251.4	4.8	6.69E-05	0.8	1.024	1.005	1.019
18X-7W, 30–32	169.73	0.3300	99.9	47.1	0.3328	327.9	31.8	0.3372	220.8	25.5	8.04E-05	0.7	1.022	1.013	1.008
19X-1W, 83–85	171.04	0.3296	257.4	42.6	0.3348	142.1	24.9	0.3356	31.5	37.1	8.41E-05	0.6	1.018	1.003	1.016
19X-3W, 77–79	173.98	0.3293	248.7	84.8	0.3344	50.7	5.0	0.3363	140.8	1.6	7.31E-05	0.7	1.021	1.006	1.016
19X-5W, 75–77	176.96	0.3269	112.5	74.0	0.3356	328.9	13.0	0.3375	236.7	9.2	7.62E-05	1.1	1.032	1.005	1.027
19X-7W, 25–27	179.27	0.3295	147.0	85.8	0.3345	331.7	4.1	0.3360	241.7	0.3	6.91E-05	0.6	1.020	1.004	1.015
20X-2W, 81–83	182.12	0.3271	203.4	68.2	0.3354	78.2	13.0	0.3375	344.1	17.2	7.24E-05	1.0	1.032	1.006	1.025
20X-4W, 77–79	185.08	0.3294	42.3	85.7	0.3352	308.5	0.3	0.3354	218.5	4.3	8.67E-05	0.6	1.018	1.001	1.018

Table T15 (continued).

Core, section, interval (cm)	Depth (mbsf)	τ_3	V ₃ (°)		V ₂ (°)		V ₁ (°)		Bulk susceptibility (SI)	Anisotropy (%)	P	L	F		
			Declination	Inclination	Declination	Inclination	Declination	Inclination							
20X-6W, 65–67	187.96	0.3292	86.0	74.2	0.3349	237.9	14.0	0.3359	329.7	7.2	7.70E-05	0.7	1.020	1.003	1.017
21X-2W, 77–79	190.82	0.3293	159.9	69.1	0.3347	28.8	14.1	0.3360	294.9	15.1	8.77E-05	0.7	1.021	1.004	1.017
21X-4W, 42–44	193.43	0.3299	19.0	68.6	0.3343	131.2	8.4	0.3358	224.3	19.6	8.70E-05	0.6	1.018	1.005	1.013
21X-6W, 90–92	196.78	0.3286	322.1	68.8	0.3337	186.5	15.5	0.3377	92.5	14.2	8.32E-05	0.9	1.028	1.012	1.016
22X-2W, 76–78	201.27	0.3293	149.4	74.1	0.3345	334.2	15.9	0.3362	243.8	1.3	9.30E-05	0.7	1.021	1.005	1.016
22X-4W, 67–69	204.18	0.3292	332.9	82.7	0.3350	188.0	6.0	0.3358	97.5	4.2	8.72E-05	0.7	1.020	1.002	1.018
22X-6W, 72–74	207.23	0.3296	15.5	77.8	0.3344	245.1	8.0	0.3360	153.8	9.2	9.14E-05	0.6	1.019	1.005	1.015
23X-2W, 109–111	211.10	0.3308	84.8	3.4	0.3332	176.1	20.9	0.3361	346.1	68.8	8.24E-06	0.5	1.016	1.009	1.007
23X-4W, 93–95	213.94	0.3303	136.6	64.6	0.3344	35.3	5.3	0.3352	302.8	24.7	6.01E-05	0.5	1.015	1.002	1.012
23X-6W, 92–94	216.93	0.3313	208.6	68.4	0.3343	20.3	21.4	0.3344	111.4	2.9	6.56E-05	0.3	1.009	1.001	1.009
24X-4W, 52–54	223.03	0.3240	110.9	46.6	0.3374	16.1	4.5	0.3386	282.0	43.1	1.00E-05	1.5	1.045	1.003	1.041
24X-6W, 97–99	226.48	0.3151	354.4	38.8	0.3279	84.7	0.3	0.3570	175.1	51.2	4.47E-06	4.2	1.133	1.089	1.040
25X-4W, 58–60	232.59	0.3262	267.3	3.1	0.3347	160.0	79.6	0.3390	357.8	9.9	3.58E-06	1.3	1.039	1.013	1.026
26X-4W, 53–55	242.14	0.3309	252.9	14.9	0.3335	344.9	7.4	0.3357	100.6	73.3	1.64E-05	0.5	1.015	1.006	1.008
26X-6W, 77–79	245.38	0.3304	359.6	85.5	0.3345	228.5	2.9	0.3351	138.3	3.4	1.03E-04	0.5	1.014	1.002	1.012
27X-2W, 54–56	248.75	0.3315	292.1	72.6	0.3330	102.5	17.1	0.3356	193.3	2.8	3.01E-05	0.4	1.012	1.008	1.005
27X-4W, 93–95	252.14	0.3301	25.5	79.4	0.3346	211.5	10.6	0.3353	121.3	1.1	2.87E-05	0.5	1.016	1.002	1.014
28X-2W, 41–43	258.22	0.3309	103.3	87.3	0.3339	249.0	2.2	0.3352	339.0	1.5	3.40E-05	0.4	1.013	1.004	1.009

τ_1 , τ_2 , and τ_3 are eigenvalues, and V₃, V₂, and V₁ are eigenvectors associated with minimum, intermediate, and maximum susceptibility, respectively. Measurement field = 300 A/m, sample volume = 7 cm³. P = anisotropy degree, L = lineation, F = foliation.



Table T16. Datum tie points, Hole U1410A.

Datum tie point	Datum	Datum type	Zone	Age (Ma)	Midpoint depth (mbsf)	Distance (m)	Duration (Ma)	LSR (cm/k.y.)	Notes
D01	C1n (Brunhes)/C1r.1r (Matuyama)	Chron boundary		0.78	11.50	11.50	0.78	1.47	
D02	C1r.3r/C2n (Olduvai)	Chron boundary		1.78	17.13	5.63	1.00	0.56	
D03	T <i>Discoaster pentaradiatus</i>	Calcareous nannofossil	NN17	2.39	31.51	14.39	0.61	2.35	
D04	T <i>Discoaster hamatus</i>	Calcareous nannofossil	NN10	9.53	36.04	4.52	7.14	0.06	Condensed
D05	B <i>Discoaster hamatus</i>	Calcareous nannofossil	NN9	10.55	42.50	6.47	1.02	0.63	
D06	Tc <i>Sphenolithus belemnos</i>	Calcareous nannofossil	NN4	17.95	45.23	2.73	7.40	0.04	Condensed
D07	B <i>Sphenolithus belemnos</i>	Calcareous nannofossil		19.03	48.23	3.00	1.08	0.28	
D08	B <i>Discoaster druggii</i>	Calcareous nannofossil	NN2	22.82	51.50	3.27	3.79	0.09	Condensed
D09	T <i>Sphenolithus ciperoensis</i>	Calcareous nannofossil	NN1	24.43	51.50	0.00	1.61	0.00	Hiatus
D10	T <i>Sphenolithus distentus</i>	Calcareous nannofossil	NP25	26.84	57.88	6.38	2.41	0.26	Average rate =
D11	T <i>Reticulofenestra umbilicus</i> (>14 µm)	Calcareous nannofossil	NP23	32.02	64.21	6.34	5.18	0.12	0.17 cm/k.y.
D12	Inferred hiatus			39.40	64.21	0.00	7.38	0.00	Hiatus
D13	C19r/C20n	Chron boundary		42.30	121.55	57.34	2.90	1.98	
D14	C20n/C20r	Chron boundary		43.43	151.27	29.72	1.13	2.63	
D15	C20r/C21n	Chron boundary		45.72	197.39	46.99	2.29	2.05	
D16	C21n/C21r	Chron boundary		47.35	218.06	21.08	1.62	1.30	
D17	B <i>Lamptonium fabaeforme constrictum</i>	Radiolarian	RP9	50.05	239.65	20.31	2.70	0.75	Average rate =
D18	B <i>Coccolithus crassus</i> *	Calcareous nannofossil		51.64	250.62	10.97	1.59	0.69	0.66 cm/k.y.
D19	B <i>Buryella clinata</i>	Radiolarian	RP7	53.35	258.70	8.08	1.71	0.47	

* = From Agnini et. al. (2007) recalibrated to GTS2012. LSR = linear sedimentation rate. T = top, Tc = top common, B = base.



Table T17. Carbonate content and accumulation rates, Site U1410. (Continued on next three pages.)

Age (Ma)	LSR (cm/k.y.)	Dry density (g/cm ³)	CaCO ₃ (wt%)	MAR (g/cm ² /k.y.)	CAR (g/cm ² /k.y.)	nCAR (g/cm ² /k.y.)
0.2	1.47	0.96	33.17	1.41	0.47	0.95
0.4	1.47	0.89	34.19	1.31	0.45	0.86
0.6	1.47	1.26	49.29	1.86	0.92	0.94
0.8	0.56	1.04	48.22	0.59	0.28	0.30
1.0	0.56	1.02	54.70	0.58	0.31	0.26
1.2	0.56	0.93	43.72	0.53	0.23	0.30
1.4	0.56	0.82	14.87	0.46	0.07	0.40
1.6	0.56	0.85	30.09	0.48	0.14	0.34
1.8	2.35	0.93	46.04	2.19	1.01	1.18
2.0	2.35	0.91	43.08	2.14	0.92	1.22
2.2	2.35	0.99	27.43	2.33	0.64	1.69
2.4	0.06	1.06	14.81	0.07	0.01	0.06
2.6	0.06	1.06	12.86	0.07	0.01	0.06
2.8	0.06	1.05	12.54	0.07	0.01	0.06
3.0	0.06	1.04	12.22	0.07	0.01	0.06
3.2	0.06	1.03	11.90	0.07	0.01	0.06
3.4	0.06	1.02	11.58	0.06	0.01	0.06
3.6	0.06	1.01	11.26	0.06	0.01	0.06
3.8	0.06	1.01	10.93	0.06	0.01	0.06
4.0	0.06	1.02	10.59	0.07	0.01	0.06
4.2	0.06	1.03	10.25	0.07	0.01	0.06
4.4	0.06	1.05	9.90	0.07	0.01	0.06
4.6	0.06	1.06	9.56	0.07	0.01	0.06
4.8	0.06	1.08	9.22	0.07	0.01	0.06
5.0	0.06	1.09	8.88	0.07	0.01	0.06
5.2	0.06	1.11	8.54	0.07	0.01	0.06
5.4	0.06	1.12	8.20	0.07	0.01	0.07
5.6	0.06	1.14	7.86	0.07	0.01	0.07
5.8	0.06	1.15	7.51	0.07	0.01	0.07
6.0	0.06	1.16	7.17	0.07	0.01	0.07
6.2	0.06	1.17	6.84	0.07	0.01	0.07
6.4	0.06	1.14	6.54	0.07	0.01	0.07
6.6	0.06	1.12	6.23	0.07	0.00	0.07
6.8	0.06	1.10	5.93	0.07	0.00	0.07
7.0	0.06	1.07	5.63	0.07	0.00	0.06
7.2	0.06	1.05	5.32	0.07	0.00	0.06
7.4	0.06	1.03	5.02	0.07	0.00	0.06
7.6	0.06	1.00	4.71	0.06	0.00	0.06
7.8	0.06	0.98	4.41	0.06	0.00	0.06
8.0	0.06	0.95	4.10	0.06	0.00	0.06
8.2	0.06	0.93	3.80	0.06	0.00	0.06
8.4	0.06	0.91	3.49	0.06	0.00	0.06
8.6	0.06	0.89	4.21	0.06	0.00	0.05
8.8	0.06	0.89	5.88	0.06	0.00	0.05
9.0	0.06	0.88	7.54	0.06	0.00	0.05
9.2	0.06	0.88	9.21	0.06	0.01	0.05
9.4	0.06	0.87	10.88	0.06	0.01	0.05
9.6	0.63	0.87	11.97	0.55	0.07	0.48
9.8	0.63	0.86	8.48	0.54	0.05	0.50
10.0	0.63	0.91	12.68	0.57	0.07	0.50
10.2	0.63	0.94	16.00	0.60	0.10	0.50
10.4	0.63	0.91	7.37	0.58	0.04	0.54
10.6	0.04	0.90	3.80	0.03	0.00	0.03
10.8	0.04	0.90	3.54	0.03	0.00	0.03
11.0	0.04	0.90	3.27	0.03	0.00	0.03
11.2	0.04	0.90	3.00	0.03	0.00	0.03
11.4	0.04	0.90	2.74	0.03	0.00	0.03
11.6	0.04	0.90	2.47	0.03	0.00	0.03
11.8	0.04	0.90	2.21	0.03	0.00	0.03
12.0	0.04	0.90	1.94	0.03	0.00	0.03
12.2	0.04	0.90	1.67	0.03	0.00	0.03
12.4	0.04	0.90	1.41	0.03	0.00	0.03
12.6	0.04	0.90	1.14	0.03	0.00	0.03
12.8	0.04	0.90	0.88	0.03	0.00	0.03
13.0	0.04	0.90	0.99	0.03	0.00	0.03
13.2	0.04	0.91	1.88	0.03	0.00	0.03
13.4	0.04	0.91	2.79	0.03	0.00	0.03
13.6	0.04	0.91	3.70	0.03	0.00	0.03
13.8	0.04	0.91	4.62	0.03	0.00	0.03



Table T17 (continued). (Continued on next page.)

Age (Ma)	LSR (cm/k.y.)	Dry density (g/cm ³)	CaCO ₃ (wt%)	MAR (g/cm ² /k.y.)	CAR (g/cm ² /k.y.)	nCAR (g/cm ² /k.y.)
14.0	0.04	0.91	5.53	0.03	0.00	0.03
14.2	0.04	0.92	6.44	0.03	0.00	0.03
14.4	0.04	0.92	7.35	0.03	0.00	0.03
14.6	0.04	0.92	8.27	0.03	0.00	0.03
14.8	0.04	0.92	9.18	0.03	0.00	0.03
15.0	0.04	0.92	10.09	0.03	0.00	0.03
15.2	0.04	0.93	11.00	0.03	0.00	0.03
15.4	0.04	0.93	11.91	0.03	0.00	0.03
15.6	0.04	0.93	12.83	0.03	0.00	0.03
15.8	0.04	0.93	13.74	0.03	0.01	0.03
16.0	0.04	0.93	14.65	0.03	0.01	0.03
16.2	0.04	0.93	15.56	0.03	0.01	0.03
16.4	0.04	0.94	16.48	0.03	0.01	0.03
16.6	0.04	0.94	17.37	0.04	0.01	0.03
16.8	0.04	0.94	17.69	0.03	0.01	0.03
17.0	0.04	0.93	17.72	0.03	0.01	0.03
17.2	0.04	0.93	17.76	0.03	0.01	0.03
17.4	0.04	0.92	17.80	0.03	0.01	0.03
17.6	0.04	0.92	17.83	0.03	0.01	0.03
17.8	0.04	0.91	17.87	0.03	0.01	0.03
18.0	0.28	0.91	17.90	0.25	0.05	0.21
18.2	0.28	0.89	17.66	0.25	0.04	0.20
18.4	0.28	0.85	16.87	0.24	0.04	0.20
18.6	0.28	0.81	15.46	0.23	0.04	0.19
18.8	0.28	0.78	12.64	0.22	0.03	0.19
19.0	0.28	0.74	9.77	0.21	0.02	0.19
19.2	0.09	0.71	7.25	0.06	0.00	0.06
19.4	0.09	0.72	7.32	0.06	0.01	0.06
19.6	0.09	0.73	7.91	0.06	0.01	0.06
19.8	0.09	0.75	8.50	0.06	0.01	0.06
20.0	0.09	0.76	9.08	0.07	0.01	0.06
20.2	0.09	0.77	9.67	0.07	0.01	0.06
20.4	0.09	0.79	10.26	0.07	0.01	0.06
20.6	0.09	0.80	10.84	0.07	0.01	0.06
20.8	0.09	0.81	11.43	0.07	0.01	0.06
21.0	0.09	0.82	11.53	0.07	0.01	0.06
21.2	0.09	0.82	10.52	0.07	0.01	0.06
21.4	0.09	0.82	9.47	0.07	0.01	0.06
21.6	0.09	0.81	8.42	0.07	0.01	0.06
21.8	0.09	0.81	7.37	0.07	0.01	0.07
22.0	0.09	0.80	6.32	0.07	0.00	0.07
22.2	0.09	0.80	5.27	0.07	0.00	0.07
22.4	0.09	0.79	4.22	0.07	0.00	0.07
22.6	0.09	0.79	3.17	0.07	0.00	0.07
22.8	0.09	0.79	2.96	0.07	0.00	0.07
23.0	0.00	0.81	3.32	0.00	0.00	0.00
23.2	0.00	0.82	3.69	0.00	0.00	0.00
23.4	0.00	0.83	4.06	0.00	0.00	0.00
23.6	0.00	0.85	4.43	0.00	0.00	0.00
23.8	0.00	0.86	4.79	0.00	0.00	0.00
24.0	0.00	0.87	5.16	0.00	0.00	0.00
24.2	0.00	0.88	5.53	0.00	0.00	0.00
24.4	0.00	0.90	5.90	0.00	0.00	0.00
24.6	0.27	0.91	6.26	0.24	0.02	0.23
24.8	0.27	0.92	6.63	0.24	0.02	0.23
25.0	0.27	0.94	6.80	0.25	0.02	0.23
25.2	0.27	0.95	6.47	0.25	0.02	0.24
25.4	0.27	0.96	6.11	0.25	0.02	0.24
25.6	0.27	0.96	6.30	0.25	0.02	0.24
25.8	0.27	0.93	7.27	0.25	0.02	0.23
26.0	0.27	0.91	8.69	0.24	0.02	0.22
26.2	0.27	0.91	11.60	0.24	0.03	0.21
26.4	0.27	0.94	11.81	0.25	0.03	0.22
26.6	0.27	1.00	10.24	0.26	0.03	0.24
26.8	0.27	1.05	8.75	0.28	0.02	0.25
27.0	0.12	1.07	10.07	0.13	0.01	0.12
27.2	0.12	1.06	12.75	0.13	0.02	0.11
27.4	0.12	1.04	15.44	0.13	0.02	0.11
27.6	0.12	1.03	18.12	0.13	0.02	0.10



Table T17 (continued). (Continued on next page.)

Age (Ma)	LSR (cm/k.y.)	Dry density (g/cm ³)	CaCO ₃ (wt%)	MAR (g/cm ² /k.y.)	CAR (g/cm ² /k.y.)	nCAR (g/cm ² /k.y.)
27.8	0.12	1.02	20.81	0.13	0.03	0.10
28.0	0.12	1.02	21.33	0.13	0.03	0.10
28.2	0.12	1.04	18.49	0.13	0.02	0.10
28.4	0.12	1.05	15.61	0.13	0.02	0.11
28.6	0.12	1.07	13.72	0.13	0.02	0.11
28.8	0.12	1.07	14.38	0.13	0.02	0.11
29.0	0.12	1.08	15.17	0.13	0.02	0.11
29.2	0.12	1.08	15.96	0.13	0.02	0.11
29.4	0.12	1.09	16.75	0.13	0.02	0.11
29.6	0.12	1.09	17.34	0.13	0.02	0.11
29.8	0.12	1.09	17.46	0.13	0.02	0.11
30.0	0.12	1.08	17.56	0.13	0.02	0.11
30.2	0.12	1.08	17.65	0.13	0.02	0.11
30.4	0.12	1.07	17.74	0.13	0.02	0.11
30.6	0.12	1.07	16.50	0.13	0.02	0.11
30.8	0.12	1.07	14.30	0.13	0.02	0.11
31.0	0.12	1.07	12.10	0.13	0.02	0.12
31.2	0.12	1.07	9.91	0.13	0.01	0.12
31.4	0.12	1.06	7.71	0.13	0.01	0.12
31.6	0.12	1.06	5.51	0.13	0.01	0.12
31.8	0.12	1.06	3.77	0.13	0.01	0.13
32.0	0.12	1.06	4.33	0.13	0.01	0.12
32.2	0.00	1.06	5.21	0.00	0.00	0.00
32.4	0.00	1.06	6.08	0.00	0.00	0.00
32.6	0.00	1.06	6.96	0.00	0.00	0.00
32.8	0.00	1.05	7.84	0.00	0.00	0.00
33.0	0.00	1.05	8.72	0.00	0.00	0.00
33.2	0.00	1.05	9.59	0.00	0.00	0.00
33.4	0.00	1.05	10.47	0.00	0.00	0.00
33.6	0.00	1.05	11.35	0.00	0.00	0.00
33.8	0.00	1.05	12.23	0.00	0.00	0.00
34.0	0.00	1.04	13.10	0.00	0.00	0.00
34.2	0.00	1.04	13.98	0.00	0.00	0.00
34.4	0.00	1.04	14.86	0.00	0.00	0.00
34.6	0.00	1.04	15.74	0.00	0.00	0.00
34.8	0.00	1.04	16.61	0.00	0.00	0.00
35.0	0.00	1.04	17.49	0.00	0.00	0.00
35.2	0.00	1.03	18.37	0.00	0.00	0.00
35.4	0.00	1.03	19.24	0.00	0.00	0.00
35.6	0.00	1.03	20.12	0.00	0.00	0.00
35.8	0.00	1.03	21.00	0.00	0.00	0.00
36.0	0.00	1.03	21.88	0.00	0.00	0.00
36.2	0.00	1.02	22.75	0.00	0.00	0.00
36.4	0.00	1.02	23.63	0.00	0.00	0.00
36.6	0.00	1.02	24.51	0.00	0.00	0.00
36.8	0.00	1.02	25.39	0.00	0.00	0.00
37.0	0.00	1.02	26.26	0.00	0.00	0.00
37.2	0.00	1.02	27.14	0.00	0.00	0.00
37.4	0.00	1.01	28.02	0.00	0.00	0.00
37.6	0.00	1.01	28.89	0.00	0.00	0.00
37.8	0.00	1.01	29.77	0.00	0.00	0.00
38.0	0.00	1.01	30.65	0.00	0.00	0.00
38.2	0.00	1.01	31.53	0.00	0.00	0.00
38.4	0.00	1.01	32.40	0.00	0.00	0.00
38.6	0.00	1.00	33.28	0.00	0.00	0.00
38.8	0.00	1.00	34.16	0.00	0.00	0.00
39.0	0.00	1.00	35.04	0.00	0.00	0.00
39.2	0.00	1.00	35.91	0.00	0.00	0.00
39.4	1.98	1.00	36.78	1.97	0.72	1.25
39.6	1.98	1.00	41.14	1.98	0.81	1.16
39.8	1.98	1.01	43.63	1.99	0.87	1.12
40.0	1.98	1.00	41.75	1.97	0.82	1.15
40.2	1.98	0.98	48.30	1.93	0.93	1.00
40.4	1.98	1.04	29.72	2.05	0.61	1.44
40.6	1.98	1.07	35.45	2.12	0.75	1.37
40.8	1.98	1.06	49.33	2.09	1.03	1.06
41.0	1.98	1.07	45.44	2.11	0.96	1.15
41.2	1.98	1.03	57.47	2.03	1.17	0.87
41.4	1.98	1.05	45.63	2.07	0.94	1.12



Table T17 (continued).

Age (Ma)	LSR (cm/k.y.)	Dry density (g/cm ³)	CaCO ₃ (wt%)	MAR (g/cm ² /k.y.)	CAR (g/cm ² /k.y.)	nCAR (g/cm ² /k.y.)
41.6	1.98	1.03	58.75	2.03	1.19	0.84
41.8	1.98	1.03	49.40	2.04	1.01	1.03
42.0	1.98	1.08	35.56	2.14	0.76	1.38
42.2	1.98	1.11	37.31	2.19	0.82	1.37
42.4	2.63	1.04	31.07	2.74	0.85	1.89
42.6	2.63	1.07	38.34	2.80	1.07	1.73
42.8	2.63	1.04	52.77	2.74	1.45	1.30
43.0	2.63	1.05	43.08	2.77	1.20	1.58
43.2	2.63	1.09	37.39	2.86	1.07	1.79
43.4	2.63	1.05	41.78	2.76	1.15	1.61
43.6	2.05	1.00	46.74	2.04	0.96	1.09
43.8	2.05	1.03	53.36	2.11	1.13	0.98
44.0	2.05	0.95	41.64	1.95	0.81	1.14
44.2	2.05	0.98	47.71	2.00	0.96	1.05
44.4	2.05	1.01	45.66	2.07	0.94	1.12
44.6	2.05	1.03	38.76	2.10	0.82	1.29
44.8	2.05	1.09	47.18	2.23	1.05	1.18
45.0	2.05	1.22	43.86	2.50	1.10	1.41
45.2	2.05	1.20	44.52	2.45	1.09	1.36
45.4	2.05	1.21	42.40	2.49	1.06	1.43
45.6	2.05	1.23	48.03	2.52	1.21	1.31
45.8	1.29	1.23	47.40	1.60	0.76	0.84
46.0	1.29	1.23	44.86	1.60	0.72	0.88
46.2	1.29	1.29	47.66	1.67	0.79	0.87
46.4	1.29	1.29	40.90	1.68	0.69	0.99
46.6	1.29	1.37	67.67	1.77	1.20	0.57
46.8	1.29	1.33	89.11	1.73	1.54	0.19
47.0	1.29	1.30	85.37	1.68	1.44	0.25
47.2	1.29	1.23	84.89	1.59	1.35	0.24
47.4	0.75	1.16	87.51	0.87	0.76	0.11
47.6	0.75	1.18	84.77	0.89	0.76	0.14
47.8	0.75	1.20	83.14	0.90	0.75	0.15
48.0	0.75	1.31	84.77	0.99	0.84	0.15
48.2	0.75	1.48	87.15	1.11	0.97	0.14
48.4	0.75	1.32	87.79	0.99	0.87	0.12
48.6	0.75	1.21	88.44	0.91	0.80	0.11
48.8	0.75	1.18	87.66	0.89	0.78	0.11
49.0	0.75	1.15	86.58	0.87	0.75	0.12
49.2	0.75	1.16	86.04	0.87	0.75	0.12
49.4	0.75	1.19	85.53	0.89	0.76	0.13
49.6	0.75	1.22	85.03	0.92	0.78	0.14
49.8	0.75	1.26	84.94	0.95	0.81	0.14
50.0	0.75	1.27	85.50	0.96	0.82	0.14
50.2	0.69	1.16	86.46	0.80	0.69	0.11
50.4	0.69	1.21	88.30	0.84	0.74	0.10
50.6	0.69	1.20	86.02	0.83	0.71	0.12
50.8	0.69	1.39	90.49	0.95	0.86	0.09
51.0	0.69	1.38	90.66	0.95	0.86	0.09
51.2	0.69	1.37	89.95	0.95	0.85	0.10
51.4	0.69	1.44	90.71	0.99	0.90	0.09
51.6	0.69	1.43	91.89	0.99	0.91	0.08
51.8	0.47	1.53	90.50	0.72	0.65	0.07
52.0	0.47	1.58	89.52	0.75	0.67	0.08
52.2	0.47	1.45	90.58	0.69	0.62	0.07
52.4	0.47	1.37	90.52	0.65	0.59	0.06
52.6	0.47	1.36	90.68	0.64	0.58	0.06
52.8	0.47	1.36	91.24	0.65	0.59	0.06
53.0	0.47		90.55	0.00	0.00	0.00

LSR = linear sedimentation rate, MAR = mass accumulation rate, CAR = carbonate accumulation rate, nCAR = noncarbonate accumulation rate.



Table T18. Geochemistry of headspace gas samples, Hole U1410A.

Core, section, interval (cm)	Depth (mbsf)	Methane (ppmv)
342-U1410-		
1H-6, 0–5	7.50	2.11
2H-7, 0–5	17.50	2.20
3H-7, 0–5	27.00	2.26
4H-7, 0–5	36.50	2.78
5H-7, 0–5	45.61	2.71
6H-7, 0–5	55.41	2.89
7H-7, 0–5	63.55	2.77
8H-7, 0–5	74.50	2.79
9H-7, 0–5	83.15	2.79
11H-7, 0–5	102.61	3.27
12H-7, 0–5	112.50	3.10
13H-7, 0–5	120.97	3.37
14H-7, 0–5	131.22	4.34
15H-7, 0–5	140.49	3.87
16H-7, 0–5	150.36	4.13
17X-7, 0–5	159.91	3.30
18X-7, 0–5	169.42	3.86
19X-7, 0–5	179.01	3.82
20X-7, 0–5	188.61	4.69
21X-7, 0–5	197.37	4.42
22X-7, 0–5	208.00	3.65
23X-7, 0–5	217.50	6.00
24X-6, 0–5	225.50	5.14
25X-4, 0–5	232.00	4.22
26X-2, 0–5	238.60	6.72
27X-6, 0–5	254.20	4.15
28X-2, 0–5	257.80	4.19

Table T19. Interstitial water constituents, Hole U1410A.

Core, section, interval (cm)	Depth (mbsf)	pH	Alkalinity (mM)	Ammonium (μM)	Salinity	Cl^- (mM)	Na^+ (mM)	SO_4^{2-} (mM)	HPO_4^{2-} (μM)	Mn^{2+} (μM)	Fe^{2+} (μM)	Ca^{2+} (mM)	Mg^{2+} (mM)	K^+ (mM)	B (μM)
342-U1310A-															
1H-5, 145–150	7.45	7.45	3.544	42	38	551.989	470.685	28.871	BDL	7.702	ND	11.36	53.862	14.929	375.538
2H-6, 145–150	17.45	7.51	3.545	105	37	555.186	477.705	27.764	BDL	6.631	5.272	11.382	53.639	15.132	374.944
3H-6, 145–150	26.95	7.47	3.433	50	37	561.292	481.021	27.159	BDL	7.432	10.861	11.6	53.098	16.318	523.419
4H-6, 145–150	36.45	7.57	3.843	44	37	553.43	474.916	27.324	BDL	7.115	5.747	11.944	53.275	14.894	579.423
5H-6, 106–111	45.56	7.41	3.222	63	37	545.828	476.271	26.526	BDL	6.281	5.617	12.203	52.299	14.752	489.01
6H-6, 136–141	55.36	7.44	3.75	58	37	556.715	480.495	27.366	BDL	6.393	5.233	13.165	54.065	12.484	516.206
7H-6, 147–152	63.50	7.32	3.803	52	37	580.964	473.982	26.861	BDL	5.805	1.467	13.414	53.282	11.736	559.207
8H-6, 140–150	74.40	7.25	3.591	78	37	560.976	486.185	25.829	BDL	5.519	46.856	13.806	51.873	12.638	507.657
9H-6, 140–150	83.05	7.17	3.62	44	36	553.411	477.408	26.278	BDL	5.319	49.008	14.124	50.691	11.538	512.154
11H-6, 101–111	102.51	7.14	3.905	74	37	546.272	474.283	24.397	BDL	6.476	71.14	14.885	49.071	11.63	502.417
12H-6, 140–150	112.40	7.15	3.917	49	37	551.084	480.479	25.53	BDL	6.832	58.565	15.756	49.297	10.636	504.39
13H-6, 140–150	120.87	7.14	4.196	100	37	561.386	488.687	25.285	BDL	7.329	77.807	16.587	49.847	9.529	457.296
14H-6, 112–122	131.12	7.06	4.001	120	37	549.331	478.322	25.093	BDL	7.63	44.514	16.707	48.723	8.576	446.519
15H-6, 91–101	140.39	7.001	4.396	47	37	555.47	485.628	24.704	BDL	9.26	35.271	17.538	48.904	8.118	472.294
16H-6, 126–136	150.26	7.007	4.744	56	37	537.585	465.726	24.21	BDL	9.831	22.243	17.67	47.376	7.012	529.422
17X-6, 133–141	159.83	6.961	4.76	52	37	549.872	474.491	24.072	BDL	11.67	31.492	18.356	47.989	11.184	482.604
18X-6, 122–132	169.32	6.932	4.994	82	37	557.461	481.917	24.657	BDL	11.763	24.256	19.122	47.824	11.555	494.823
19X-6, 121–131	178.91	6.959	5.151	74	37	557.425	487.646	23.918	BDL	12.456	33.862	19.689	46.963	11.549	476.939
20X-6, 121–131	188.51	7.018	5.061	107	37	550.797	478.777	23.972	BDL	14.872	23.869	19.875	46.202	11.162	507.848
22X-6, 140–150	207.90	7.026	4.305	95	37	576.232	468.218	22.562	BDL	8.862	2.427	20.402	44.327	10.97	456.129
23X-6, 140–150	217.40	6.872	4.82	109	37	551.099	479.456	23.618	BDL	6.061	0.323	20.349	43.912	11.699	407.422
25X-3, 140–150	231.90	6.821	5.194	79	38	555.392	482.376	23.132	BDL	3.943	0.316	21.188	43.831	10.94	396.9
26X-1, 140–150	238.50	7.016	5.289	119	38	563.387	493.388	24.016	BDL	3.799	0.257	22.122	44.064	11.083	383.896
27X-5, 140–150	254.10	6.851	5.656	155	37	556.977	480.682	21.716	BDL	10.882	0.21	23.532	39.205	10.345	478.828

BDL = below detection limit ($\text{HPO}_4^{2-} = 0.2 \mu\text{M}$), calculated as two times the standard deviation of multiple measures of a blank. ND = not detected.



Table T20. Sedimentary sample and bulk elemental geochemistry, Hole U1410A. (Continued on next two pages.)

Core, section, interval (cm)	Depth (mbsf)	CaCO ₃ (wt%)	IC (wt%)	TC (wt%)	TN (wt%)	TOC (wt%)
342-U1410A-						
1H-1, 148–149	1.48	48.02	5.76	5.92	0.06	0.16
1H-2, 38–39	1.88	50.36	6.04	6.47	0.08	0.43
1H-3, 61–62	3.61	19.698	2.362	1.69	0.08	BDL
1H-4, 46–47	4.96	24.393	2.925	3.13	0.06	0.21
1H-5, 31–32	6.31	34.712	4.162	4.55	0.11	0.39
1H-6, 20–21	7.70	66.405	7.962	7.66	0.03	BDL
2H-1, 39–40	8.89	39.71	4.761	4.98	0.03	0.22
2H-2, 38–39	10.38	50.147	6.012	6.08	0.04	0.07
2H-3, 38–39	11.88	46.452	5.569	5.95	0.08	0.38
2H-4, 38–39	13.38	60.91	7.303	7.47	0.05	0.17
2H-5, 38–39	14.88	8.025	0.962	1.35	0.11	0.39
2H-6, 38–39	16.38	35.062	4.204	4.73	0.11	0.53
2H-7, 18–19	17.68	44.481	5.333	5.90	0.06	0.57
3H-1, 38–39	18.38	61.207	7.339	7.68	0.05	0.34
3H-2, 38–39	19.88	40.174	4.817	4.92	0.04	0.10
3H-3, 38–39	21.38	38.652	4.634	4.85	0.08	0.22
3H-4, 38–39	22.88	50.68	6.076	6.29	0.05	0.21
3H-5, 38–39	24.38	40.793	4.891	5.18	0.05	0.29
3H-6, 38–39	25.88	26.169	3.138	3.27	0.07	0.13
3H-7, 18–19	27.18	31.629	3.792	3.64	0.06	BDL
4H-1, 38–39	27.88	22.018	2.64	3.04	0.09	0.40
4H-2, 38–39	29.38	23.796	2.853	3.23	0.08	0.38
4H-3, 38–39	30.88	13.237	1.587	1.88	0.10	0.29
4H-4, 35–36	32.35	11.073	1.328	1.77	0.36	0.44
4H-5, 38–39	33.88	6.951	0.833	1.22	0.11	0.39
4H-6, 38–39	35.38	3.345	0.401	0.72	0.12	0.32
4H-7, 18–19	36.68	12.808	1.536	1.97	0.13	0.43
5H-1, 60–61	37.60	6.87	0.824	1.34	0.14	0.52
5H-2, 38–39	38.88	12.216	1.465	1.64	0.13	0.18
5H-3, 38–39	40.38	17.832	2.138	2.70	0.14	0.56
5H-4, 38–39	41.88	3.997	0.479	0.64	0.07	0.16
5H-5, 38–39	43.38	0.691	0.083	0.20	0.07	0.12
5H-6, 25–26	44.75	17.662	2.118	2.20	0.05	0.08
5H-7, 13–14	45.74	17.927	2.149	2.25	0.06	0.10
6H-1, 38–39	46.88	16.287	1.953	2.05	0.06	0.10
6H-2, 38–39	48.38	6.762	0.811	0.92	0.05	0.11
6H-3, 38–39	49.88	11.857	1.422			
6H-4, 38–39	51.38	2.738	0.328	0.43	0.06	0.10
6H-5, 38–39	52.88	6.908	0.828	2.04	0.06	1.21
6H-6, 38–39	54.38	5.904	0.708	0.77	0.05	0.06
6H-7, 16–17	55.57	8.089	0.97	1.14	0.08	0.17
7H-1, 38–39	56.38	12.79	1.533	1.58	0.06	0.05
7H-2, 38–39	57.90	8.191	0.982	1.15	0.07	0.17
7H-3, 15–16	59.20	22.467	2.694	2.84	0.07	0.15
7H-4, 30–31	59.97	13.404	1.607	1.74	0.07	0.13
7H-5, 30–31	61.19	17.342	2.079	2.16	0.07	0.08
7H-6, 30–31	62.33	17.787	2.133	2.27	0.07	0.14
7H-7, 38–39	63.93	3.413	0.409	0.66	0.06	0.25
8H-1, 38–39	65.88	37.161	4.456	4.45	0.07	BDL
8H-2, 38–39	67.38	36.307	4.353	4.62	0.08	0.27
8H-3, 38–39	68.88	51.347	6.156	6.44	0.04	0.28
8H-4, 38–39	70.38	29.52	3.539	3.74	0.07	0.20
8H-5, 38–39	71.88	54.953	6.589	6.67	0.05	0.08
8H-6, 38–39	73.38	38.405	4.605	4.67	0.05	0.07
8H-7, 9–10	74.59	58.643	7.031	7.28	0.06	0.25
9H-1, 24–25	75.24	37.961	4.551			
9H-2, 38–39	76.88	34.174	4.097	4.36	0.07	0.26
9H-3, 12–13	78.12	47.947	5.749			
9H-4, 38–39	79.03	30.851	3.699	3.88	0.07	0.18
9H-5, 38–39	80.53	75.623	9.067			
9H-6, 38–39	82.03	20.215	2.424	2.55	0.07	0.13
9H-7, 20–21	83.35	25.455	3.052	3.28	0.07	0.23
10H-1, 9–10	84.59	33.022	3.959	4.11	0.06	0.15
10H-2, 20–21	85.20	32.85	3.939	4.18	0.07	0.24
10H-3, 30–31	85.98	48.819	5.853	5.93	0.05	0.08
10H-4, 38–39	87.53	36.994	4.436	4.60	0.06	0.16

Table T20 (continued). (Continued on next page.)

Core, section, interval (cm)	Depth (mbsf)	CaCO ₃ (wt%)	IC (wt%)	TC (wt%)	TN (wt%)	TOC (wt%)
10H-5, 38–39	88.63	26.261	3.149	3.36	0.08	0.21
10H-6, 38–39	90.03	32.988	3.955	4.11	0.07	0.15
10H-7, 38–39	91.44	53.821	6.453			
11H-1, 38–39	94.38	53.513	6.416	6.58	0.05	0.16
11H-2, 38–39	95.88	47.617	5.709	5.89	0.05	0.18
11H-3, 38–39	97.38	31.328	3.756	4.05	0.08	0.29
11H-4, 38–39	98.88	80.765	9.683	10.06	0.01	0.38
11H-5, 38–39	100.38	48.142	5.772	5.92	0.06	0.15
11H-6, 23–24	101.73	42.946	5.149	5.41	0.07	0.26
11H-7, 10–11	102.71	35.597	4.268	4.42	0.08	0.15
12H-1, 38–39	103.88	56.709	6.799	6.45	0.05	BDL
12H-2, 38–39	105.38	41.627	4.991	4.96	0.07	BDL
12H-3, 38–39	106.88	84.975	10.188	9.81	0.03	BDL
12H-4, 38–39	108.38	47.336	5.675	5.67	0.07	BDL
12H-5, 38–39	109.88	33.83	4.056	4.1	0.08	0.04
12H-6, 38–39	111.38	67.466	8.089	7.55	0.03	BDL
12H-7, 17–18	112.67	43.963	5.271	5.15	0.06	BDL
13H-1, 24–25	113.24	40.134	4.812	4.93	0.07	0.12
13H-2, 38–39	113.85	47.502	5.695	5.6	0.07	BDL
13H-3, 38–39	115.35	32.639	3.913	3.92	0.08	0.01
13H-4, 38–39	116.85	30.207	3.622	3.64	0.08	0.02
13H-5, 38–39	118.35	34.751	4.167	4.05	0.08	BDL
13H-6, 38–39	119.85	40.509	4.857	4.73	0.07	BDL
13H-7, 38–39	121.35	37.475	4.493	4.64	0.08	0.15
14H-1, 38–39	122.88	29.022	3.48	3.53	0.08	0.05
14H-2, 38–39	124.38	28.188	3.38	3.33	0.08	BDL
14H-3, 38–39	125.88	33.588	4.027	3.85	0.06	BDL
14H-4, 38–39	127.38	31.84	3.817	3.69	0.08	BDL
14H-5, 38–39	128.88	39.807	4.773	4.66	0.08	BDL
14H-6, 38–39	130.38	37.299	4.472	4.67	0.1	0.20
14H-7, 18–19	131.40	41.696	4.999	4.87	0.06	BDL
15H-1, 140–141	133.40	81.663	9.791	9.38	0.02	BDL
15H-2, 38–39	133.86	52.685	6.317	6.07	0.07	BDL
15H-3, 38–39	135.36	46.086	5.526	5.23	0.06	BDL
15H-4, 38–39	136.86	37.927	4.547	4.51	0.09	BDL
15H-5, 39–40	138.37	43.744	5.245	5.68	0.08	0.44
15H-6, 20–21	139.68	47.826	5.734	5.46	0.06	BDL
15H-7, 15–16	140.64	37.716	4.522	4.35	0.08	BDL
16H-1, 39–40	141.89	44.488	5.334	5.41	0.08	0.08
16H-2, 39–40	143.39	43.41	5.205	5.31	0.07	0.11
16H-3, 39–40	144.89	33.15	3.975	4.25	0.11	0.28
16H-4, 39–40	146.39	34.637	4.153	4.26	0.09	0.11
16H-5, 31–32	147.81	38.08	4.566	4.85	0.1	0.28
16H-6, 31–32	149.31	33.855	4.059	4.09	0.07	0.03
16H-7, 15–16	150.51	29.201	3.501	3.78	0.09	0.28
17X-1, 38–39	151.38	45.086	5.406	5.33	0.08	BDL
17X-2, 38–39	152.88	72.754	8.723	8.26	0.05	BDL
17X-3, 38–39	154.38	41.769	5.008	4.88	0.07	BDL
17X-4, 37–38	155.87	34.983	4.194	4.04	0.07	BDL
17X-5, 37–38	157.37	43.254	5.186	5.1	0.06	BDL
17X-5, 73–74	157.73	77.824	9.331	9.08	0.02	BDL
17X-6, 26–27	158.76	53.577	6.424	6.05	0.04	BDL
17X-7, 13–14	160.04	48.614	5.829	5.49	0.05	BDL
18X-1, 38–39	160.98	44.042	5.281	4.84	0.05	BDL
18X-2, 40–41	162.50	41.805	5.012	4.75	0.06	BDL
18X-3, 39–40	163.99	40.169	4.816	4.41	0.04	BDL
18X-4, 39–40	165.49	40.667	4.876	4.53	0.04	BDL
18X-5, 39–40	166.99	48.82	5.853	5.46	0.06	BDL
18X-6, 29–30	168.39	54.97	6.591	6.27	0.05	BDL
18X-7, 14–15	169.56	41.593	4.987	4.7	0.06	BDL
19X-1, 41–42	170.61	49.852	5.977	5.96	0.07	BDL
19X-2, 40–41	172.10	47.25	5.665	5.47	0.06	BDL
19X-3, 40–41	173.60	32.916	3.947	3.77	0.08	BDL
19X-4, 39–40	175.09	37.204	4.461	4.19	0.06	BDL
19X-5, 39–40	176.59	44.626	5.351	4.97	0.06	BDL
19X-6, 39–40	178.09	44.191	5.298	5.04	0.03	BDL
19X-7, 14–15	179.15	45.561	5.463	5.19	0.07	BDL
20X-1, 38–39	180.18	52.441	6.287	5.92	0.04	BDL
20X-2, 40–41	181.70	45.226	5.422	5.02	0.05	BDL

Table T20 (continued).

Core, section, interval (cm)	Depth (mbsf)	CaCO ₃ (wt%)	IC (wt%)	TC (wt%)	TN (wt%)	TOC (wt%)
20X-3, 38–39	183.18	47.581	5.705	5.41	0.05	BDL
20X-4, 38–39	184.68	38.812	4.653	4.4	0.06	BDL
20X-5, 38–39	186.18	41.199	4.94	4.76	0.07	BDL
20X-6, 33–34	187.63	48.802	5.851	5.48	0.07	BDL
20X-7, 15–16	188.76	43.024	5.158	4.87	0.06	BDL
21X-1, 21–22	189.61	47.431	5.687	5.35	0.05	BDL
21X-2, 38–39	190.42	38.23	4.584	4.31	0.06	BDL
21X-3, 38–39	191.92	39.067	4.684	4.31	0.04	BDL
21X-4, 17–18	193.17	48.909	5.864	5.58	0.06	BDL
21X-5, 42–43	194.79	46.897	5.623	5.32	0.06	BDL
21X-6, 45–46	196.32	50.099	6.007	5.66	0.04	BDL
21X-7, 42–43	197.79	45.547	5.461	5.17	0.05	BDL
22X-1, 35–36	199.35	48.482	5.813	5.59	0.05	BDL
22X-2, 38–39	200.88	46.922	5.626	5.3	0.06	BDL
22X-3, 38–39	202.38	42.06	5.043	4.69	0.05	BDL
22X-4, 35–36	203.85	51.933	6.227	6.24	0.19	0.01
22X-5, 38–39	205.38	43.788	5.25	4.99	0.05	BDL
22X-6, 38–39	206.88	36.884	4.422	4.37	0.07	BDL
22X-7, 12–13	208.12	45.61	5.469	5.46	0.07	BDL
23X-1, 38–39	208.88	52.206	6.259	5.91	0.04	BDL
23X-2, 48–49	210.48	85.287	10.226	9.69	0.01	BDL
23X-3, 35–36	211.85	92.568	11.099	10.52	0.02	BDL
23X-4, 43–44	213.43	84.924	10.182	9.53	0.03	BDL
23X-5, 38–39	214.88	85.159	10.21	9.54	0.01	BDL
23X-6, 40–41	216.40	86.546	10.377	9.72	0.22	BDL
23X-7, 10–11	217.60	81.882	9.817	8.99	0	BDL
24X-1, 43–44	218.43	87.204	10.455	10.35	0	BDL
24X-2, 44–45	219.94	87.971	10.548	10.42	0	BDL
24X-3, 44–45	221.44	84.03	10.075	9.88	0.08	BDL
24X-4, 53–54	223.03	82.72	9.918	10.03	0.01	0.11
24X-5, 38–39	224.38	85.025	10.194	10.02	0.08	BDL
24X-6, 44–45	225.94	87.655	10.51	10.11	0.01	BDL
25X-1, 29–30	227.79	87.831	10.531	10.22	0	BDL
25X-2, 26–27	229.26	88.827	10.65	10.28	0	BDL
25X-3, 33–34	230.83	86.958	10.426	10.07	0.01	BDL
25X-4, 34–35	232.34	86.343	10.352	10.07	0	BDL
26X-1, 23–24	237.33	84.674	10.152	9.65	0.01	BDL
26X-2, 41–42	239.01	85.587	10.262	10.04	0.09	BDL
26X-3, 25–26	240.35	85.406	10.24	9.89	0.11	BDL
26X-4, 25–26	241.85	89.545	10.736	10.62	0.1	BDL
26X-5, 18–19	243.28	84.594	10.143	9.33	0.01	BDL
26X-6, 42–43	245.02	91.766	11.002	10.43	0.1	BDL
27X-1, 44–45	247.14	89.77	10.763	10.56	0.01	BDL
27X-2, 54–55	248.74	90.33	10.83	10.41	0.01	BDL
27X-3, 47–48	250.17	92.354	11.073	10.11	0	BDL
27X-4, 93–94	252.13	89.137	10.687	10.31	0.02	BDL
27X-5, 75–76	253.45	90.924	10.901	10.51	0	BDL
27X-6, 34–35	254.54	90.326	10.83	10.51	0	BDL
28X-1, 30–31	256.60	91.535	10.975	9.96	0	BDL
28X-2, 6–7	257.86	88.745	10.64	9.88	0	BDL

IC = inorganic carbon, TC = total carbon, TN = total nitrogen, TOC = total organic carbon. BDL = below detection limit (TOC < 0.03 wt%).



Table T21. Thermal conductivity results, Hole U1410A. (Continued on next page.)

Core, section, interval (cm)	Depth (mbsf)	Thermal conductivity (W/[m·K])			Heating power (W/m)
		Mean	Standard deviation	Observation	
342-U1410A-					
1H-3W, 75	3.01	0.993	2.41E-02	0.959*	1.612
1H-3W, 75	3.01			1.009*	1.612
1H-3W, 75	3.01			1.011*	1.612
2H-3W, 75	11.51	0.896	3.52E-02	0.846*	1.612
2H-3W, 75	11.51			0.921	1.612
2H-3W, 75	11.51			0.920	1.612
3H-3W, 75	21.01	0.971	5.50E-03	0.970	1.612
3H-3W, 75	21.01			0.965*	1.612
3H-3W, 75	21.01			0.978	1.612
4H-3W, 75	30.51	1.411	2.24E-02	1.380	1.612
4H-3W, 75	30.51			1.428	1.612
4H-3W, 75	30.51			1.426	1.612
5H-3W, 75	40.01	1.130	1.61E-02	1.107	1.612
5H-3W, 75	40.01			1.144*	1.612
5H-3W, 75	40.01			1.138*	1.612
6H-3W, 75	49.51	1.060	3.67E-02	1.008*	1.612
6H-3W, 75	49.51			1.090	1.612
6H-3W, 75	49.51			1.081	1.612
7H-3W, 31	59.05	1.179	1.45E-02	1.160	1.612
7H-3W, 31	59.05			1.183*	1.612
7H-3W, 31	59.05			1.195	1.612
8H-3A, 75	68.51	1.156	1.67E-02	1.132	1.612
8H-3A, 75	68.51			1.170*	1.612
8H-3A, 75	68.51			1.165*	1.612
9H-3A, 30	78.00	1.183	8.80E-03	1.171	1.612
9H-3A, 30	78.00			1.191*	1.612
9H-3A, 30	78.00			1.187	1.612
10H-3A, 75	85.69	1.199	2.01E-02	1.173*	1.612
10H-3A, 75	85.69			1.202*	1.612
10H-3A, 75	85.69			1.222*	1.612
11H-3A, 75	97.01	1.123	5.62E-02	1.151	1.612
11H-3A, 75	97.01			1.174	1.612
11H-3A, 75	97.01			1.045	1.612
12H-3A, 75	106.51	1.155	7.70E-03	1.154	1.612
12H-3A, 75	106.51			1.164*	1.612
12H-3A, 75	106.51			1.145	1.612
13H-3A, 75	114.98	1.150	3.70E-03	1.145*	1.612
13H-3A, 75	114.98			1.154*	1.612
13H-3A, 75	114.98			1.150*	1.612
14H-3A, 75	125.51	1.138	1.70E-02	1.114*	1.612
14H-3A, 75	125.51			1.151*	1.612
14H-3A, 75	125.51			1.149	1.612
15H-3A, 75	134.99	1.144	1.59E-02	1.151	1.612
15H-3A, 75	134.99			1.159	1.612
15H-3A, 75	134.99			1.122*	1.612
16H-3W, 75	144.51	1.166	7.80E-03	1.155	1.612
16H-3W, 75	144.51			1.174*	1.612
16H-3W, 75	144.51			1.168*	1.612
17X-3W, 75	154.01	1.135	2.20E-02	1.109*	1.612
17X-3W, 75	154.01			1.163	1.612
17X-3W, 75	154.01			1.132*	1.612
18X-3W, 75	163.61	1.198	4.70E-03	1.192	1.612
18X-3W, 75	163.61			1.203*	1.612
18X-3W, 75	163.61			1.199*	1.612
19X-3W, 75	173.21	1.182	1.14E-02	1.176	1.612
19X-3W, 75	173.21			1.172*	1.612
19X-3W, 75	173.21			1.198	1.612
20X-3W, 75	182.81	1.202	2.34E-02	1.172*	1.612
20X-3W, 75	182.81			1.229*	1.612
20X-3W, 75	182.81			1.205*	1.612
22X-3W, 75	202.01	1.222	1.01E-02	1.209	1.612
22X-3W, 75	202.01			1.234	1.612
22X-3W, 75	202.01			1.224	1.612
23X-3A, 75	211.51	1.431	2.37E-02	1.400	1.612
23X-3A, 75	211.51			1.434*	1.612
23X-3A, 75	211.51			1.458*	1.612



Table T21 (continued).

Core, section, interval (cm)	Depth (mbsf)	Thermal conductivity (W/[m·K])			Heating power (W/m)
		Mean	Standard deviation	Observation	
24X-3A, 75	221.01	1.316	9.90E-03	1.330*	1.612
24X-3A, 75	221.01			1.312*	1.612
24X-3A, 75	221.01			1.307*	1.612
25X-3A, 75	230.51	1.326	1.45E-02	1.306*	1.612
25X-3A, 75	230.51			1.339*	1.612
25X-3A, 75	230.51			1.334*	1.612
26X-3A, 75	240.11	1.387	1.53E-02	1.381*	1.612
26X-3A, 75	240.11			1.408*	1.612
26X-3A, 75	240.11			1.372*	1.612
27X-3A, 75	249.71	1.496	5.20E-03	1.494*	1.612
27X-3A, 75	249.71			1.503	1.612
27X-3A, 75	249.71			1.491*	1.612

* = result obtained directly from the TK04 processing software. Other results were generated by the IODP uploader using raw data because they were rejected by the TK04 software. Thermal conductivity mean and standard deviation calculated from thermal conductivity observations. Heating power used to perform the measurement is also listed.

Table T22. Core top and composite depth, Site U1410. (Continued on next page.)

Core	Depth		Offset (m)	Cumulative offset (m)	Comment
	(mbsf)	(m CCSF)			
342-U1410A-					
1H	0.00	0.00	0.00	0.00	
2H	8.50	7.70	-0.80	-0.80	
3H	18.00	18.70	1.50	0.70	
4H	27.50	28.95	0.75	1.45	
5H	37.00	38.20	-0.25	1.20	
6H	46.50	48.00	0.30	1.50	
7H	56.00	58.35	0.85	2.35	
8H	65.50	67.85	0.00	2.35	
9H	75.00	79.45	2.10	4.45	
10H	84.50	90.04	1.09	5.54	
11H	94.00	98.54	-1.00	4.54	
12H	103.50	108.54	0.50	5.04	
13H	113.00	117.99	-0.05	4.99	
14H	122.50	128.39	0.90	5.89	
15H	132.00	137.39	-0.50	5.39	
16H	141.50	146.89	0.00	5.39	Slumped
17X	151.00	157.64	1.25	6.64	
18X	160.60	167.04	-0.20	6.44	
19X	170.20	176.64	0.00	6.44	
20X	179.80	186.59	0.35	6.79	
21X	189.40	196.19	0.00	6.79	Disturbed
22X	199.00	205.79	0.00	6.79	
23X	208.50	226.29	11.00	17.79	
24X	218.00	236.64	0.85	18.64	
25X	227.50	247.79	1.65	20.29	
26X	237.10	257.39	0.00	20.29	
27X	246.70	266.99	0.00	20.29	
28X	256.30	276.59	0.00	20.29	
342-U1410B-					
1H	0.00	-0.10	-0.10	-0.10	
2H	3.80	4.75	1.05	0.95	
3H	13.30	13.85	-0.40	0.55	
4H	22.80	23.95	0.60	1.15	
5H	31.30	32.90	0.45	1.60	
6H	39.70	41.50	0.20	1.80	
7H	49.20	50.60	-0.40	1.40	
8H	58.70	62.00	1.90	3.30	
9H	66.80	71.05	0.95	4.25	
10H	76.30	80.73	0.18	4.43	
11H	85.80	90.72	0.49	4.92	
12H	90.80	95.72	0.00	4.92	
13H	100.30	105.92	0.70	5.62	
14H	109.80	115.22	-0.20	5.42	
15H	119.30	125.27	0.55	5.97	
16H	128.80	135.07	0.30	6.27	Tentative
17H	138.30	144.42	-0.15	6.12	Tentative/Slumped?
18H	147.80	153.67	-0.25	5.87	Slumped?
19X	153.80	160.67	1.00	6.87	
20X	163.40	170.77	0.50	7.37	Tentative
21X	173.00	180.57	0.20	7.57	Tentative
22X	182.60	190.17	0.00	7.57	Shattered liner
23X	187.60	194.97	-0.20	7.37	Tentative
24X	197.20	204.57	0.00	7.37	Tentative
25X	206.80	213.67	-0.50	6.87	Tentative
26X	216.40	236.57	13.30	20.17	
27X	226.00	246.17	0.00	20.17	Tentative
28X	235.60	255.77	0.00	20.17	
342-U1410C-					
1H	0.00	0.15	0.15	0.15	
2H	6.80	6.95	0.00	0.15	
3H	16.30	17.65	1.20	1.35	
4H	25.80	27.37	0.22	1.57	
5H	35.30	36.87	0.00	1.57	
6H	44.80	46.77	0.40	1.97	
7H	54.30	57.29	1.02	2.99	
8H	63.80	66.82	0.03	3.02	Tentative
9H	73.30	76.47	0.15	3.17	



Table T22 (continued).

Core	Depth		Offset (m)	Cumulative offset (m)	Comment
	(mbsf)	(m CCSF)			
10H	82.80	87.41	1.44	4.61	
11H	89.80	94.21	-0.20	4.41	
12H	99.30	105.11	1.40	5.81	
13H	108.80	114.96	0.35	6.16	
14H	118.30	125.86	1.40	7.56	
15H	127.80	136.76	1.40	8.96	
16H	137.30	147.36	1.10	10.06	Slumped?
17X	146.80	156.86	0.00	10.06	Slumped?
18X	156.40	166.86	0.40	10.46	
19X	166.00	176.56	0.10	10.56	Tentative
20X	175.60	186.76	0.60	11.16	
21X	185.20	196.36	0.00	11.16	Tentative
22X	194.80	205.96	0.00	11.16	
23X	204.40	216.56	1.00	12.16	
24X	214.00	230.96	4.80	16.96	
25X	223.60	240.51	-0.05	16.91	
26X	233.20	247.91	-2.20	14.71	
27X	242.80	257.51	0.00	14.71	

Table T23. Splice tie points, Site U1410.

Hole, core, section, interval (cm)	Depth		Hole, core, section, interval (cm)	Depth		Comment
	(mbsf)	(m CCSF)		(mbsf)	(m CCSF)	
342-			342-			
U1410A-1H-5, 55	6.55	6.55	Tie to	U1410A-1H-1, 0	0.00	0.00
U1410B-2H-4, 26	8.56	9.52	Tie to	U1410B-2H-2, 30	5.60	6.55
U1410A-2H-6, 114	17.14	16.34	Tie to	U1410B-3H-2, 138	15.79	16.34
U1410B-3H-5, 60	19.51	20.05	Tie to	U1410A-3H-1, 135	19.35	20.05
U1410A-3H-6, 125	26.75	27.46	Tie to	U1410B-4H-3, 51	26.31	27.46
U1410B-4H-4, 115	28.45	29.60	Tie to	U1410A-4H-1, 65	28.15	29.60
U1410A-4H-4, 76	32.76	34.20	Tie to	U1410B-5H-1, 130	32.60	34.20
U1410B-5H-5, 130	38.60	40.19	Tie to	U1410A-5H-2, 49	38.99	40.19
U1410A-5H-4, 81	42.31	43.51	Tie to	U1410B-6H-2, 51	41.71	43.51
U1410B-6H-6, 96	48.20	50.01	Tie to	U1410A-6H-2, 51	48.51	50.01
U1410A-6H-6, 66	54.66	56.16	Tie to	U1410B-7H-4, 106	54.76	56.16
U1410B-7H-6, 80	57.50	58.90	Tie to	U1410A-7H-1, 55	56.55	58.90
U1410A-7H-7, 20	63.75	66.11	Tie to	U1410B-8H-3, 111	62.81	66.11
U1410B-8H-5, 37	65.07	68.37	Tie to	U1410C-8H-2, 5	65.35	68.37
U1410C-8H-6, 75	72.05	75.08	Tie to	U1410B-9H-3, 103	70.83	75.08
U1410B-9H-5, 111	73.91	78.17	Tie to	U1410C-9H-2, 20	75.00	78.17
U1410C-9H-5, 75	80.05	83.23	Tie to	U1410B-10H-2, 100	78.80	83.23
U1410B-10H-5, 118	83.48	87.91	Tie to	U1410C-10H-1, 50	83.30	87.91
U1410C-10H-4, 80	88.10	92.71	Tie to	U1410B-11H-2, 49	87.79	92.71
U1410B-11H-4, 5	90.35	95.26	Tie to	U1410C-11H-1, 105	90.85	95.26
U1410C-11H-5, 115	96.91	101.33	Tie to	U1410A-11H-2, 129	96.79	101.33
U1410A-11H-6, 85	102.35	106.87	Tie to	U1410B-13H-1, 95	101.25	106.87
U1410B-13H-4, 90	105.70	111.33	Tie to	U1410A-12H-2, 129	106.29	111.33
U1410A-12H-5, 119	110.69	115.72	Tie to	U1410B-14H-1, 50	110.30	115.72
U1410B-14H-6, 5	117.35	122.78	Tie to	U1410A-13H-4, 132	117.79	122.78
U1410A-13H-7, 31	121.28	126.27	Tie to	U1410B-15H-1, 100	120.30	126.27
U1410B-15H-4, 60	124.40	130.38	Tie to	U1410A-14H-2, 49	124.49	130.38
U1410A-14H-6, 19	130.19	136.07	Tie to	U1410B-16H-1, 100	129.80	136.07
U1410B-16H-4, 100	134.30	140.58	Tie to	U1410A-15H-3, 21	135.19	140.58
U1410A-15H-6, 55	140.03	145.42	Tie to	U1410B-17H-1, 100	139.30	145.42
U1410B-17H-5, 140	144.79	150.90	Tie to	U1410A-16H-3, 101	145.51	150.90
U1410A-16H-5, 128	148.78	154.17	Tie to	U1410B-18H-1, 50	148.30	154.17
U1410B-18H-4, 45	152.75	158.64	Tie to	U1410A-17X-1, 100	152.00	158.64
U1410A-17X-4, 94	156.44	163.07	Tie to	U1410B-19X-2, 90	156.20	163.07
U1410B-19X-7, 50	162.71	169.56	Tie to	U1410C-18X-2, 120	159.10	169.56
U1410C-18X-5, 140	163.80	174.24	Tie to	U1410B-20X-3, 45	166.87	174.24
U1410B-20X-6, 25	171.17	178.56	Tie to	U1410C-19X-2, 50	168.00	178.56
U1410C-19X-4, 50	171.00	181.57	Tie to	U1410B-21X-1, 100	174.00	181.57
U1410B-21X-6, 10	180.60	188.16	Tie to	U1410C-20X-1, 140	177.00	188.16
U1410C-20X-7, 10	184.61	195.77	Tie to	U1410B-23X-1, 80	188.40	195.77
U1410B-23X-5, 40	194.00	201.36	Tie to	U1410C-21X-4, 50	190.20	201.36
U1410C-21X-6, 120	193.90	205.07	Tie to	U1410B-24X-1, 50	197.70	205.07
U1410B-24X-3, 20	200.40	207.78	Tie to	U1410A-22X-2, 49	200.99	207.78
U1410A-22X-6, 118	207.68	214.47	Tie to	U1410B-25X-1, 80	207.60	214.47
U1410B-25X-4, 40	211.70	218.56	Tie to	U1410C-23X-2, 50	206.40	218.56
U1410C-23X-CC, 27	214.07	226.23	Append to	U1410A-23X-1, 5	208.55	226.34
U1410A-23X-6, 13	216.13	233.91	Tie to	U1410C-24X-2, 145	216.95	233.91
U1410C-24X-6, 10	221.60	238.57	Tie to	U1410B-26X-2, 50	218.40	238.57
U1410B-26X-5, 100	223.40	243.56	Tie to	U1410C-25X-3, 5	226.65	243.56
U1410C-25X-5, 45	230.05	246.97	Tie to	U1410B-27X-1, 80	226.80	246.97
U1410B-27X-7, 60	235.31	255.48	Append to	U1410B-28X-1, 5	235.65	255.82
U1410B-28X-3, 115	239.75	259.92	Tie to	U1410A-26X-2, 103	239.63	259.92
U1410A-26X-4, 139	242.99	263.28	Append to	U1410A-27X-1, 13	246.83	267.12
U1410A-27X-6, 60	254.80	275.09	Append to	U1410A-28X-1, 13	256.43	276.72
U1410A-28X-CC, 32	258.65	278.94				

